THERMAL HYDRAULICS ANALYSIS OF THE MIT RESEARCH REACTOR IN SUPPORT OF A LOW ENRICHMENT URANIUM (LEU) CORE CONVERSION

by

YU-CHIH KO

B.S. Engineering and System Science, 2002
M.S. Engineering and System Science, 2004
National Tsing-Hua University, Taiwan

Submitted to the Department of Nuclear Science and Engineering in Partial Fulfillment of the Requirements for the Degree of

Master of Science in Nuclear Science and Engineering
at the
Massachusetts Institute of Technology
[February 2008]
January 2008

Signature of Author: _____
Department of Nuclear Science and Engineering
January 8, 2008

Certified by: _____
Dr. Lin-wen Hu, Thesis Supervisor
Nuclear Reactor Laboratory

_____
Professor Mujid S. Kazimi, Thesis Co-supervisor
Department of Nuclear Science and Engineering

_____
Dr. Thomas Newton, Thesis Reader
Nuclear Reactor Laboratory

Accepted by: _____
Professor Jacquelyn C. Yanch
Chairman, Department Committee on Graduate Students

THERMAL HYDRAULICS ANALYSIS OF THE MIT RESEARCH REACTOR IN SUPPORT OF A LOW ENRICHMENT URANIUM (LEU) CORE CONVERSION
by

YU-CHIH KO

Submitted to the Department of Nuclear Science and Engineering on January 8, 2007 in Partial Fulfillment of the Requirements for the Degree of Master of Science in Nuclear Science and Engineering

Abstract

The MIT research reactor (MITR) is converting from the existing high enrichment uranium (HEU) core to a low enrichment uranium (LEU) core using a high-density monolithic UMo fuel. The design of an optimum LEU core for the MIT reactor is evolving. The objectives of this study are to benchmark the in-house computer code for the MITR, and to perform the thermal hydraulic analyses in support of the LEU design studies. The in-house multi-channel thermal-hydraulics code, MULCH-II, was developed specifically for the MITR. This code was validated against PLTEMP for steady-state analysis, and RELAP5 and temperature measurements for the loss of primary flow transient. Various fuel configurations are evaluated as part of the LEU core design optimization study. The criteria adopted for the LEU thermal hydraulics analysis for this study are the limiting safety system settings (LSSS), to prevent onset of nucleate boiling during steady-state operation, and to avoid a clad temperature excursion during the loss of flow transient.

The benchmark analysis results showed that the MULCH-II code is in good agreement with other computer codes and experimental data, and hence it is used as the main tool for this study. In ranking the LEU core design options, the primary parameter is a low power peaking factor in order to increase the LSSS power and to decrease the maximum clad temperature during the transient. The LEU fuel designs with 15 to 18 plates per element, fuel thickness of 20 mils, and a hot channel factor less than 1.76 are shown to comply with these thermal-hydraulic criteria. The steady-state power can potentially be higher than 6 MW, as requested in the power upgrade submission to the Nuclear Regulatory Commission.

Thesis Supervisor: Lin-wen Hu
Title: Associate Director of MIT Nuclear Reactor Laboratory
Thesis Co-supervisor: Mujid S. Kazimi
Title: Professor of Nuclear Science and Engineering

Acknowledgements

I would like to express my sincere appreciation to my thesis advisors, Dr. Lin-wen Hu and Professor Mujid Kazimi for all of their guidance and patience. This thesis cannot be completed without their assistance. I am especially grateful to Dr. Lin-wen Hu. She helped me in many ways during the past one and half years. My study at MIT has a wonderful beginning because of her support and encouragement.

I want to thank Dr. Thomas Newton, my thesis reader, for his help and support. I am also indebted to Dr. Arne Olsen and Dr. Floyd Dunn at ANL who prepared the initial PLTEMP and RELAP5 input decks. My colleagues in the LEU conversion project and my thermal-hydraulic group always make me happy, thank you, everybody.

Special thanks go to Rui Hu, my senior and good friend for his assistance on using the RELAP5 code. His patience and generosity are mostly appreciated.

I would like to thank my family. Although we cannot see each other during these days, your support and love drive me to fulfill my dream.

Finally, I must express my thanks to my dear wife, Yen-Chia Lin. Her supports, encouragement, love and selflessness is the answer whenever there is a question mark in my mind.

Table of Contents

Appendix

List of Figures

List of Tables

Chapter 1
Introduction

1.1 Objectives

The MIT research reactor (MITR) is converting from using high enrichment uranium (HEU) core to low enrichment uranium (LEU) core. The design of an LEU is currently ongoing. It is expected that MIT will finish the conversion by 2014. The objectives of this study are to benchmark the in-house computer code for the MITR, and to perform the thermal hydraulic analyses in support of the LEU design studies. The in-house multi-channel thermal-hydraulics code, MULCH-II, which was developed specifically for MITR, is used as the main tool for thermal-hydraulic calculations. Computer codes routinely used by the RERTR program, such as PLTEMP and RELAP5, and MITR measurement data are used for the benchmark study. The second objective of this study is to evaluate various design options in order to support the LEU core optimization study. The criteria adopted for the LEU thermal hydraulics analysis for this study are the limiting safety system settings (LSSS), to prevent onset of nucleate boiling during steady-state operation, and the loss of flow analysis to avoid a clad temperature excursion during the transient.

1.2 The Reduced Enrichment for Research and Test Reactors Program

In order to minimize the amount of weapons-grade uranium in the civilian world, efforts to use low enriched uranium (LEU) in research reactors have lasted for several decades. LEU is defined as being less than 20% enriched in U-235. Although the use of LEU fuel has some drawbacks, for example, possible losses of neutron fluxes, current concerns about terrorists building an HEU weapon have promoted increased attention to LEU fuels. The Reduced Enrichment for Research and Test Reactors (RERTR) Program was established in 1978. It is established to "develop the technical means to convert the reactors and isotope production processes from the use of HEU to the use of low enriched uranium through the development of new LEU fuels and targets." [1]. The RERTR program has been under the National Nuclear Security Administration since 2004 as part of the Global Threat Reduction Initiative (GTRI) [2] to better coordinate several nonproliferation programs together under GTRI. Under the auspices of the RERTR program, a total of eleven U.S. reactors have been converted by end of 2006 [3]. Eight U.S. reactors were scheduled to be converted using currently developed LEU fuels. In addition, six HEU-fueled U.S. reactors, including MIT research reactor, are unable to use currently qualified LEU fuels because of their compact core design and high power

density. These six reactors require the development of high-density LEU fuel for conversion. As of 2005, 39 research reactors in 22 countries have converted to LEU fuel through the work of the RERTR program.

1.3 Description of the MIT Reactor

The MIT Reactor has been in operation providing neutrons for research since 1958. The original reactor (MITR-I) was a heavy-water moderated and cooled reactor using HEU aluminide fuel. After a re-evaluation of needs and further core optimization studies, the current reactor (MITR-II) was built. The MITR-II core differs significantly from the original design in that it uses light water to cool and moderate a close-packed array of finned, plate-type elements. Initial criticality of the MITR-II was achieved on August 14, 1975 [4].

Figure 1-1 is an isometric view of the present MIT Research Reactor (MITR-II or MITR). It is licensed for 5 MW operation. The MITR uses a close-packed array of finned, plate-type elements. Fuel elements are surrounded by a heavy-water reflector which is in turn surrounded by the original graphite reflector. The fuel elements made of UAl_x cermet (HEU) are rhomboid in shape and each contains fifteen plates. The normal core configuration is twenty-four fuel elements with three positions available for in-core experiments. This core design was chosen to maximize the thermal neutron flux in the reflector regions where the experimental beam ports are located.

Reactor control is provided by six boron-impregnated stainless-steel shim blades and one cadmium regulating rod. Forced flow removes heat from the primary, heavy water, and graphite region with all heat loads being deposited in a common secondary cooling system. There are two anti-siphon valves located in the upper core tank to prevent complete drainage because of a siphon effect in the event of a break in the inlet primary piping. Four natural circulation valves, that are located next to the flow guide, provide a natural circulation flow path for decay heat removal. The pressure in the system is practically atmospheric, and coolant temperature is approximately 50 °C (120 °F).

Relicensing documents were submitted to US Nuclear Regulatory Commission (NRC) for 6 MW operation. The new license request, dubbed MITR-III, is for the same core configuration and operating conditions as the MITR-II. The 20% power uprate is realized by recapturing the excess safety margin in the MITR-II design. As described in the Safety Analysis Report (SAR) [4], the basis for the MITR-III's thermal-hydraulic design is that, under conditions of forced convection, the primary coolant system can remove the energy produced during routine 6.0 MW operation of the reactor without

onset of nucleate boiling (ONB). Another design feature is that the system should be able to remove at least 100 kW of heat from the fuel elements by natural convection without the onset of nucleate boiling. Provisions are also taken into account in the coolant system design so that fuel integrity is maintained during all credible transients, such as a loss of primary coolant flow because of a pump coast-down.

The objective of the thermal-hydraulic design of the MITR II is to maintain the structural integrity of the fuel elements which are made of a UAlx matrix enclosed in an 6061 aluminum alloy clad. Al-6061 melts at approximately 660 °C (1200 °F). However, it begins to soften at about 450 °C (842 °F), and the avoidance of this temperature is the safety limit criterion. There are several heat transfer phenomena that could lead to elevated temperatures should they occur. These are:

a) Critical Heat Flux (CHF) at Low Quality: This phenomenon refers to departure from nucleate boiling (DNB). Vapor bubbles form on the fuel clad surface. Initially, this increases heat transfer because of the latent heat that is removed by bubble formation. However, if the heat flux rises, the bubbles coalesce so that patches of vapor exist and heat transfer then decreases because heat must now be conducted through a gas. For a given flow rate, CHF is the heat flux at which this sudden decrease in heat transfer occurs.

b) Critical Heat Flux (CHF) at High Quality: This phenomenon is similar to that described above except that the initiating event is not a departure from nucleate boiling but rather dryout where vapor accumulates in the channel center and gradually strips liquid from the clad surface.

c) Onset of Flow Instabilities (OFI): Flow instabilities refer to the phenomenon where vapor forms in a coolant channel and, as a result of the volume that is required by the vapor, liquid is displaced. This displacement may result in channel blockage with less coolant flowing to the channel in question and more to adjacent ones. OFI is a concern for cores with a multi-channel design.

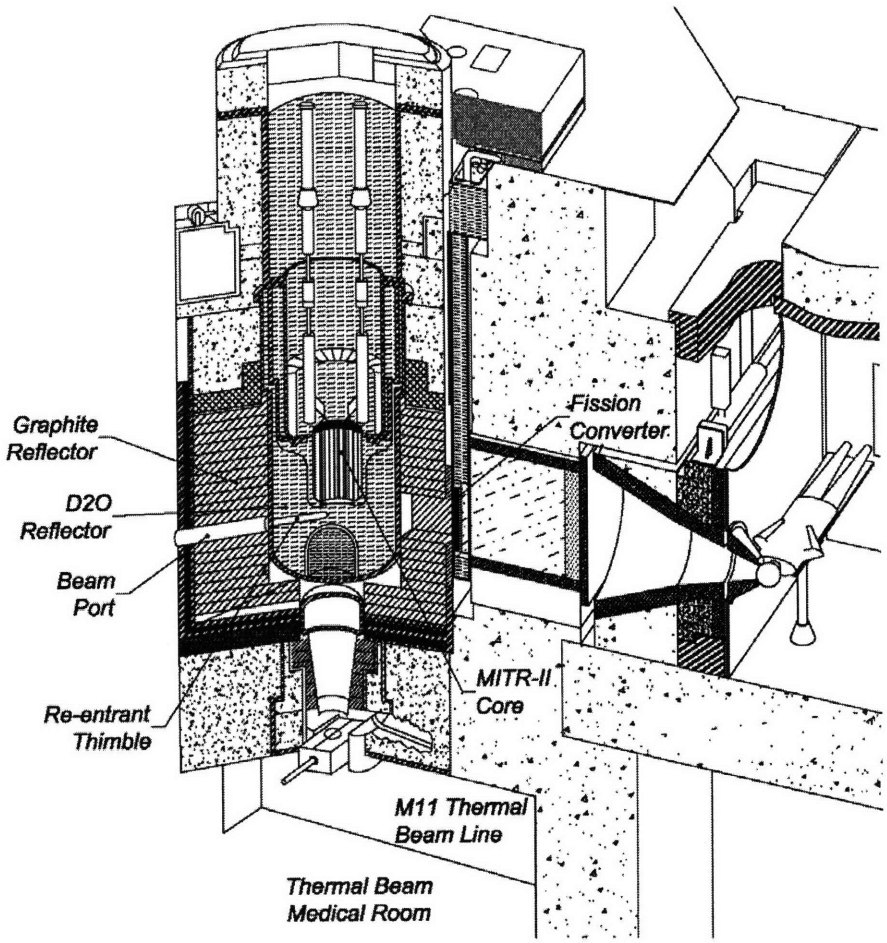

Figure 1-1 Isometric View of the MIT Research Reactor

1.4 Computer Codes Utilized in this Study

1.4.1 The MIT in-house code: MULti-CHannel-II

An in-house thermal hydraulics code, MULti-CHannel-II or MULCH-II, was developed for the steady-state, thermal hydraulic limits, and loss of primary flow analysis of the MITR [5,6,7]. This code uses a model of the MITR-II, coupling power distributions with momentum and energy conservation equations to obtain system design parameters and safety limits. The MULCH-II code features the multi-channel analysis, natural circulation

and anti-siphon valve models, fin effectiveness model and correlations for low pressure systems. In addition, the MULCH-II code is capable of modeling forced to natural circulation during a loss of primary flow transient and calculating the safety limits and limiting safety system settings for licensing applications.

The solution procedure for the code is a two step process [8]. First, the primary and secondary loop parameters are solved for each node using energy conservation equations. If the operational mode is natural circulation, then both momentum and energy equations are solved for the nodes in the core tank region. Second, the core parameters are solved for both the hot and the average channels, each of which consists of ten axial nodes. The second step may require iterations if the difference between the hot channel and the average channel pressure drops exceeds a preset value. This could occur because of variation in local coolant densities or flow instability. The hot channel operating parameters are then compared with pre-selected criteria to verify if the thermal hydraulic limits are exceeded.

The MULCH-II code can be used for the following purposes: (1) to determine system design parameters such as pressure drop, flow rate, temperatures, and heat exchanger capacities, etc.; (2) to analyze transients such as loss of primary flow and loss of heat sink, and (3) to establish safety limits and limiting safety system settings.

The MULCH-II code has been validated previously against steady-state MITR data, empirical correlations for the onset of flow instability, and temperature data obtained from loss of flow transient experiments. The steady-state data were taken from the hourly operation log [9]. The operation conditions cover a wide range of cooling tower outlet temperatures and heat exchanger fouling factors. The transient experimental data were obtained from pump coast-down experiments that were performed during the MITR-II's initial startup in 1997 [10]. Calculations of onset of flow instability compared satisfactorily with correlations derived from experimental data. The MULCH-II code input instruction is attached as Appendix A

1.4.2 The PLTEMP/ANL code

PLTEMP/ANL is a FORTRAN program that obtains a steady-state flow and temperature solution for a nuclear reactor core, or for a single fuel assembly [11]. This code is developed and maintained by Argonne National Laboratory (ANL) and has been used for other LEU conversion studies. The PLTEMP/ANL code was benchmarked with *Mathematica* and experimental data [11, 12].

PLTEMP/ANL was designed to represent flow and temperature conditions in a single hot channel, a single fuel subassembly, or a reactor core consisting of up to five different types of fuel assemblies, and up to 30 fuel assemblies of each type. Each fuel assembly consists of one or more plates or tubes separated by coolant channels. Flow distribution was calculated to obtain uniform pressure drops across all flow paths, either in the core or in a given fuel subassembly. Axial power peaking factors were supplied for each fuel plate of each fuel subassembly. Bypass flow through non-fueled channels could also be specified.

PLTEMP/ANL incorporates a variety of thermal-hydraulic correlations with which to determine safety margins such as onset of nucleate boiling (ONB), departure from nucleate boiling (DNB), and onset of flow instability (FI). Coolant properties for either light or heavy water are obtained from FORTRAN functions rather than from tables. The code is intended for thermal-hydraulic analysis of research reactor performance in the sub-cooled boiling regime. Both turbulent and laminar flow regimes can be modeled.

1.4.3 The RELAP5-3D code

The RELAP5 series of computer codes has been maintained at the Idaho National Laboratory (INL) under sponsorship of the U.S. Department of Energy, the U.S. Nuclear Regulatory Commission, members of the International Code Assessment and Applications Program (ICAP), members of the Code Applications and Maintenance Program (CAMP), and members of the International RELAP5 Users Group (IRUG) [13]. RELAP5-3D, the latest code version in the series of RELAP5 codes, is a highly generic code that can calculate the behavior of a reactor coolant system during a transient. In addition, it can be used for simulation of a wide variety of hydraulic and thermal transients in both nuclear and non-nuclear systems involving mixtures of vapor, liquid, non-condensable gas, and non-volatile solute. The RELAP5 core was benchmarked with experimental data and is used widely in the nuclear power industry [14, 15, 16].

RELAP5-3D features multi-dimensional components to allow users to more accurately model the multi-dimensional flow behavior that can be exhibited in any component or region of a Light Water Reactor (LWR) system. In this thesis, RELAP5-3D code will be used for benchmark study for both steady state and loss of primary coolant transient. Besides, it is also used to calculate thermal-hydraulic performance of LEU fuel to optimize the LEU core design.

Chapter 2
The Low Enrichment Uranium Fuel Design

2.1 Introduction

A number of lower density LEU fuels have been qualified by the RERTR program since its inception. These include UAlx-Al fuel (uranium density of 2.3 g/ cm^3), U_3O_8-Al fuel (up to 3.2 gU/ cm^3), $UZrH_x$ fuel (up to 3.7 gU/cm^3), U_3Si_2-Al (up to 4.8 g/ cm^3) and so on. High density U-Mo alloys are currently the fuels under testing and development by the RERTR program [3].

In order to qualify LEU fuels for use, the RERTR program must supply all of the information to a regulatory authority (NRC in the U.S.) required to approve its use. [17] This includes thermal and material technical data, small scale and large scale irradiation testing and measurements, as well as qualification of fuel fabricators and fabrication processes [18]. It is also necessary to consider reprocessing parameters for the fuel.

Once the fuel is qualified for use, a reactor must apply to the licensing authority to use the fuel in its facility. The U.S. Department of Energy has set a goal to convert U.S. reactors by 2014, high density dispersion and monolithic fuels are targeted to be qualified by 2010.

2.2 LEU Core Design Objectives and Constraints

2.2.1 Constraints

The objective of the LEU core design is to prevent any reduction in neutron flux available to experiments due to the conversion to LEU fuel, as well as increasing the flexibility for meeting the needs of in-core experiments. Material in this section follows that of [19] pp. 53-55. Portions that are verbatim are indicated by quotations.

"The conversion of the MIT Reactor will be funded, at least in part, by the U.S. Department of Energy under the RERTR program. Because the resources and budget are not limitless, the conversion of the MIT Reactor will have to be made with funding constraints. Modification of the reactor beyond the existing core structure would be expensive and most likely not fundable within RERTR guidelines, although such complete renovation could possibly bring significant gains for experimental needs. Thus,

it would be more cost effective that any modifications as part of the LEU conversion of the MITR will have to be made within the existing core structure."

2.2.2 Criteria for LEU Fuel Selection

In order to select an LEU fuel and core design, a number of criteria should be met. These include both safety and utilization goals and are listed below [19]:

1. Equivalent to or greater thermal flux than the HEU core at the same power level.

2. Equivalent to or greater fast flux than the HEU core at the same power level.

3. Negative moderator temperature and void coefficients.

4. Fuel cycle length equivalent or longer than the HEU core.

5. Adequate blade worth and shutdown margins.

6. Sufficient excess reactivity to overcome xenon poisoning and Doppler broadening, under restart conditions.

7. Adequate subcooled margin in all channels. The criterion in an LEU core is to avoid the onset of nucleate boiling (ONB) even in the hottest channels and the channels with lowest coolant flow.

8. Adequate natural circulation cooling for low power and shutdowns.

2.3 Material of the Proposed LEU Fuel

It has been concluded that the monolithic uranium-molybdenum (U-Mo) fuel is currently the only viable option for LEU fuel that has sufficient density to be used in the MITR [20]. At present, a LEU design for the MIT Reactor is proposed using high density monolithic U-Mo fuel with molybdenum content of 10%. This fuel has a density of 17.5 g/cm^3. Use of fuels with higher molybdenum content (therefore with a slightly lower density) is also possible. However, the addition of a percentage or two of molybdenum will have little effect on either neutronic performance or thermal performance [19].

2.4 Configuration of the Proposed LEU Fuel

Figure 2-1 shows the configuration of the proposed LEU core design. This design was proposed by T. H. Newton in 2006 as part of his PhD thesis [21]. It consisted of half-sized fuel elements made up of nine U-Mo LEU fuel plates of 0.55 mm thickness with 0.25 mm finned aluminum cladding. In this configuration, fuel is placed close to a centrally located in-core sample assembly (ICSA), thus enhancing the fast flux. For both HEU and LEU, there are three rings in the core. A-ring is the innermost ring, B-ring is in between and C-ring is the outermost ring. To optimize the in-core flux, solid beryllium dummies with solid lead dummies are utilized. Half-sized fuel elements arranged within the A-ring and B-ring are also utilized in an attempt of in-core flux optimization.

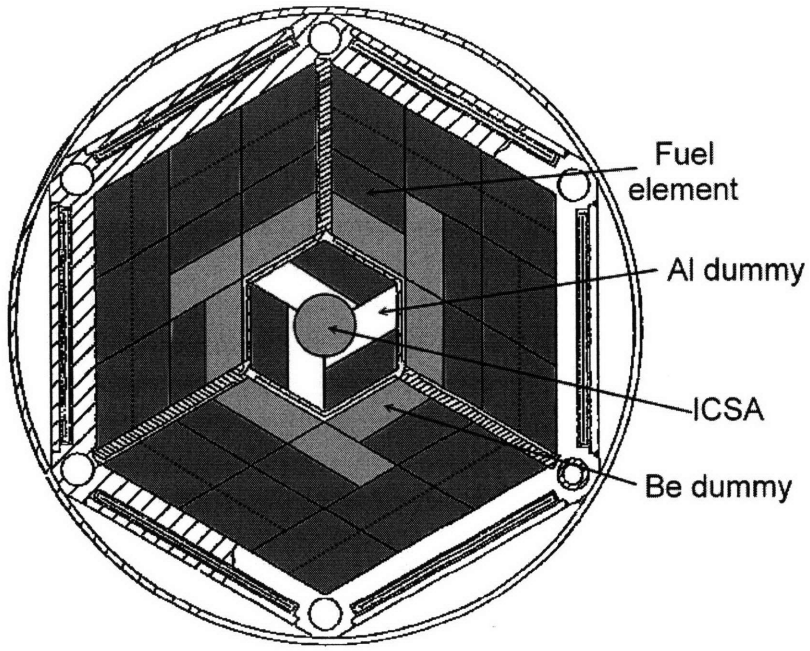

Figure 2-1 Configuration of the proposed LEU core design [21]

2.5 Features of the Proposed LEU Fuel

The LEU core design for the MIT Reactor has been developed to best meet the needs of the experimental users of the reactor. This design was made flexible enough to meet the changing needs of experimenters. Table 2-1 lists the properties and configuration of HEU and LEU core [22]. Given that the LEU fuel density is much higher than the HEU fuel, it is possible to obtain the necessary ^{235}U content in the same core volume.

U-Mo alloy is currently the proposed LEU fuel. Comparing with the UAlx fuel used in HEU, the melting point and conductivity of U-Mo fuel are slightly lower than those of UAlx fuel. However, these are not seen as significant barriers to its use, since the fuel plates are thin and the temperature gradient is small during normal operations, and the limiting condition of reactor transients is dependent on the softening point of the aluminum cladding, 450 °C, much lower than the fuel melting temperature of ~ 1200 °C .

The number of fuel plates in the LEU core is grater than that of the HEU core, which will decrease the average heat generation per plate. The higher fuel density will result in a much larger uranium loading, although the plates used in the LEU core are thinner. The fissile mass in the LEU core is twice as that of the HEU core, which results in an overall lower neutron flux at a given power level. However, the LEU core configuration was designed to optimize neutron flux delivery to experimental positions.

Table 2-1 Comparison of HEU and LEU core characteristics

	HEU core	LEU*
	Fuel Properties	
Fuel material	UAlx	Monolithic U-7Mo
Fuel material density (g/cm^3)	3.44	17.55
Uranium density (g U/cm^3)	1.54	16.32
Fuel melting point (°C)	1400	~1200
U-235 weight per plate (kg)	0.031	0.057
Thermal conductivity – fresh fuel (W/m K)	42.5	17.6
Thermal conductivity – irradiated fuel (W/m K)	42.1	17.4
Enrichment	93%	20%
	Configuration	
Number of fuel elements/core	23	42
Number of fuel plates/element	15	9
Number of total fuel plates	345	378
Fuel thickness (mm)	0.76	0.55
Aluminum cladding thickness (mm)	0.38	0.25
Number of fins per fuel plate	220	220
Fin height (mm)	0.254	0.254
Fin Width (mm)	0.254	0.254

*This is the reference LEU core proposed by Thomas Newton [22].

Chapter 3
Modeling and Benchmarking: Steady State Analysis

3.1 Introduction

The objective of this benchmark study is to evaluate the capability and accuracy of the MITR's in-house thermal-hydraulics code, MULCH-II. Since MULCH-II will be used to perform the thermal-hydraulic calculation for the proposed LEU core design, it is very important to assure the adequacy of using the MULCH-II code. Two different types of scenario, steady state and loss of primary coolant accident, are analyzed. In this chapter, PLTEMP/ANL (version 3.0) and RELAP5-3D (version 2.3.6) are chosen to benchmark the MULCH-II code. Results of steady-state analyses are summarized and compared.

3.2 Steady State Conditions

The MIT Research Reactor is currently being relicensed for 6 MW operation. It is intended to operate at or below a steady-state thermal power level of 6.0 MW with a primary coolant flow rate of 2000 gpm, a coolant outlet temperature of 55 °C, and a coolant level at overflow [23]. The MITR's thermal-hydraulic design basis is that, under conditions of forced convection, the primary coolant system can remove the energy produced during routine 6.0 MW operation of the reactor and transfer it to the secondary coolant system without the onset of nucleate boiling.

These operating conditions are set for the simulation cases. In the following paragraph, the terms "MULCH", "PLTEMP" and "RELAP5" will be used instead of "MULCH-II", "PLTEMP/ANL" and "RELAP5-3D" code for simplicity.

3.3 Comparison of the Input Parameters

The initial PLTEMP input deck for the MITR 6 MW power uprate was assembled by Dr. Arne Olsen at ANL [11]. The input parameters for PLTEMP are "plate width", "fuel length" and "unfueled width" to model the fuel plate geometry and to calculate the heated area. MULCH, which was developed specifically for MITR, considers "fuel meat length", "fuel length" and "fin effectiveness". The fin effectiveness of the MULCH code is a multiplication factor used in conjunction with the coolant heat transfer coefficient to account for the heat transfer augmentation due to the longitudinal fins on the clad surface. Since PLTEMP (version 3.0) does not include the fin effectiveness as in the case of MULCH-II code, the parameter "plate width" was increased to incorporate the larger heat

transfer area.

The RELAP5 input deck for the MITR 6 MW power uprate was assembled. However, there is also no such fin effectiveness model in the RELAP5 input. To incorporate the fin effectiveness as in the case of MULCH code, the plate surface area in the RELAP5 input was intentionally increased by a factor of 1.9. Details of the RELAP5 model for the MIT reactor will be described in Chapter 4.

The MULCH code does not model the temperature distribution within the fuel plate since during steady-state and credible transient scenarios the temperature difference between fuel centerline and clad outer surface is small. MULCH does take into account the conduction resistance between fuel meat outer surface and coolant due to crud. The crud means oxidation layers formed during regular reactor operation. MULCH can provide the crud outer surface temperatures and the temperature difference between coolant and the crud. MULCH can also provide the clad outer surface temperatures by setting crud thickness to zero. In this benchmark study, it is assumed that there is no crud formed on the clad surface. Appendix B summarizes the calculated temperature difference between fuel centerline and coolant for the hot channel (hot channel factor = 2.0) as a function of reactor power.

In MULCH, PLTEMP and RELAP5, there are 10 axial nodes for hot and average channel. Node 0 is the coolant inlet temperature and Node 10 is the coolant outlet temperature.

3.4 Comparison of MULCH and PLTEMP code

3.4.1 Description of Simulation Cases

There are two simulation cases which are used to compare the MULCH and PLTEMP code. Table 3-1 lists the input parameters for these two simulation cases. Case 1 (Without fins) is the simplified case which does not take into account the fin effectiveness. This case is selected to facilitate direct comparison of MULCH and PLEMP. Case 2 is the "best estimate" case set up to consider the heat transfer of fins. For MULCH code, the fin effectiveness is 1.9. For PLTEMP, the parameter "plate width" is changed to 0.1062 to incorporate the effect of fins (0.05588*1.9 = 0.1062). Analyses reported below are based on a steady-state reactor power of 6 MW for the existing HEU core. The core consists of 22 fuel elements and 15 plates per element. The MULCH and PLTEMP input files are attached in Appendix C and Appendix D, respectively.

Table 3-1 Description of simulation cases

	MULCH-II		PLTEMP/ANL	
Simulated Case	Plate width (m)	Fin effectiveness	Plate width (m)	Fin effectiveness
Case 1 (Without fins)	0.05588	0.0	0.05588	NA
Case 2 (Best estimate)	0.05588	1.9	0.1062*	NA

* For PLTEMP, a larger plate width is used to incorporate the fin effectiveness. 0.05588*1.9 = 0.1062, the number to simulate the increased surface area due to fins.

3.4.2 Simulation Results

3.4.2.1 Comparison of coolant and cladding temperature

Figure 3-1 is the comparison of coolant temperature for both Case 1 and Case 2. Coolant temperature is determined by energy conservation which is a function of power (integrated heat flux) and coolant inlet temperature, thus Case 1 and Case 2 have identical coolant temperature. Fin effectiveness has no influence on energy conservation and the prediction of steady state coolant temperature. As shown in Fig.3-1, the coolant temperatures predicted by MULCH and PLTEMP are very close because the same values of input parameters have been used.

Figure 3-2 is the comparison of clad temperature for Case 1. Figure 3-2 shows that the prediction of MULCH and PLTEMP are almost the same. Figure 3-3 is the comparison of clad temperature for Case 2. As shown in Fig. 3-3, PLTEMP predicts slightly lower cladding temperature than MULCH which is consistent with the coolant temperature difference.

3.4.2.2 Comparison of axial temperature distribution

Table 3-2 summarizes the coolant and clad temperature difference for Case 1. It shows that the maximum coolant temperature difference between MULCH and PLTEMP occurs at node 4, which is also the hottest node. The maximum clad temperature difference occurs at node 5. This difference is relatively small comparing to the difference in

coolant temperature. In general, MULCH predicts higher coolant and clad temperature than PLTEMP does. The temperature difference in the hot channel is greater than it is in the average channel due to higher heat flux. It is noted that the first five nodes have higher temperature difference than the following nodes due to bottom peaking of the power distribution. One possible reason for the discrepancy in coolant temperature is that MULCH reports maximum node temperature (e.g., coolant temperature at node outlet) while PLTEMP reports the node-average temperature.

Table 3-3 summarizes the coolant and clad temperature difference for Case 2. It shows that the maximum clad temperature difference also occurs at node 4, which is consistent with the coolant temperature difference. Comparing Table 3-2 and Table 3-3, it should be noted that the clad temperature difference in Case 2 is much greater than it is in Case 1. This is because the fin effectiveness affects the heat transfer area, thus affects the clad temperature distribution as well. Since MULCH and PLTEMP use different ways to take into account the fin effectiveness, it is reasonable that greater clad temperature difference will appear when the existence of fin is considered (Case 2). Namely, the results from the two codes will be slightly different due to the contribution of the fins.

It should also be noted that the significant figures of temperature provided by MULCH and PLTEMP are different. MULCH can provide one digit after decimal point. In contrast, PLTEMP can provide three digits after the decimal point. These differences can be seen in the following Table 3-4. In author's opinion, the predicted values of MULCH and PLTEMP each have about a 10% uncertainty.

3.4.2.3 Comparison of hot channel heat flux, coolant and cladding temperature difference, and heat transfer coefficient

Table 3-4 summarizes the comparison of hot channel heat flux and heat transfer coefficient for the Case 1. It shows that the heat flux is exactly the same because the same values of reactor power and heat transfer area are given for the two codes. To calculate the heat transfer coefficient, MULCH and PLTEMP adopt different correlations. PLTEMP uses Dittus-Boelter [24] for single phase and Bergles-Rohsenow [25] for two-phase heat transfer coefficient. MULCH uses Chen's correlation [26] to calculate both single and two-phase heat transfer coefficient. However, assuming no boiling occurs in steady state, Chen's correlation will reduce to standard Dittus-Boelter during single phase flow, thus the heat transfer coefficient predicted by the two codes should be roughly the same as shown in Table 3-4.

Table 3-5 summarizes the comparison of hot channel heat flux and heat transfer coefficient for the Case 2. Comparing with Table 3-4, it can be seen that the fin does have

impacts on the results. Apparently, heat flux is decreased approximately by a factor of 1.9, which is equal to the value of fin effectiveness. Besides, heat transfer coefficients are slightly affected by the existence of fin. It can also be found in both Table 3-4 and 3-5 that basically PLTEMP predicts higher temperature difference between coolant and clad than MULCH does. However, the difference is less than 5% and is insignificant.

3.4.2.4 Comparison of core pressure drop

The results of pressure drop through the core region were compared. The comparison is as follows: MULCH predicts the pressure drop is about 50081 Pa. This is in agreement with PLTEMP's prediction of 50,000 Pa.

3.5 Comparison of MULCH and RELAP5 code

3.5.1 Description of Simulation Case

There is only one case performed by RELAP5 for the steady state analysis. This case is the "best estimate" case set up to ensure both codes predict the same results as initial conditions for loss of primary transient simulations described in Chapter 4. For MULCH code, the fin effectiveness is 1.9. For RELAP5, the plate surface area is intentionally increased by a factor of 1.9 to incorporate the effect of fins.

3.5.2 Simulation Results

3.5.2.1 Comparison of coolant and cladding temperature

Figure 3-4 shows a comparison of coolant temperature. As mentioned in 3.4.2.1, coolant temperature is determined by energy conservation, therefore, in Fig. 3-4, the calculated coolant temperatures are about the same. Figure 3-5 is the comparison of cladding temperature. The results show that the cladding temperatures in the average channel are almost the same. For the hot channel, MULCH predicts a higher cladding temperature than RELAP5 does. The temperature difference of cladding, especially in the hot channel, is possibly due to the fin effectiveness and different heat transfer correlations that MULCH and RELAP5 use. The correlations which RELAP5 employs are described in 3.5.2.3.

3.5.2.2 Comparison of axial temperature difference

In Table 3-6, the temperature differences for coolant and cladding outer surface for each axial node are summarized. Table 3-6 shows that MULCH and RELAP5 predict about the same coolant temperature in both the hot and average channels and the same cladding

temperature in the average channel (within a difference of 0.1 °C). The higher temperature difference occurs at the cladding temperature in hot channel. The maximum temperature difference between MULCH and RELAP5 occurs at node 4, which is also the hottest node. The cladding temperature difference in the hot channel is higher than the others because of higher heat flux. It is noted that the first five nodes have greater temperature difference than the following nodes due to bottom peaking of the power distribution. These results are consistent with the results of comparison between MULCH and PLTEMP.

3.5.2.3 Comparison of hot channel heat flux, coolant and cladding temperature difference, and heat transfer coefficient

Table 3-7 summarizes the comparison of hot channel heat flux and heat transfer coefficient. Under the steady state conditions, i.e., no boiling occurs, the values of heat transfer coefficient should be roughly the same. However, Table 3-7 shows that RELAP5 predicts slightly higher heat transfer coefficients than MULCH does. The discrepancy could be attributed to the heat transfer correlations. MULCH uses Chen's correlation for both single and two-phase heat transfer. For RELAP5, single phase heat transfer correlations are calculated relying on evaluating forced turbulent convection, forced laminar convection, and natural convection and selecting the maximum of these three. The correlations are by Dittus-Boelter [24], Kays [27], and Churchill-Chu [28], respectively. Two-phase heat transfer correlations are calculated by Chen's correlation for nucleate boiling and transition boiling; by Bromley correlation for film boiling.

3.5.2.4 Comparison of core pressure drop

The pressure drop through the core region is calculated to be about 50,081 Pa by MULCH. This is slightly higher than RELAP5's prediction of 49,399 Pa.

3.6 Conclusions

In this chapter, two cases are simulated using PLTEMP and one case is simulated using RELAP5 to benchmark MULCH for steady state analyses. Assuming fin effectiveness is zero, the results predicted by MULCH and PLTEMP are very close. To consider the existence of fins, since both PLTEMP and RELAP5 cannot model the fin effectiveness, heat transfer area on cladding surface is increased intentionally to incorporate the effect of fins. In these best estimate cases, results are different in a narrow range among PLTEMP, RELAP5 and MULCH. Since the steady state results of MULCH are in agreement with PLTEMP and RELAP5, it is concluded that MULCH is qualified to perform steady state analysis for the MIT reactor.

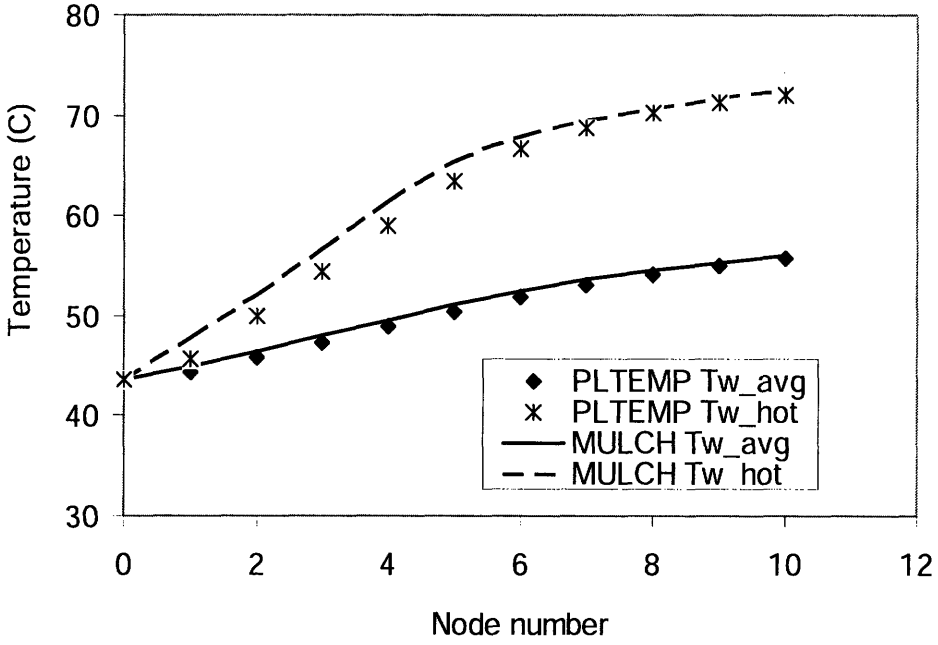

Figure 3-1 Comparison of coolant temperature for both Case 1 and Case 2

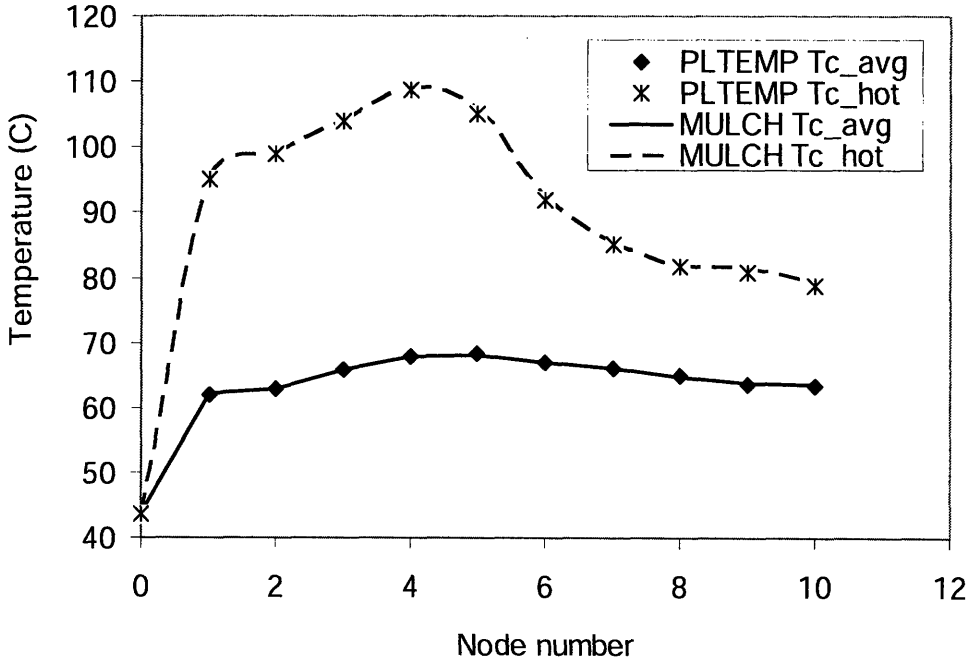

Figure 3-2 Comparison of clad surface temperature for Case 1

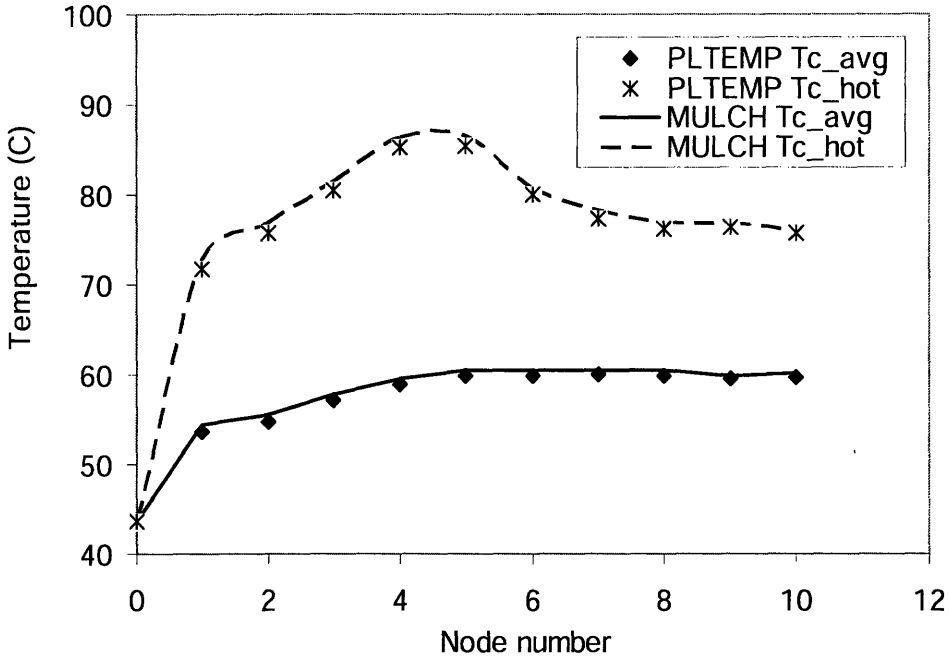

Figure 3-3 Comparison of clad surface temperature for Case 2

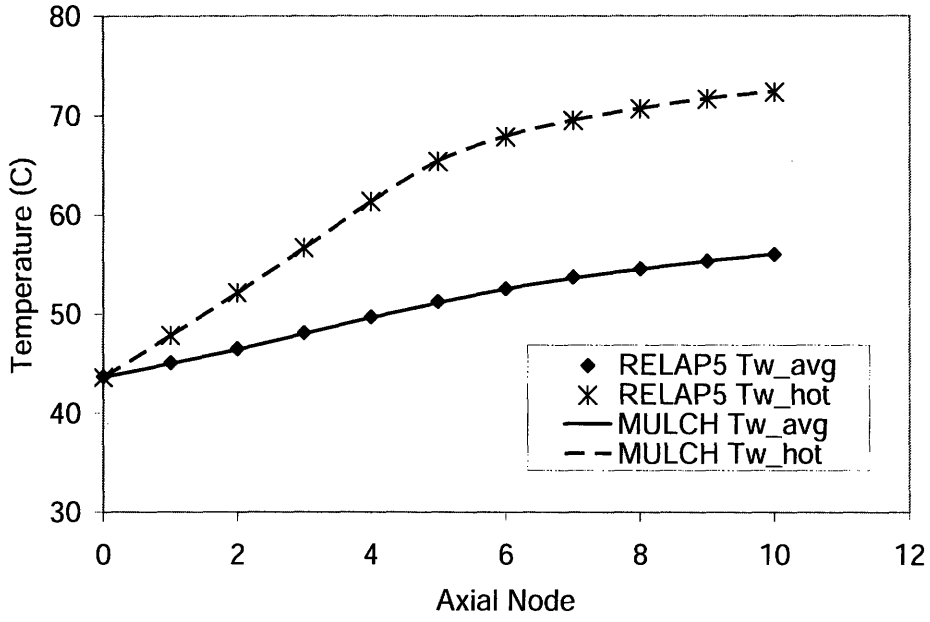

Figure 3-4 Comparison of coolant temperature (RELAP5)

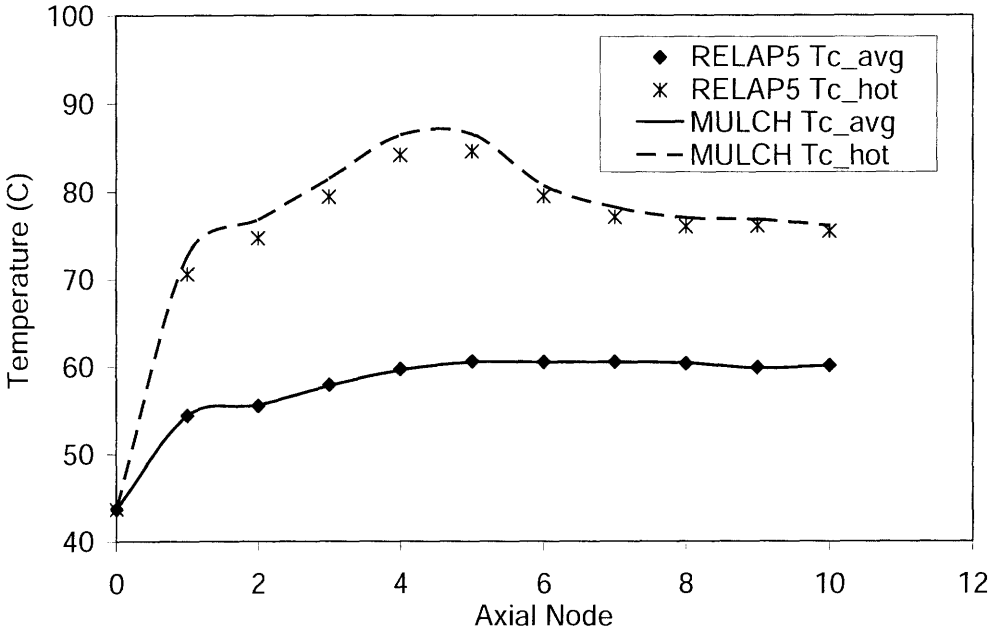

Figure 3-5 Comparison of clad surface temperature (RELAP5)

Table 3-2 Temperature difference* between MULCH and PLTEMP (Case 1)

	Hot Channel		Average Channel	
Node	Cladding (°C)	Coolant (°C)	Cladding (°C)	Coolant (°C)
1	0.251	2.088	0.056	0.672
2	0.22	2.105	0.074	0.631
3	0.268	2.173	-0.002	0.733
4	0.339	2.261	0.028	0.739
5	0.637	1.984	-0.016	0.662
6	0.523	1.205	-0.133	0.633
7	0.315	0.732	0.015	0.501
8	0.193	0.525	-0.126	0.351
9	0.607	0.453	0.276	0.293
10	0.466	0.319	0.232	0.27

* Temperature difference = MULCH – PLTEMP

Table 3-3 Temperature difference between MULCH and PLTEMP (Case 2)

	Hot Channel		Average Channel	
Node	Cladding (°C)	Coolant (°C)	Cladding (°C)	Coolant (°C)
1	1.028	2.088	0.75	0.672
2	1.03	2.105	0.804	0.631
3	1.078	2.173	0.728	0.733
4	1.198	2.261	0.736	0.739
5	1.17	1.984	0.707	0.662
6	0.755	1.205	0.653	0.633
7	0.846	0.732	0.568	0.501
8	0.757	0.525	0.581	0.351
9	0.53	0.453	0.312	0.293
10	0.465	0.319	0.351	0.27

Table 3-4 Comparison of hot channel heat flux, temperature difference and heat transfer coefficient (Case 1: Without Fins)

	Heat Flux q" (W/m^2)		Temperature Difference* Tc – Tw (°C)		Heat Transfer Coefficient h (W/m^2 °C)	
Node	MULCH	PLTEMP	MULCH	PLTEMP	MULCH	PLTEMP
1	8.01E+05	8.01E+05	47.5	49.337	1.69E+04	1.62E+04
2	8.23E+05	8.23E+05	47.1	48.985	1.75E+04	1.68E+04
3	8.59E+05	8.59E+05	47.5	49.405	1.81E+04	1.74E+04
4	8.93E+05	8.93E+05	47.8	49.722	1.87E+04	1.80E+04
5	7.71E+05	7.71E+05	40.3	41.647	1.91E+04	1.85E+04
6	4.77E+05	4.77E+05	24.5	25.182	1.94E+04	1.89E+04
7	3.13E+05	3.13E+05	15.9	16.317	1.97E+04	1.92E+04
8	2.23E+05	2.23E+05	11.2	11.532	1.99E+04	1.93E+04
9	1.86E+05	1.86E+05	9.7	9.546	1.91E+04	1.95E+04
10	1.32E+05	1.32E+05	6.9	6.753	1.91E+04	1.95E+04

*Temperature Difference = cladding temperature (Tc) – coolant temperature (Tw)

Table 3-5 Comparison of hot channel heat flux, temperature difference and heat transfer coefficient (Case2: With Fins)

	Heat Flux q" (W/m^2)		Temperature Difference Tc – Tw (°C)		Heat Transfer Coefficient h (W/m^2 °C)	
Node	MULCH	PLTEMP	MULCH	PLTEMP	MULCH	PLTEMP
1	4.21E+05	4.21E+05	24.9	25.96	1.69E+04	1.62E+04
2	4.33E+05	4.33E+05	24.7	25.775	1.75E+04	1.68E+04
3	4.52E+05	4.52E+05	24.9	25.995	1.82E+04	1.74E+04
4	4.70E+05	4.70E+05	25.1	26.163	1.87E+04	1.80E+04
5	4.06E+05	4.05E+05	21.1	21.914	1.92E+04	1.85E+04
6	2.51E+05	2.51E+05	12.8	13.25	1.96E+04	1.89E+04
7	1.65E+05	1.65E+05	8.7	8.586	1.89E+04	1.92E+04
8	1.17E+05	1.17E+05	6.3	6.068	1.86E+04	1.93E+04
9	9.77E+04	9.77E+04	5.1	5.023	1.92E+04	1.94E+04
10	6.95E+04	6.95E+04	3.7	3.554	1.88E+04	1.95E+04

Table 3-6 Temperature difference* between MULCH and RELAP5 (Steady State)

Node	Hot Channel		Average Channel	
	Cladding (°C)	Coolant (°C)	Cladding (°C)	Coolant (°C)
1	2.10	-0.02	0.00	-0.07
2	2.10	-0.04	0.10	-0.10
3	2.10	-0.04	-0.10	-0.07
4	2.20	-0.01	-0.10	-0.08
5	1.90	0.05	-0.10	-0.12
6	1.20	0.06	-0.02	-0.04
7	1.10	0.02	-0.02	-0.08
8	1.00	0.05	0.08	-0.03
9	0.70	0.08	-0.09	0.01
10	0.60	0.09	-0.01	0.03

* Temperature difference = MULCH – RELAP5.

Table 3-7 Comparison of hot channel heat flux, temperature difference and heat transfer coefficient (Steady State)

	Heat Flux q" (W/m^2)		Temperature Difference* Tc – Tw (°C)		Heat Transfer Coefficient h (W/m^2 °C)	
Node	MULCH	RELAP5	MULCH	RELAP5	MULCH	RELAP5
1	4.21E+05	4.21E+05	24.9	22.68	1.69E+04	1.86E+04
2	4.33E+05	4.33E+05	24.7	22.56	1.75E+04	1.92E+04
3	4.52E+05	4.52E+05	24.9	22.76	1.82E+04	1.99E+04
4	4.70E+05	4.70E+05	25.1	22.89	1.87E+04	2.05E+04
5	4.06E+05	4.06E+05	21.1	19.25	1.92E+04	2.11E+04
6	2.51E+05	2.51E+05	12.8	11.66	1.96E+04	2.15E+04
7	1.65E+05	1.65E+05	8.7	7.62	1.90E+04	2.17E+04
8	1.17E+05	1.17E+05	6.3	5.35	1.86E+04	2.19E+04
9	9.77E+04	9.77E+04	5.1	4.48	1.92E+04	2.18E+04
10	6.95E+04	6.95E+04	3.7	3.19	1.88E+04	2.18E+04

*Temperature Difference = cladding temperature (Tc) – coolant temperature (Tw)

Chapter 4
Modeling and Benchmarking: Loss of Primary Flow Analysis

4.1 Introduction

The MIT Research Reactor is intended to operate with a primary coolant flow rate of 2000 gpm under steady state conditions. A low primary flow (below 1900 gpm) will automatically initiate a scram. There are two initiating events that can cause a loss of primary coolant flow accident [29]. The first is a loss of off-site electrical power which will stop the primary pumps and scram the reactor by dropping all six shim blades simultaneously. This is a credible scenario. The second is a pump coast down accident that occurs because of primary pump power supply failures or malfunctions of the pump motors. This is not considered to be a credible accident because the probability for both pumps to fail at the same time is very small.

In this chapter, analyses were performed for a loss-of-flow (LOF) accident. The benchmark study consists of two parts. First, LOF accidents initiated by pump coast down are simulated by RELAP5 and MULCH based on a steady-state reactor power of 6 MW with an initial flow rate at 2000 gpm for the existing highly enriched uranium core. Second, the measurements from MITR-II startup test are used to compare with the prediction of MULCH and RELAP5.

4.2 Natural circulation in the MIT Reactor

The MITR is equipped with natural circulation and anti-siphon valves as passive safety features to promote the removal of decay heat from the core whenever forced convection flow is not sufficient. These valves are particularly important for a loss of flow transient during operation, when natural circulation becomes the primary means of cooling the core. There are four natural circulation valves (NCVs) located at the bottom of the core tank and two anti-siphon valves (ASVs) installed in the core tank at the elevation of the primary inlet pipe. Both the NCVs and ASVs are ball-type check valves. Under forced convection, the valves are shut because the ball is forced to the top of the shaft by the coolant pressure, thereby blocking the top aperture of the valves. When the primary flow is not sufficient to maintain the holding pressure, the ball begins to drop so that the valves will be open.

Figure 4-1 and 4-2 illustrate the forced and natural convection circulation paths in MITR. When a transient or accident causes the pressure drops, for example, pump coast down occurs, NCVs and ASVs will start to open. Natural convection flow is then established

within the core tank because of the buoyancy force of the heated coolant in the core region. The hot coolant exiting the core rises within the core tank, mixes with cold coolant in the outlet plenum, reverses direction and flows through the natural convection and/or anti-siphon valves, and then goes back through the core region thereby completing the natural circulation loop.

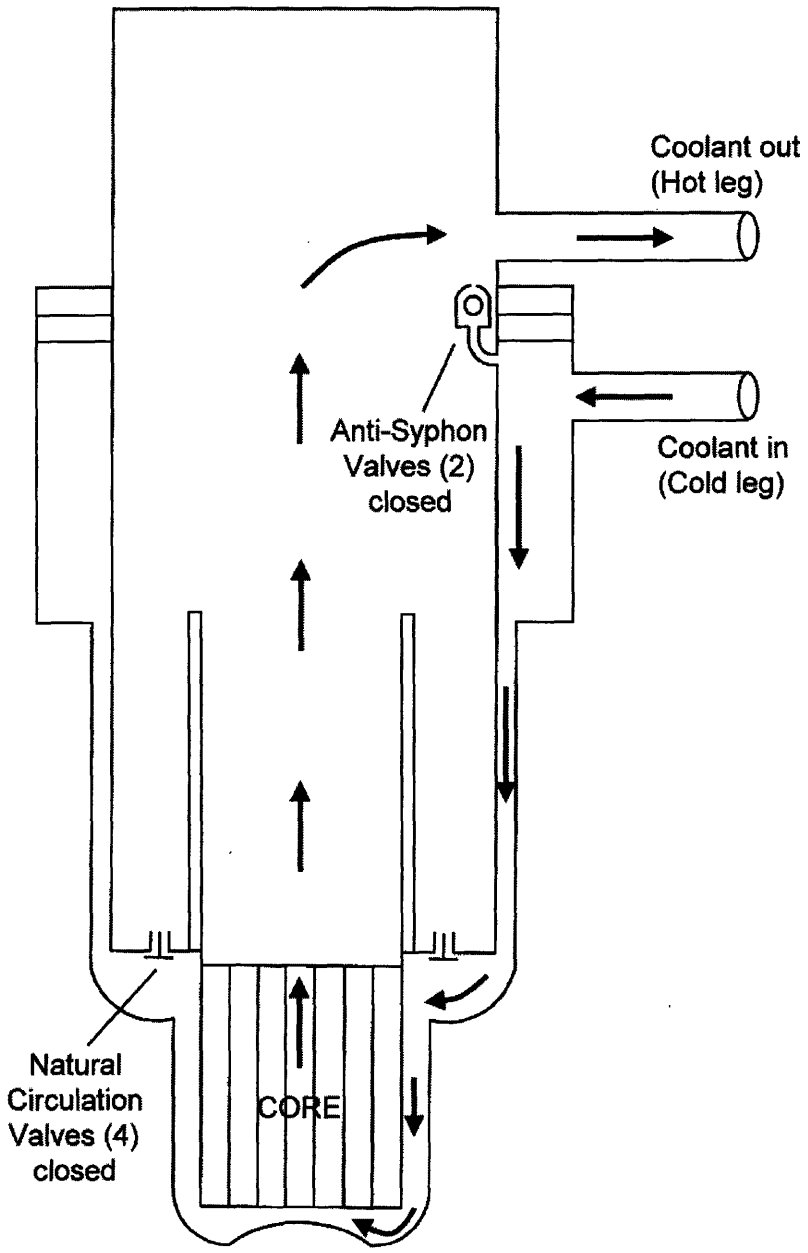

Figure 4-1 Forced convection in MIT reactor

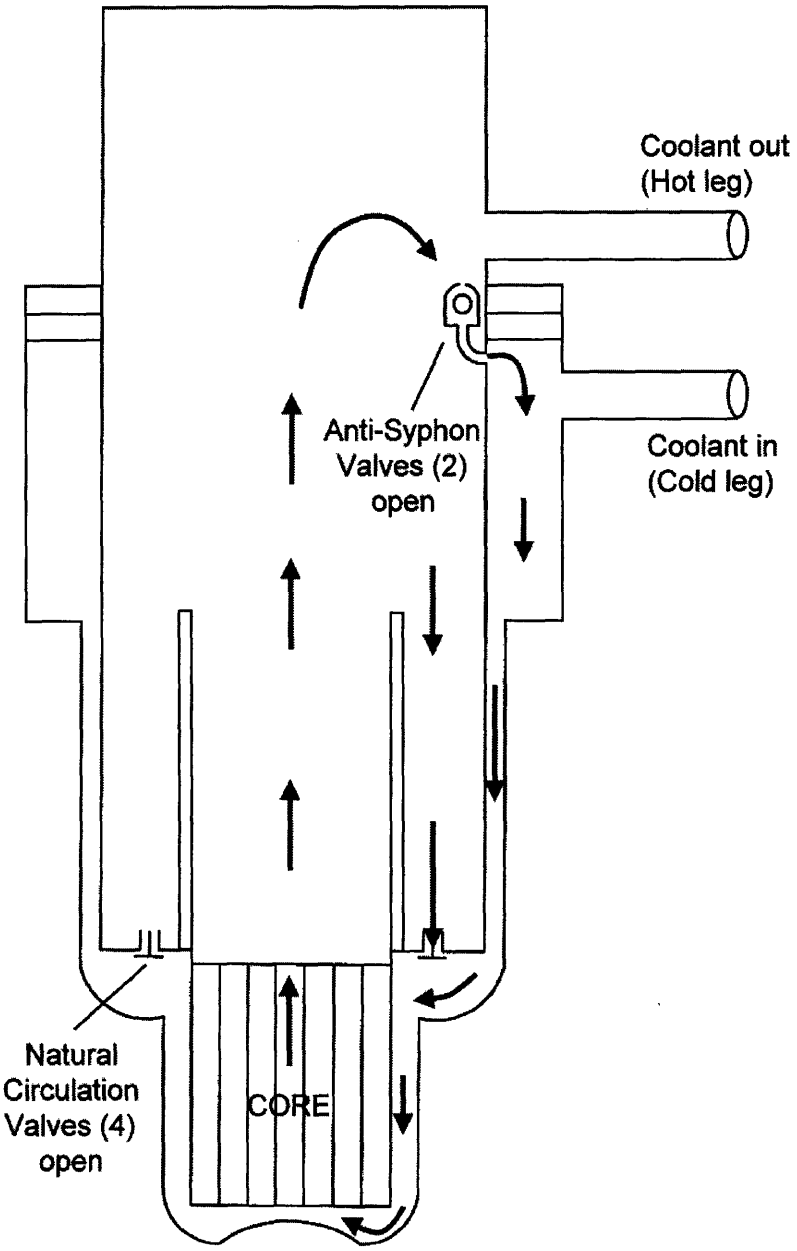

Figure 4-2 Natural convection in MIT reactor

4.3 MITR Modeling for Loss of Primary Flow Accident

Figure 4-3 illustrates the control volumes and the flow paths modeled for MITR [30]. Table 4-1 summarizes the MITR primary system parameters [31]. Figure 4-4 and 4-5 are the simplified primary loop control volumes of MULCH and RELAP5 code, respectively. The anti-siphon valves (ASVs) and natural circulation valves (NCVs) are shown in the figures. Both ASV and NCV are very important components for establishing natural circulation during the loss of primary flow transients. Comparing Figure 4-4 and 4-5, it can be found that RELAP5 divides the primary loop into more control volumes. In the RELAP5 MITR model, mixing area is split into 3 sub-regions and the average channel, hot channel and bypass flow are separate control volumes. The RELAP5 input for MITR is given in Appendix E.

4.4 Transient Scenario and Assumptions

As mentioned in 4.1, there are two initiating events that can cause a loss of primary coolant flow accident. In this benchmark study, the initiating event is assumed to be a pump coast down accident without loss of off-site power. Figure 4-6 shows the pump coast down curve of the MIT reactor [10].

When a pump coast down accident occurs, the reactor will shut down automatically upon receiving a low primary coolant flow scram signal. In the MITR-II initial startup natural convection tests, a scram delay time of 0.41 seconds [32] is assumed. It takes about 0.86 seconds from the initiation of scram to reach 80% of full insertion of the shim bank. A more conservative value of 0.9 seconds is assumed for analysis where in reality it takes about 0.51 seconds in the startup test. In the loss of primary flow simulation, MULCH assumes the reactor will shut down 2.3 seconds (one second for signal transmission and 1.3 seconds for shim blade insertion) after the initiating event. The reactor will scram by a step reactivity insertion at 2.3 seconds. This is a conservative assumption compared to the startup test measurement.

For RELAP5, it is also assumed a one-second signal transmission delay as consistent with MULCH. However, the reactor will scram by a ramp reactivity insertion. It is assumed that the reactivity insertion of -7.5 beta will be attained within one second right after the scram signal de-energizes the shim blade magnets. This assumption is based on MITR shim bank height of 10" as shown in Fig 4-7 [23]. It shows the MITR shim bank integral curve of a burnt core. For a fresh core the shim bank worth will be greater. Since MITR refuelings are normally performed so that the criticality is reached at a shim bank height of 7 to 9 inches, the assumption of -7.5 beta reactivity insertion is very conservative because it assumes less reactivity insertion than what a normal scram will have.

In the simulation cases, MULCH predicts the NCV and ASV will open at the same time, which is 4.4 seconds after the initiating event. For RELAP5, we use this timing as an assumption to force open NCV and ASV at time equal to 4.4 second. It is reasonable

since RELAP5 adopts the same pump coast down curve as MULCH. The transient scenario is detailed in Table 4-2.

To calculate the decay power, MULCH uses a simplified correlation which is based on point kinetic equations with 7 precursor groups [5]. For RELAP5, the decay power model is based on an approximation of the ANS Proposed Standard [13]. RELAP5 provides several standards, such as the 1973 ANSI/ANS Standard, 1979 ANSI/ANS Standard and the exact 1994 ANSI/ANS Standard etc., for the decay power calculation. In this study, the 1979 ANSI/ANS Standard is chosen to calculate the decay power.

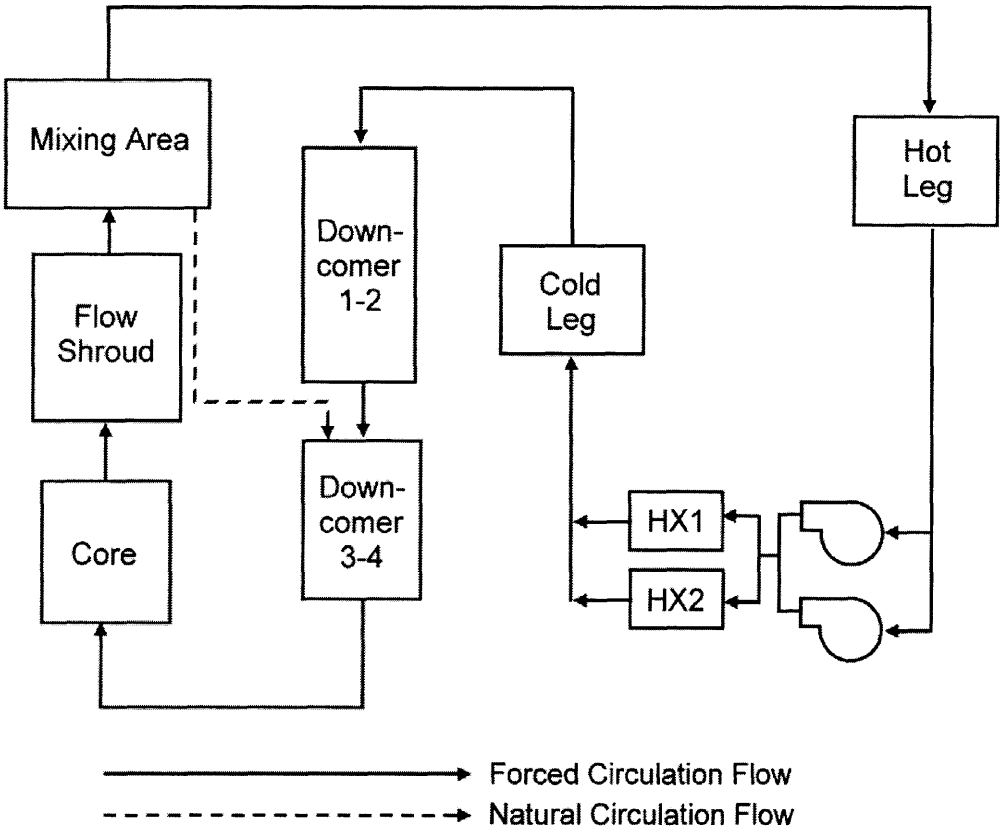

Figure 4-3 Schematic of MITR flow paths

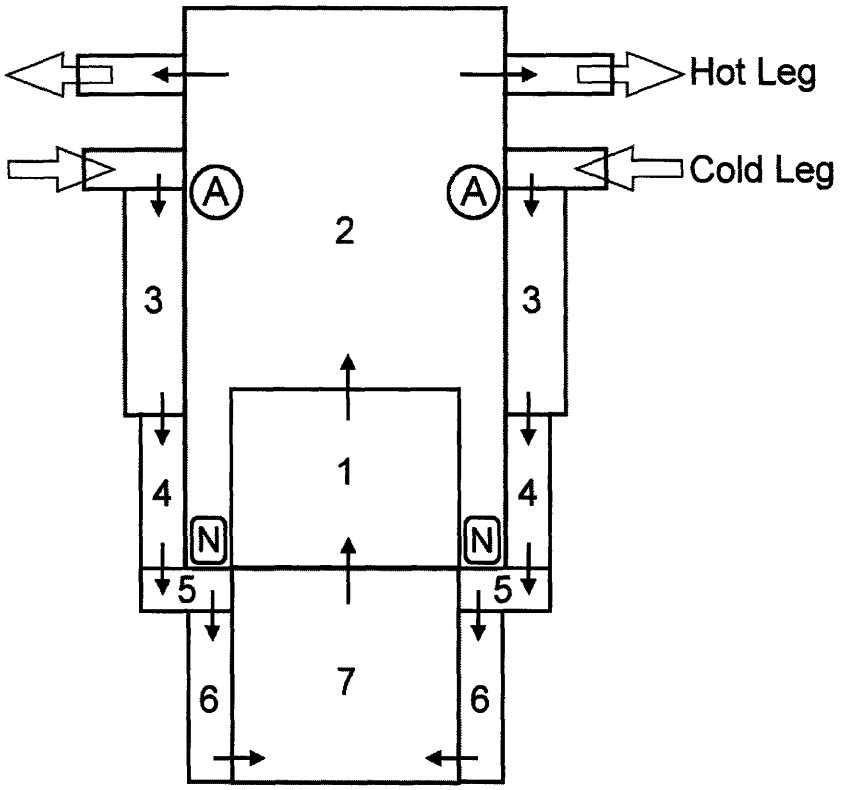

CV1: Flow Shroud
CV2: Mixing Area
CV3: Downcomer 1
CV4: Downcomer 2
CV5: Downcomer 3
CV6: Downcomer 4
CV7: Fuel Element
A: Anti-Siphon Valve (ASV)
N: Natural Convection Valve (NCV)

Figure 4-4 MITR primary loop control volumes (MULCH code)

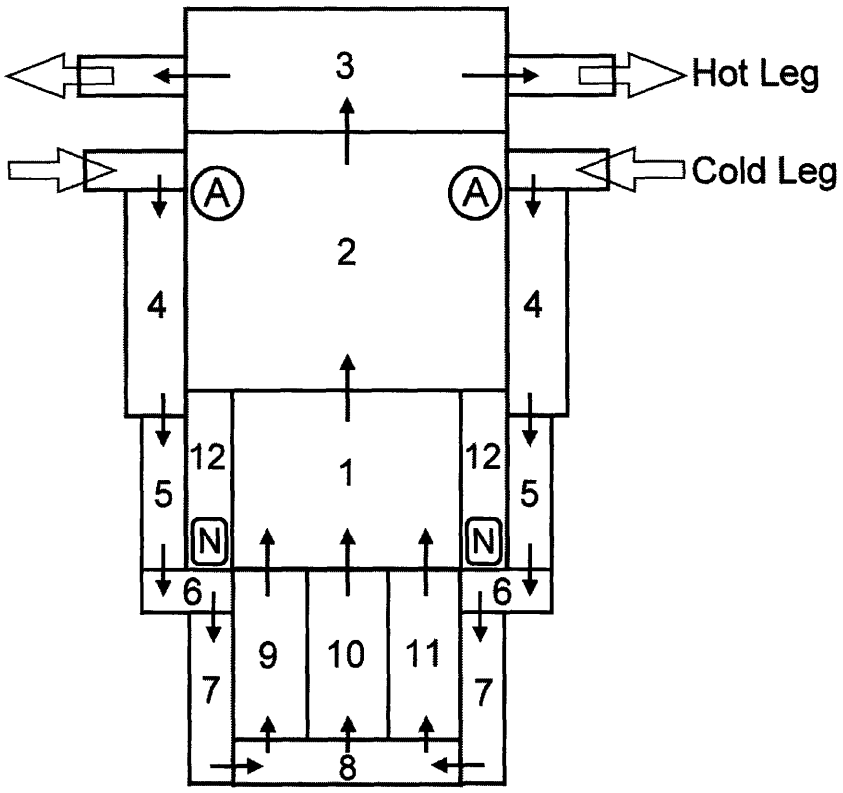

CV1: Flow Shroud
CV2: Mixing Area 1
CV3: Mixing Area 2
CV4: Downcomer 1
CV5: Downcomer 2
CV6: Downcomer 3
CV7: Downcomer 4
CV8: Fuel Bottom
CV9: Avg. Channel
CV10: Hot Channel
CV11: Bypass Flow
CV12: Mixing Area 3
A: Anti-Siphon Valve (ASV)
N: Natural Convection Valve (NCV)

Figure 4-5 MITR primary loop control volumes (RELAP5 code)

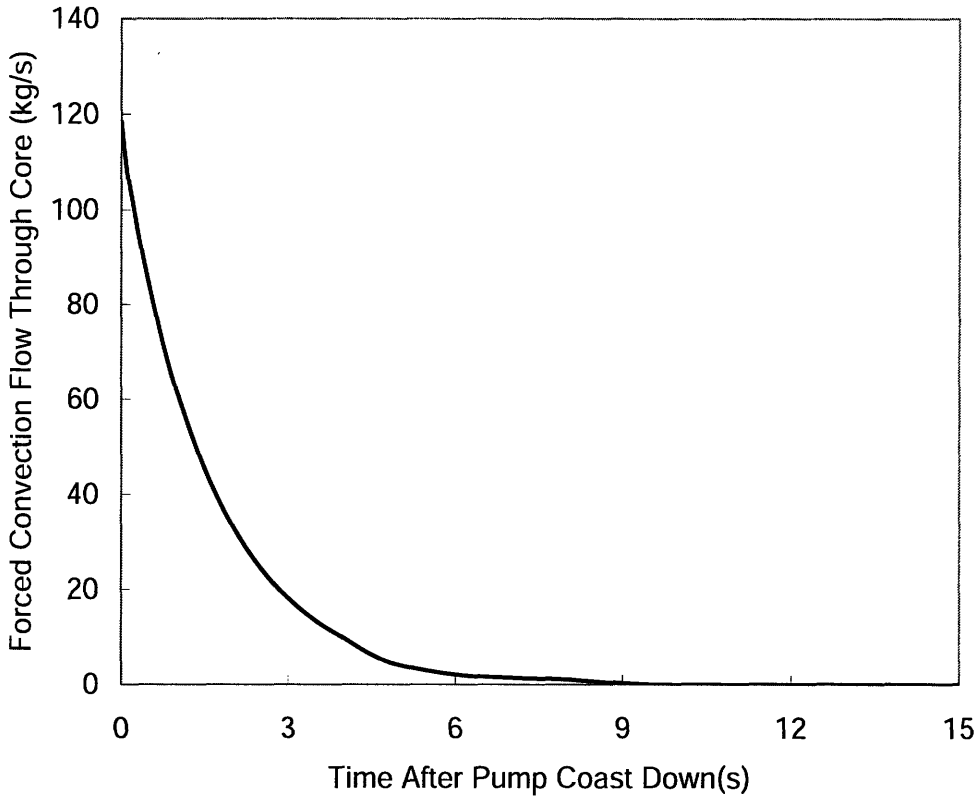

Figure 4-6 MITR pump coast down curve

Table 4-1 MITR primary system parameters (adopted from [5])

	Flow area per channel (m^2)	Volume per channel (m^3)	De (m)	Inlet elevation, Zin (m)	outlet elevation, Zout (m)	Zout – Zin	K factor	Number of channels
Core	1.249 E-4	8.243 E-5	2.1864 E-3	7.13	7.79	0.66	2.05	330
Flow Shroud	0.130	0.099	0.387	7.79	8.55	0.76	0.00	1
Mixing Area	0.923	1.920	1.084	8.55	9.77	1.22	0.00	1
Hot Leg	0.032	0.427	0.203	9.77	2.69	-7.08	4.58	1
Heat Exchanger	0.0689	1.68 E-4	7.04 E-3	2.69	2.69	0.0	7.30	1770
Cold Leg	0.032	0.468	0.203	2.69	9.66	6.97	2.17	1
Downcomer 1	0.339	0.413	0.180	9.66	8.44	-1.22	0.0	1
Downcomer 2	0.111	0.076	0.063	8.44	7.75	-0.69	0.30	1
Downcomer 3	4.4 E-3	0.016	0.220	7.75	7.74	-0.01	0.18	1
Downcomer 4	0.029	0.018	0.040	7.74	7.13	-0.61	0.0	1

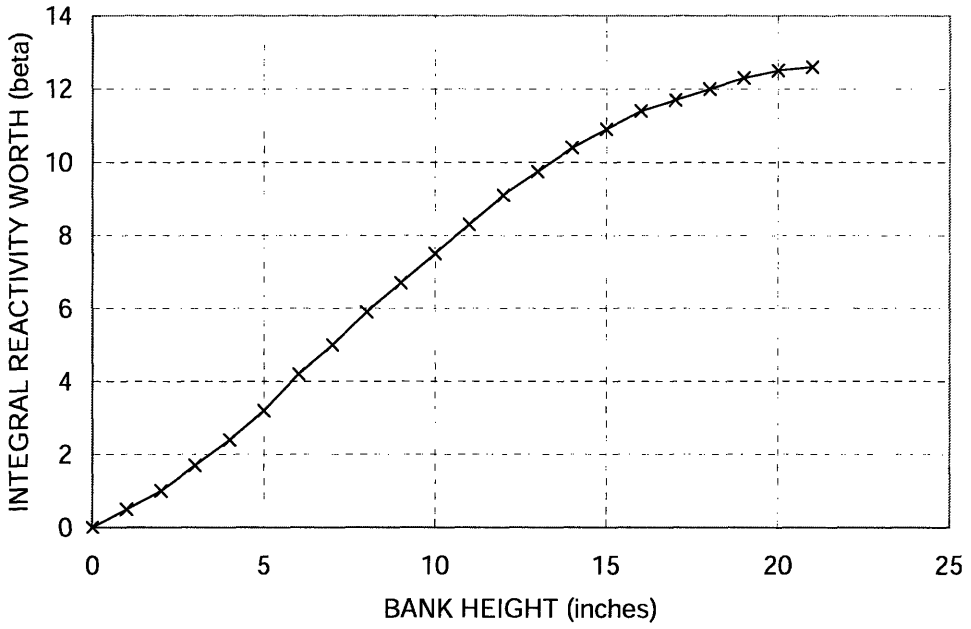

Figure 4-7 MITR Shim Bank Integral Curve

Table 4-2 Scenario of the loss-of-flow (LOF) case

Time (sec)	Event
0.0	Loss of primary flow (Pump coast-down)
2.3	Reactor scram
4.4	ASV and NCV open

4.5 Simulation Results

4.5.1 Comparison of flow rates

Figure 4-8 through 4-12 show the flow rate of all anti-siphon valves, all natural circulation valves, core, average channel and hot channel, respectively. In Fig.4-8 and 4-9, positive flow rate means it is an "up-flow" or "bypass flow"; if negative, it is a "down-flow" or "natural circulation flow". As shown in Fig. 4-8, the flow passing through ASV is always a down-flow during the transient. RELAP5 predicts the ASV flow rate which is always higher than the prediction of MULCH. Furthermore, RELAP5 predicts the ASV flow rate reaches a much lower level at the first few seconds of the transient, however, the steady state (after the natural circulation is established) ASV flow rate is close to that predicted by MULCH.

Table 4-3 summarizes the change of ASV and NCV flow rate through the transient. In Table 4-3, MULCH predicts the steady state ASV flow rate of 1.37 (kg/s), which is slightly less than RELAP5's prediction. RELAP5 predicts ASV would have a steady state flow rate of 1.40 (kg/s). In contrast to the flow through ASVs, Fig. 4-9 shows that at first the flow passing through NCVs is an up-flow since the pump still works due to inertia and the axial location of NCV is relatively low. After the natural circulation is fully established, NCVs start to have a down-flow. MULCH predicts the NCV would have a down flow (natural circulation flow) at time equal to 18.4 second. RELAP5 predicts the natural circulation flow established at time equal to 15.0 second. Again, RELAP5 predicts a higher steady state NCV flow rate than MULCH. For RELAP5 and MULCH, the steady state NCV flow rate is 0.51 (kg/s) and 0.29 (kg/s) respectively.

The core flow rate is shown in Fig. 4-10. Table 4-4 summarizes the change of core flow rate through the transient. At the beginning of the transient, MULCH predicts a higher core flow rate than RELAP5. After ASVs and NCVs open (at 4.4 second), the core flow rate of RELAP5 becomes greater than MULCH. Once the natural circulation flow is established, the core flow rate would be steady and equal to the summation of ASV and NCV flow rate. It can be found in Table 4-4 that RELAP5 predicts a higher steady state core flow rate than MULCH, which is consistent with the results shown in Fig. 4-8 and 4-9. The steady state core flow rate of RELAP5 and MULCH are 1.91 (kg/s) and 1.52 (kg/s) respectively. Figure 4-11 and 4-12 are the flow rate in average channel and hot channel. As shown in Fig. 4-11, the flow rate in average channel has similar behavior to core flow rate. However, Fig. 4-12 shows that RELAP5 predicts there is a small flow oscillation in hot channel. This flow oscillation is due to boiling in hot channel and results in temperature spike on hot channel clad temperature. It should also be noted that the flow rate in hot channel is smaller than average channel due to the flow disparity for hot channel. In both MULCH and RELAP5, the factor of 0.864 is used for the flow disparity.

4.5.2 Comparison of coolant and cladding temperature

Figure 4-13 through 4-15 are comparisons of coolant temperature in the average channel. Node #1, #5, and #10 represent the entrance, the mid-point, and the outlet of the channel, respectively. As shown in Fig 4-13 to 4-15, both MULCH and RELAP5 predict a peak at the beginning due to the reduction in primary flow, and then the temperature gradually increases. RELAP5 predicts the coolant temperature in average channel would start to decrease due to the fully developed natural circulation flow. MULCH does not show the temperature decreasing trend but it is expected that the similar decreasing trend will happen later. These results are consistent with the abovementioned since RELAP5 predicts the NCV would transition to down-flow earlier than MULCH (RELAP5: 15.0 second; MULCH: 18.4 second, Fig 4-9). Basically RELAP5 predicts higher coolant temperature in average channel. This is because the different heat transfer correlations used in the two codes. In addition to that, the fin effectiveness and the difference in decay power may also account for this discrepancy. The decay power correlation will be discussed later in this section.

Figure 4-16 to 4-18 show the coolant temperature in the hot channel. In general, MULCH predicts higher hot channel coolant temperature than RELAP5 because of different two-phase heat transfer model. Figure 4-17 shows MULCH predicts the coolant temperature would finally stay at 107.46 °C, which is the saturation temperature corresponding to the system pressure. In Fig. 4-17 and 4-18, MULCH predicts that node #5 reaches the saturation temperature faster than node #10 because of the greater heat generation in node #5 (the normalized power distribution, as shown in Fig. 5-3, will discuss in chapter 5). RELAP5 predicts a temperature oscillation due to boiling and flow disparity. However, RELAP5 predicts that the hot channel coolant temperature does not reach the saturation temperature.

Figure 4-19 to 4-24 are comparison of cladding temperature in average and hot channel. As shown in Fig. 4-19 to 4-21, the two codes predict similar trend of cladding temperature in average channel. Figure 4-22 to 4-24 shows that RELAP5 also predicts a temperature oscillation which is corresponding to the hot channel flow rate and coolant temperature. Like coolant temperature, RELAP shows a higher cladding temperature than MULCH in the average channel and a lower cladding temperature in the hot channel.

4.5.3 Comparison of decay power

To calculate the decay power, MULCH uses a simplified correlation which is based on point kinetic equations with 7 precursor groups. The 7 group constants are summarized in Table 4-5. For RELAP5, the decay power model is based on an approximation of the ANS Proposed Standard. In this study, the 1979 ANSI/ANS Standard is chosen for RELAP5 to calculate the decay power. The DKPOWR code is also used to benchmark the decay power calculation.

The DKPOWR code was first developed to combine exponential pulse-function expressions for fission-product decay power with calculated fission histories to determine total fission-product decay power following fuel irradiation. The code used decay power pulse functions fit to CINDER-10ENDF/B-IV summation calculations or fits to combinations of calculated and measured decay power data for U^{235} and Pu^{239} as incorporated in the "ANSI/ANS-5.1-1979 Standard for Decay Heat Power in Light Water Reactors" [33]. Documentation for the code is currently being developed for distribution by the Electric Power Research Institute [34].

Figure 4-25 shows the results of decay power. In Fig. 4-25, it can be observed that MULCH, RELAP5 (ANS 1979) and DKPOWR predict similar trend of decay power. MULCH predicts a total decay energy of 8347.6 kJ during the transient, which is slightly less than RELAP5 (ANS 1979)'s prediction of 8564.0 kJ.

The total power is also compared. Figure 4-26 shows the difference of predicted total power between RELAP5 and MULCH. The difference is assuming due to the reactivity insertion. MULCH assumes the reactor will scram by a step reactivity insertion at 2.3 second. For RELAP5, the reactor will receive the scram signal in one second and a ramp reactivity insertion follows. The ramp reactivity insertion of -7.5 beta will be reached within one second right after signal arrived. This assumption is based MITR shim bank height of 10" and is very conservative as mentioned in section 4.4. Table 4-6 summarizes the change of total power through the transient. As shown in Table 4-6, MULCH predicts a total energy of 21236.8 kJ during the transient, which is slightly greater than RELAP5 (ANS 1979)'s predicted value of 21147.8 kJ.

4.6 Comparison of Calculated and Measured Coolant Temperature

4.6.1 General Information of the experimental data

The measurements from MITR-II startup test are used to compare with the prediction of MULCH and RELAP5. The loss of primary flow transient in MITR-II has been studied in detail by Bamdad [4]. He took experimental data during a series of loss of flow transients. For each transient, the outlet temperatures from two or three fuel elements were measured every fifteen to thirty seconds. Temperature measurements were made by inserting stainless steel clad chromel-alumel type K thermocouples into various positions. Table 4-7 shows a summary of thermocouples and places in reactor core. Figure 4-27 shows the cross section of MITR-II core and Fig. 4-28 shows the in-core thermocouples. Thermocouple installation and wiring is shown in construction and startup procedure of MITR-II [9]. The main design criteria was to affix the holder so that it could not break free during both primary operation and yet would have minimum effect on the element flow. To measure the fuel element outlet temperature the thermocouple tip is positioned in the element exit plenum under the end nozzle bale. Since the distance to channel exit is less than one inch, the measured temperature may not be the mixed mean element outlet temperature.

4.6.2 Comparison of predicted and measured outlet coolant temperatures

There are three cases used to compare the measurements and calculated results. These three cases have different steady state power and operating hours before reactor shut down. The descriptions of the three cases are summarized in Table 4-8. For simulation cases, the initiating event is the pump coast-down accident and the same assumptions are employed as stated in 4.4. Measured data from thermocouple TC-6, TC-7, and TC-9 are used to compare with the predicted values of coolant outlet temperature. Notice that the thermocouples are located in different positions. It is expected that the measured temperature from fuel element B-6 would fall between the predicted average and peak temperatures (within experimental error).

Figure 4-29 through 4-31 show the comparison between MULCH and measurements. It can be observed that the predicted values lie above and below the measured values. There are two sources for the difference between measured and predicted values of outlet temperature. In the early phase of the transient, the predicted power peak appears to be shifted to the right of the measured peak (i.e., it is predicted to occur later). This may be because MULCH has a simplified neutron kinetics model which adopts a step reactivity insertion. The longer-term temperatures reflect the decay heat generation rate in the core. MULCH calculates heat generation rate is a function of the decay precursor concentrations, which are related to the operating history of the reactor prior to the experiments. The predicted temperatures were based on the assumption that the reactor had been operating infinitely at the power level used for each experiment. Because the predicted long-term outlet temperatures are accurate for runs with longer operating histories, the difference between the measured and predicted long-term outlet temperatures in Fig. 4-29b are assumed to be due to the short operating history prior to the experiment.

Figure 4-32 through 4-34 show the comparison between RELAP5 and measurements. It can be found that RELAP5 seems to over-predict the peak temperature. However, in general RELAP5 has better performance and the predicted trend and values are closer to the measured values.

Comparison between MULCH, RELAP5 and measurements are shown in Figure 4-35 through 4-40. In sum, RELAP5 works well and the results match the main trend of the experimental data. MULCH, although is somewhat less conservative than RELAP5 in terms of the prediction of transient behavior, can still be used for safety analysis since the predicted peak values are always higher than the experimental data. Furthermore, MULCH is preferable because of the following advantages: 1) It is fast and easy to run; 2) The MULCH input deck requires much fewer parameters compared to RELAP5; 3) MULCH code can facilitate the thermal hydraulics limits analysis as well as best estimate. 4) The MULCH source code is open so the code can be easily modified to incorporate additional functions.

4.7 Conclusions

Loss of primary flow transients are studied to benchmark the MULCH code by using the RELAP5-3D code. Results of loss of primary flow transients show that RELAP5 predicts higher ASV, NCV and core flow when the natural circulation established. For the comparison of temperature, RELAP5 predicts higher coolant and cladding temperature in average channel but lower coolant and cladding temperature in hot channel. The decay power is also compared. Results show that MULCH predicts a total decay power of 8347.6 kJ during the transient, which is slightly less than RELAP5's prediction of 8564.0 kJ.

The calculated outlet coolant temperatures are compared with measurements. Results show that RELAP5 seems to over-predict the peak temperature but the predicted trend and values match the measured values well. MULCH is less conservative than RELAP5 in terms of the prediction of transient behavior; however it can be used for safety analysis since the predicted peak values are always higher than the experimental data. For detailed cases, RELAP5 may be used to obtain more accurate results.

Based on the benchmark analysis results, the MULCH code could be used for the LEU core conversion analysis. In the future, sensitivity study for decay power should be performed. The point kinetics model in MULCH should also be improved. It can be expected that MULCH will predict better results for loss of primary flow transient if the step reactivity insertion is replaced ramp reactivity insertion.

Table 4-3 Comparison of ASV and NCV flow rate

Time (sec)	ASV flow rate (kg/s)		NCV flow rate (kg/s)	
	MULCH	RELAP5	MULCH	RELAP5
0.0	0.00	0.00	0.00	0.00
4.0	0.00	0.00	0.00	0.00
4.5	-0.11	-0.47	1.16	0.69
5.0	-0.35	-1.72	1.89	1.93
5.5	-0.53	-1.96	1.74	1.90
6.0	-0.76	-2.34	1.53	1.73
6.5	-0.96	-2.20	1.32	1.56
7.0	-1.10	-2.15	1.11	1.42
7.5	-1.19	-2.01	0.92	1.29
8.0	-1.25	-1.92	0.75	1.18
9.0	-1.30	-2.07	0.57	0.96
10.0	-1.31	-2.30	0.56	0.75
15.0	-1.35	-1.59	0.24	-0.03
20.0	-1.36	-1.43	-0.11	-0.41
25.0	-1.37	-1.40	-0.27	-0.48
30.0	-1.37	-1.40	-0.29	-0.51

Table 4-4 Comparison of core flow rate

Time (sec)	Core flow rate (kg/s)	
	MULCH	RELAP5
0.0	115.1	115.2
1.0	63.2	56.9
1.5	46.5	41.7
2.0	34.2	30.6
2.5	25.2	22.5
3.0	18.6	16.7
3.5	13.6	12.3
4.0	9.96	9.04
4.5	5.80	5.63
5.0	3.46	3.62
6.0	1.74	2.60
7.0	1.08	2.10
8.0	0.77	1.82
9.0	0.68	1.66
10.0	0.69	1.56
15.0	1.02	1.69
20.0	1.35	1.89
25.0	1.51	1.91
30.0	1.52	1.91

Table 4-5 Decay heat fission product group constants in MULCH-II code

Group (i)	β_{Di}	λ_{Di} (s^{-1})
1	0.097	1.280
2	0.220	0.152
3	0.237	1.93E-2
4	0.187	1.88E-3
5	0.132	1.43E-4
6	0.072	1.25E-4
7	0.055	2.20E-7

Table 4-6 Comparison of total power

Time (sec)	Total Power (kW)		
	MULCH	RELAP5 (ANS 1973)	RELAP5 (ANS 1979)
0.0	6000.0	6000.0	6000.0
1.0	6000.0	6000.0	6000.0
1.5	6000.0	2598.7	2585.7
2.0	6000.0	1160.4	1149.6
2.5	384.3	854.9	847.8
3.0	363.1	747.6	742.3
3.5	349.0	684.2	679.4
4.0	338.8	653.4	648.4
4.5	330.9	627.2	621.7
5.0	324.3	604.5	598.2
6.0	313.4	566.8	558.7
7.0	304.4	536.5	526.7
8.0	296.5	511.5	500.2
9.0	289.6	490.4	477.9
10.0	283.4	472.5	459.0
15.0	260.9	410.0	394.3
20.0	246.7	370.9	355.1
25.0	236.7	342.9	327.5
30.0	228.9	321.5	306.4
Total energy within 30 seconds (kJ)	21236.8	21533.8	21147.8

Table 4-7 Thermocouple Position in MITR-II Startup Test

T/C number	Position Element	Place
6	C-13	mixed outlet
7	C-15	mixed outlet
8	A-2	mixed outlet
9	B-6	mixed outlet
10	3Gu6	graphite plug
11	spider hole #3	bottom of core inlet
12	A-2	T/C on inside of the last place 4" from bottom, toward A-3
13	A-2	T/C on center plate of the element 0.1" from bottom, away from A-3
16		cadmium shutter

Table 4-8 Description of simulation cases

	Description
Case 1	Steady-steady power of 4.83 MWth for 18 hours.
Case 2	Steady-steady power of 4.0 MWth for11.5 hours
Case 3	Steady-steady power of 3.5 MWth for 6 hours and 37 minutes.

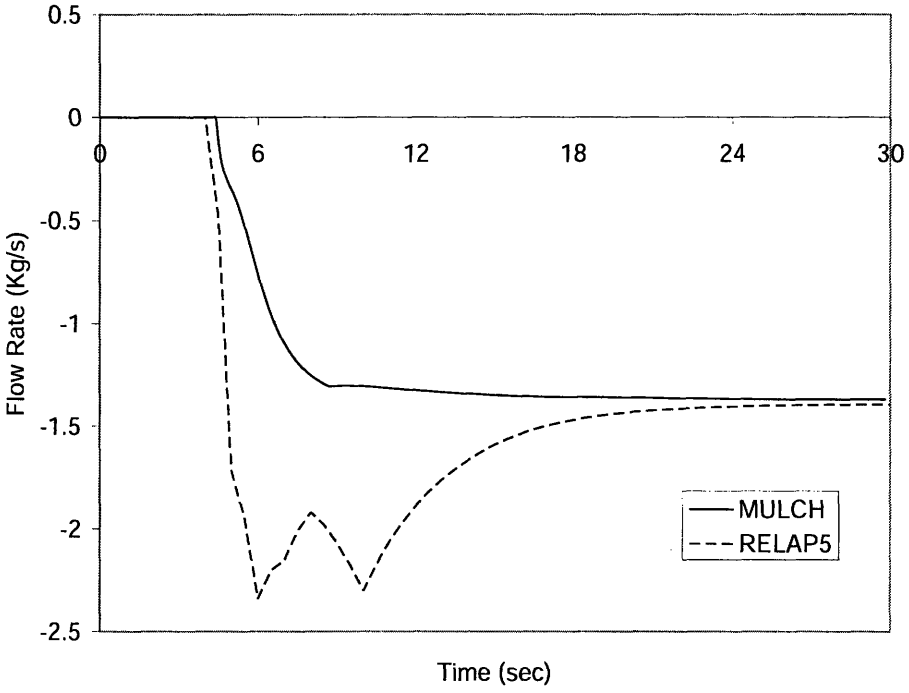

Figure 4-8 Comparison of ASV flow rate

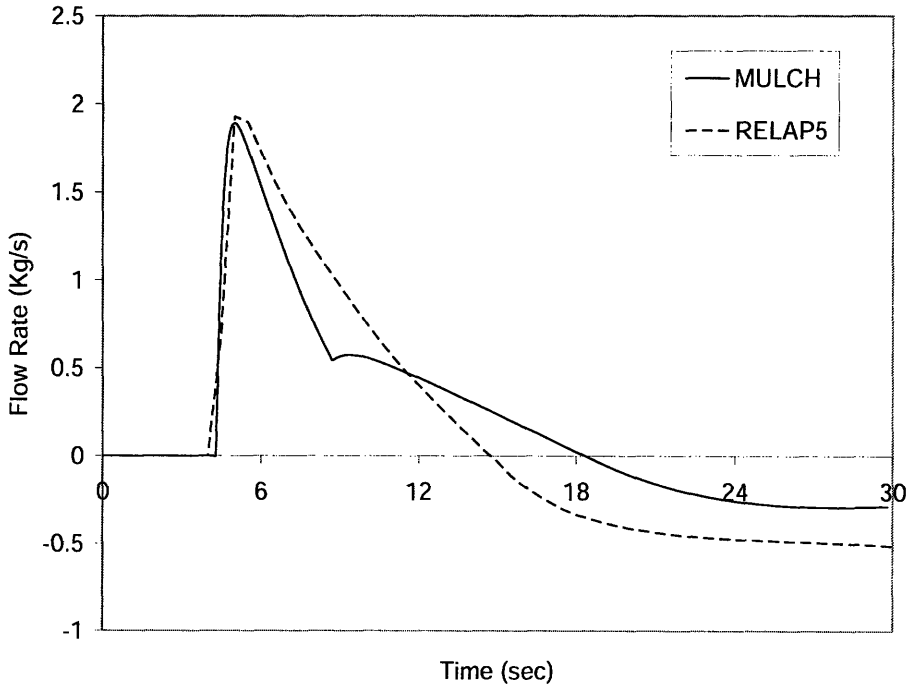

Figure 4-9 Comparison of NCV flow rate

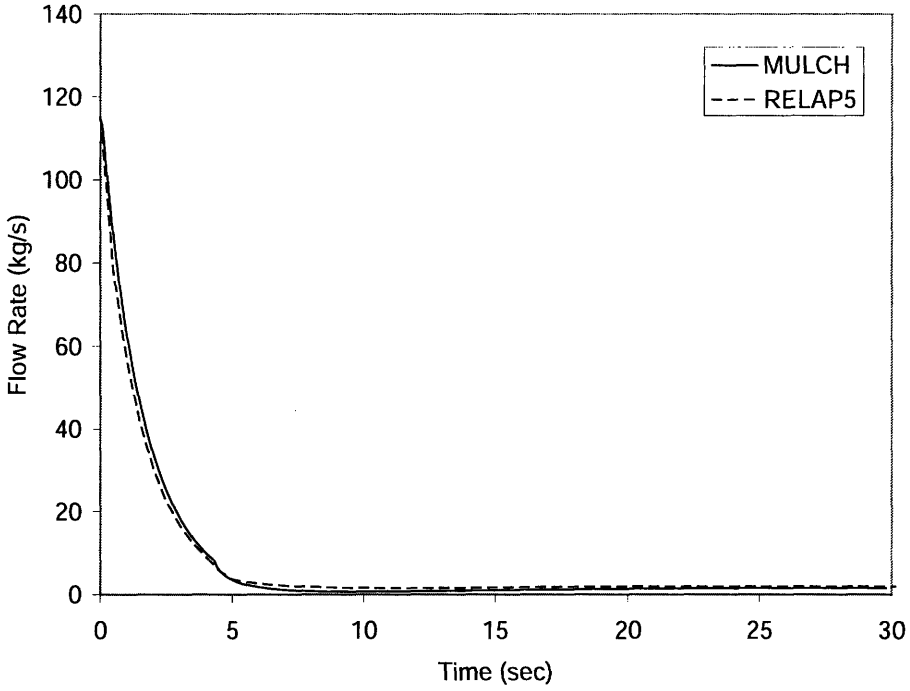

Figure 4-10 Comparison of core flow rate

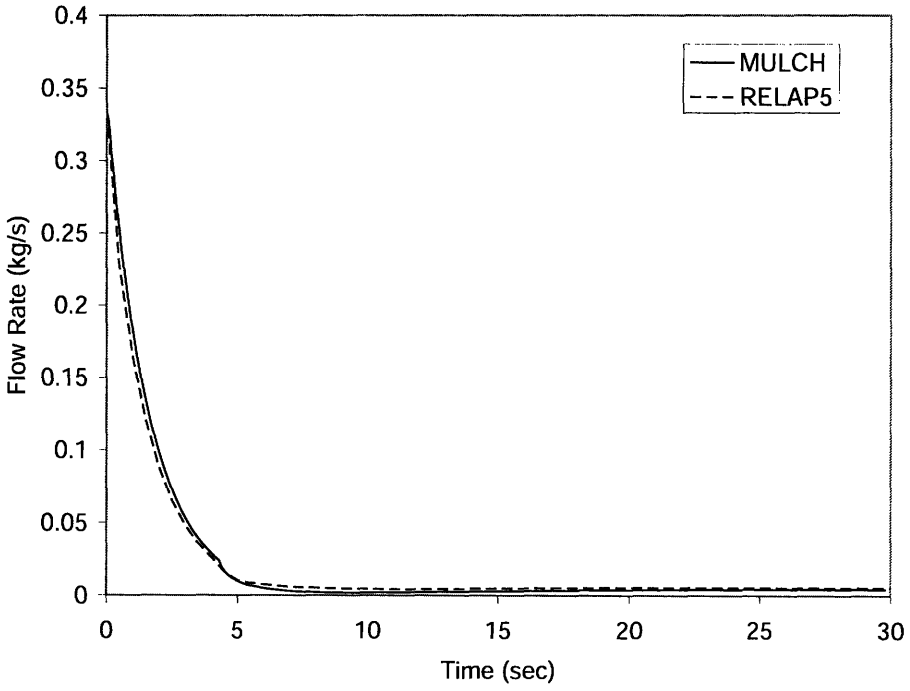

Figure 4-11 Comparison of flow rate in average channel

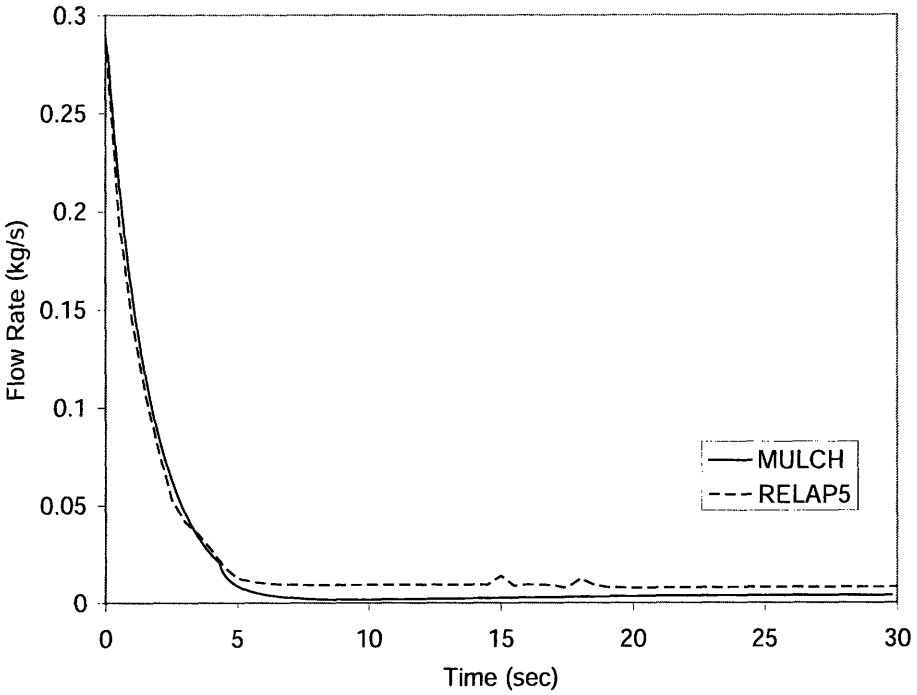

Figure 4-12 Comparison of flow rate in hot channel

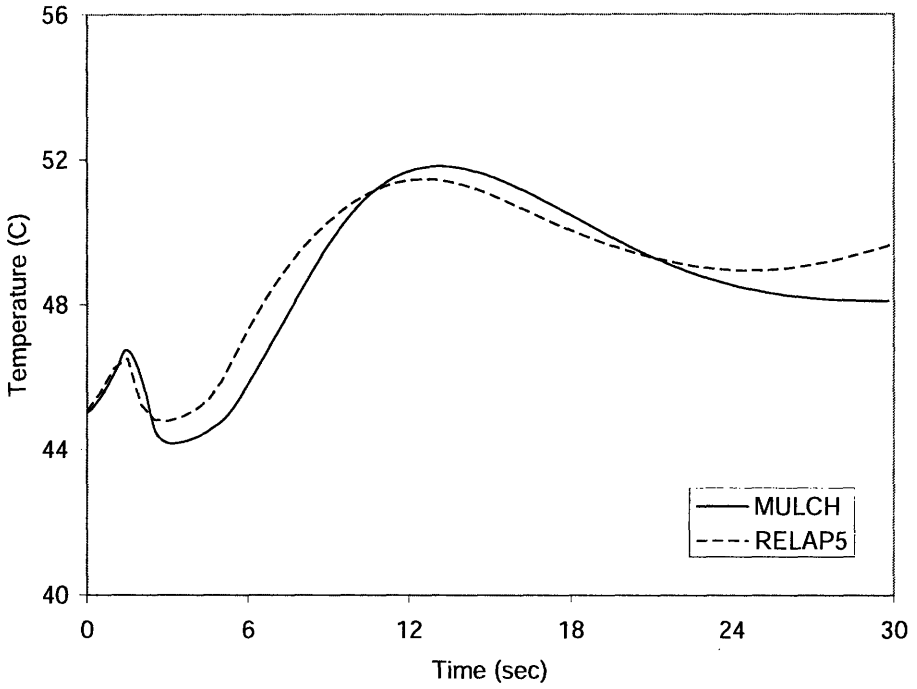

Figure 4-13 Comparison of coolant temperature (Avg. channel, node#1)

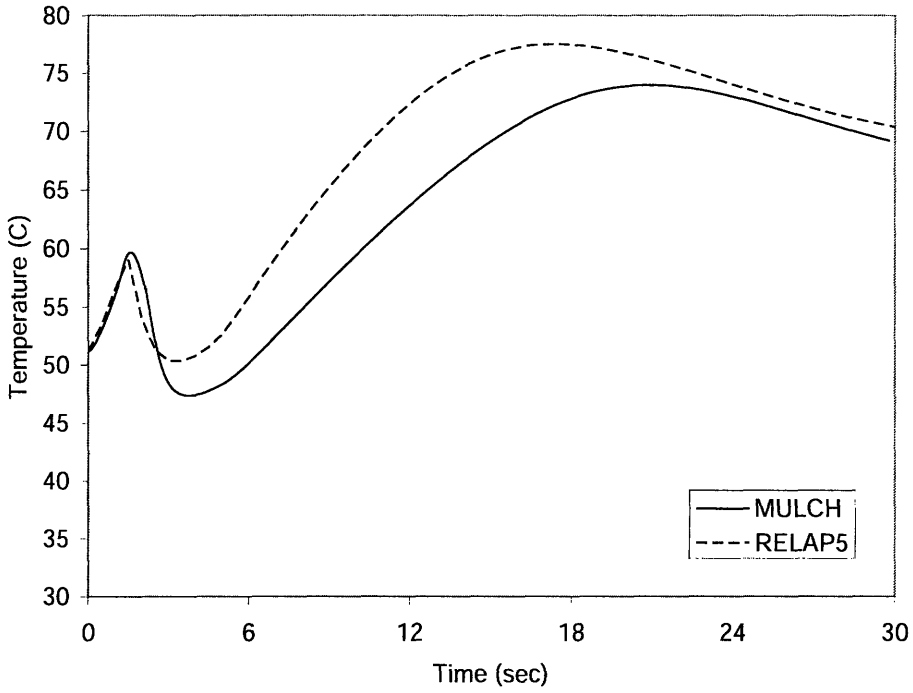

Figure 4-14 Comparison of coolant temperature (Avg. channel, node#5)

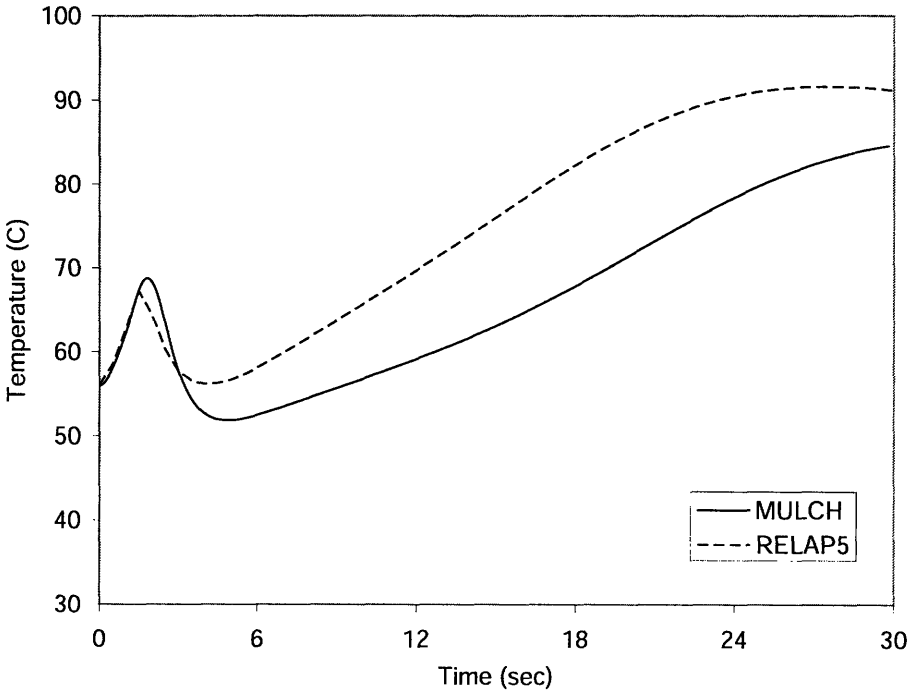

Figure 4-15 Comparison of coolant temperature (Avg. channel, node#10)

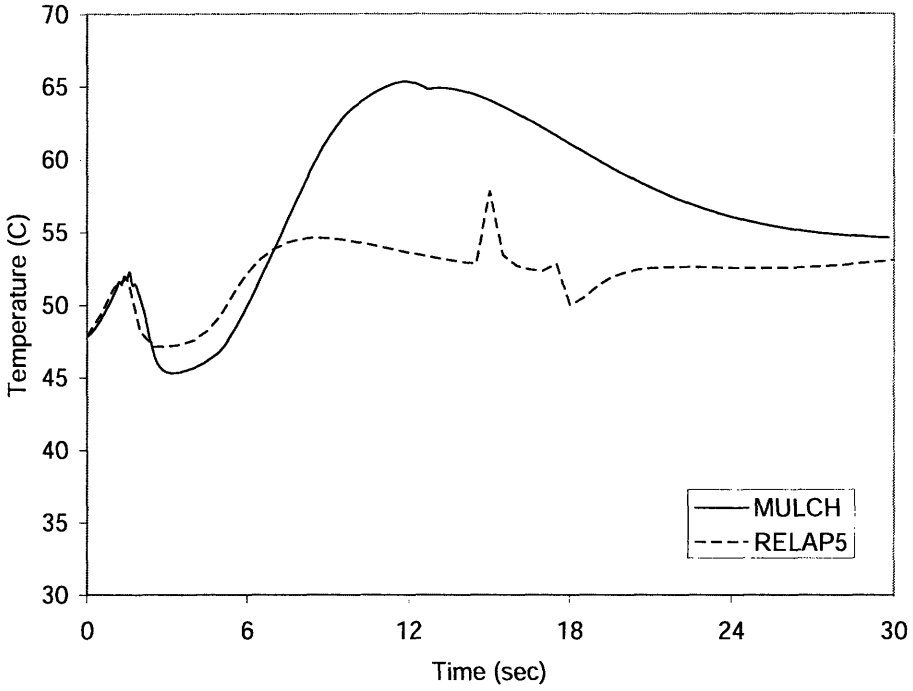

Figure 4-16 Comparison of coolant temperature (Hot channel, node#1)

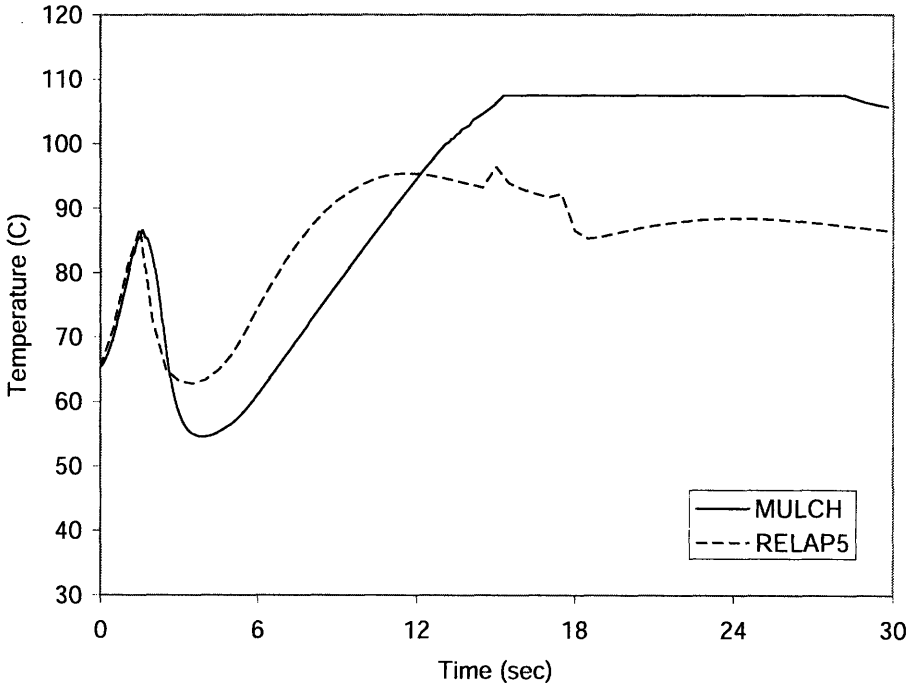

Figure 4-17 Comparison of coolant temperature (Hot channel, node#5)

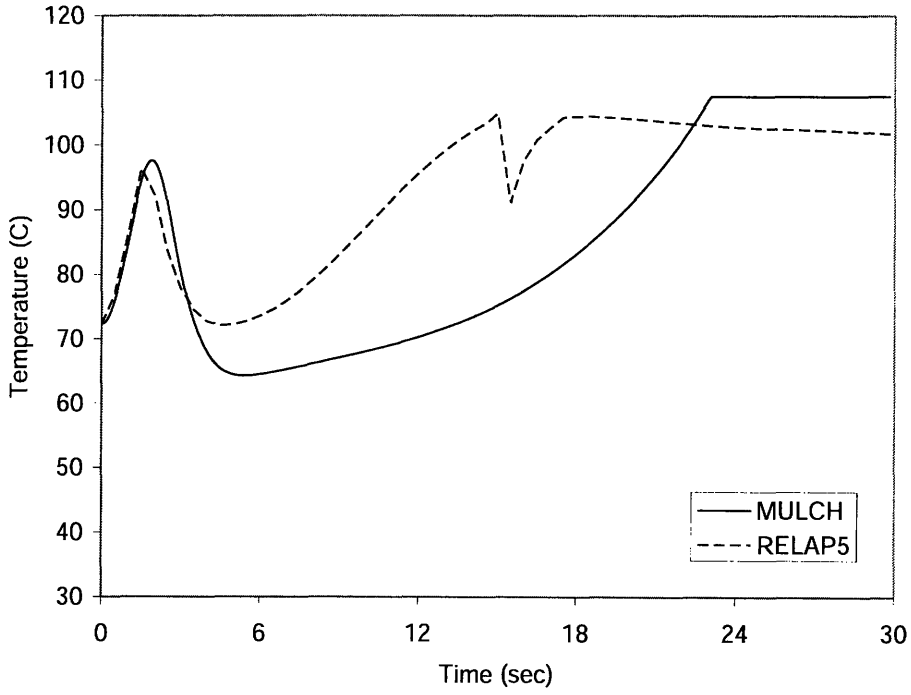

Figure 4-18 Comparison of coolant temperature (Hot channel, node#10)

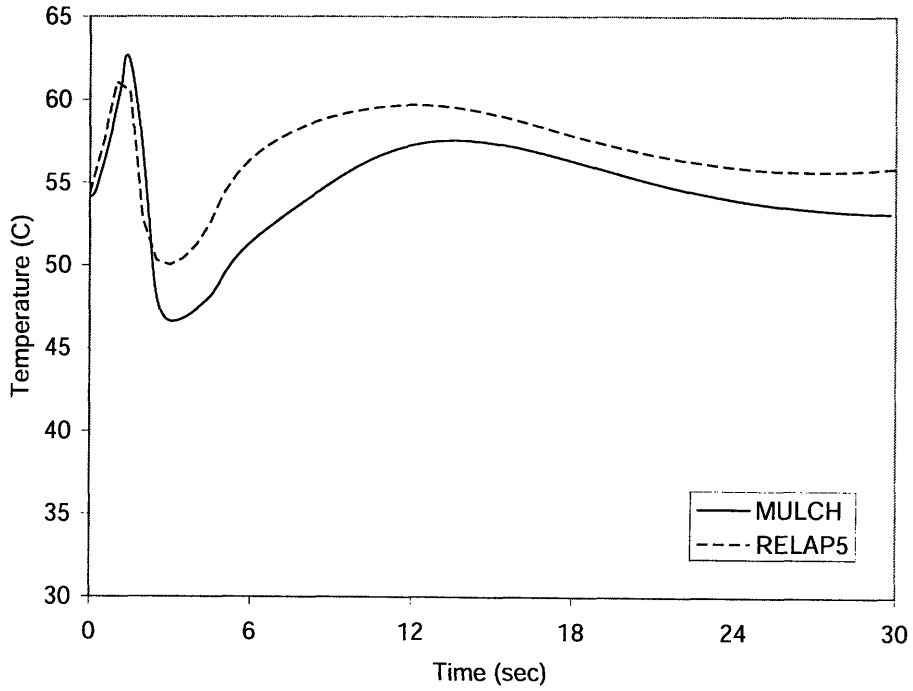

Figure 4-19 Comparison of cladding temperature (Avg. channel, node#1)

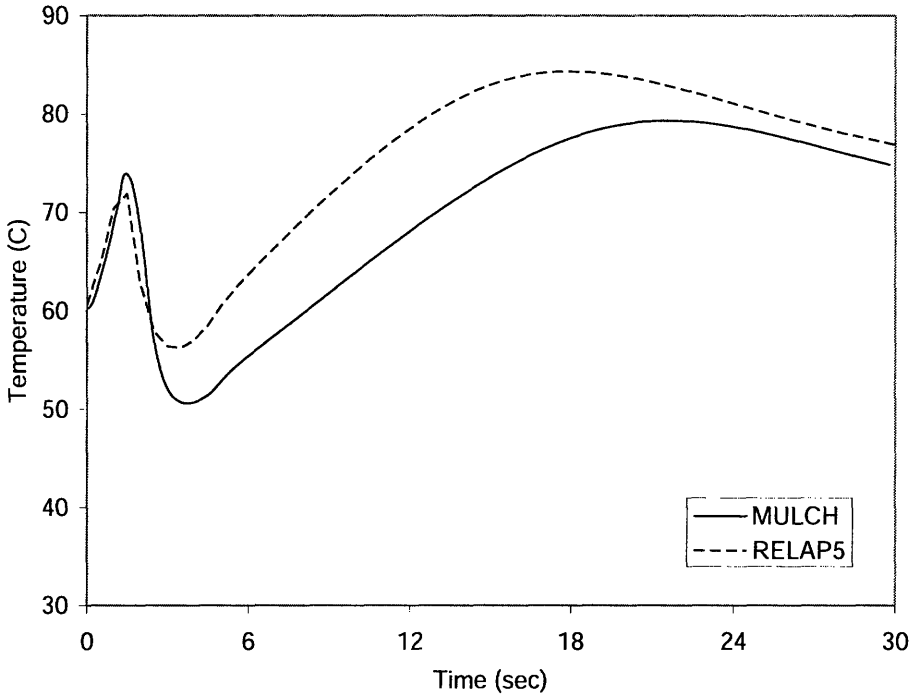

Figure 4-20 Comparison of cladding temperature (Avg. channel, node#5)

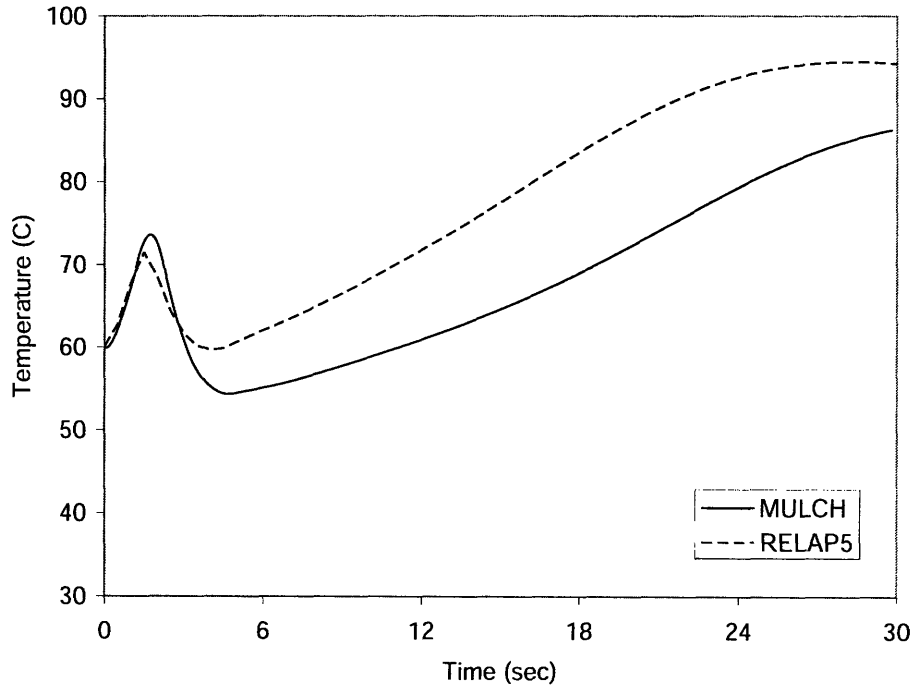

Figure 4-21 Comparison of cladding temperature (Avg. channel, node#10)

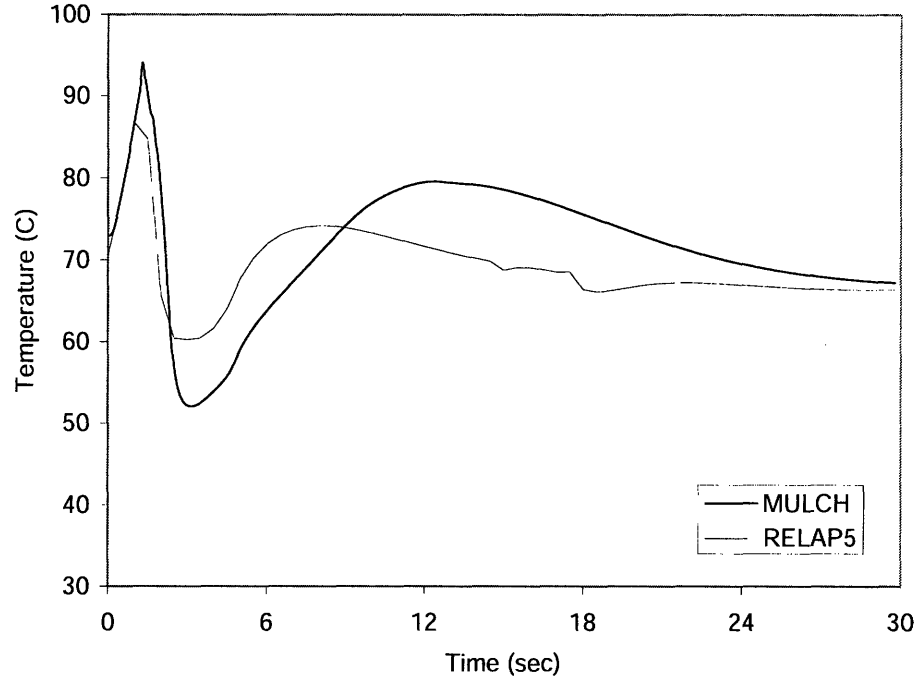

Figure 4-22 Comparison of cladding temperature (Hot channel, node#1)

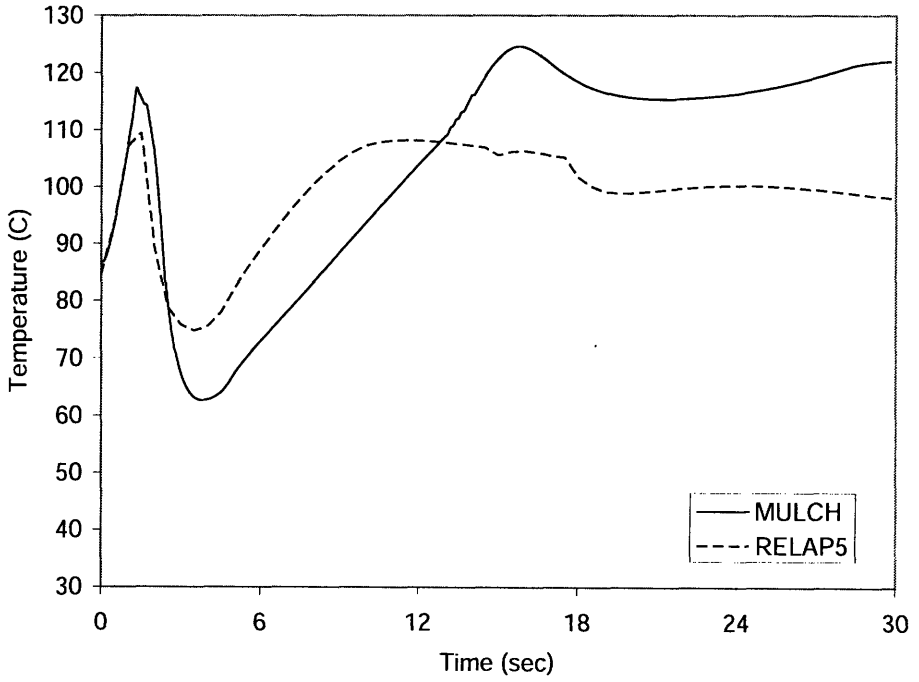

Figure 4-23 Comparison of cladding temperature (Hot channel, node#5)

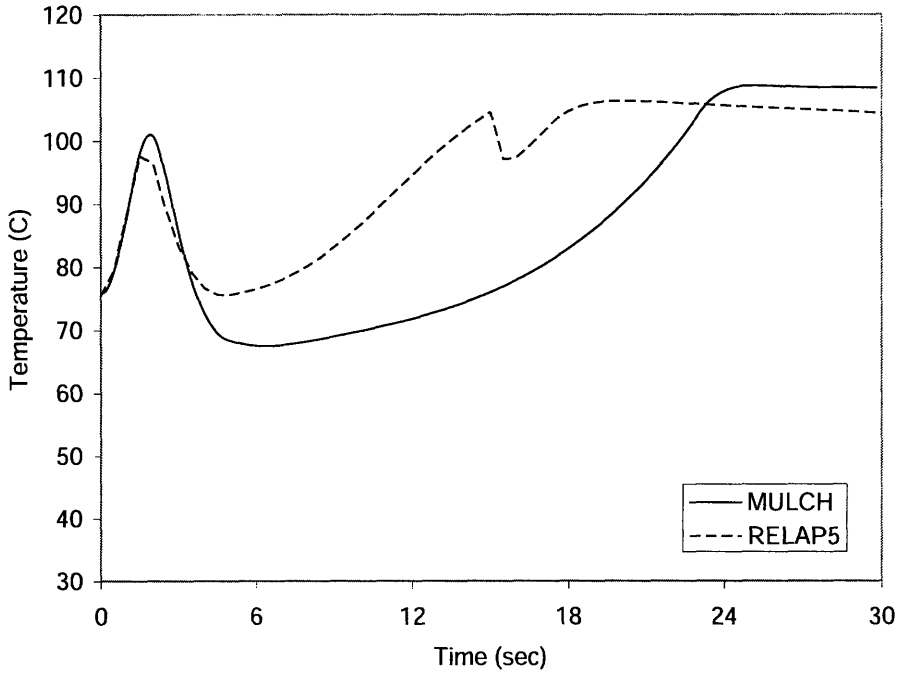

Figure 4-24 Comparison of cladding temperature (Hot channel, node#10)

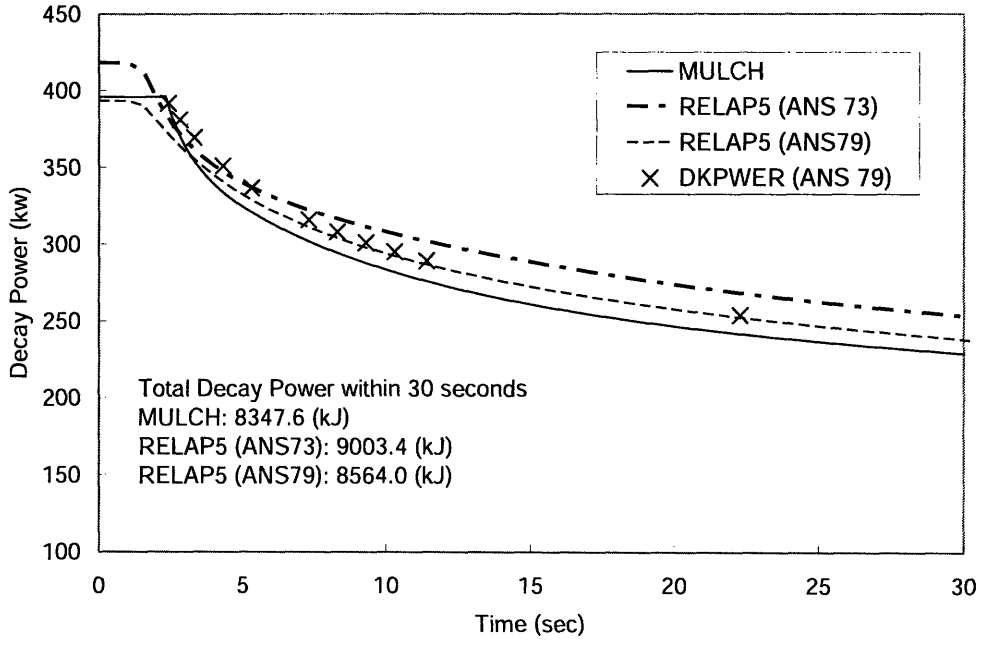

Figure 4-25 Comparison of decay power

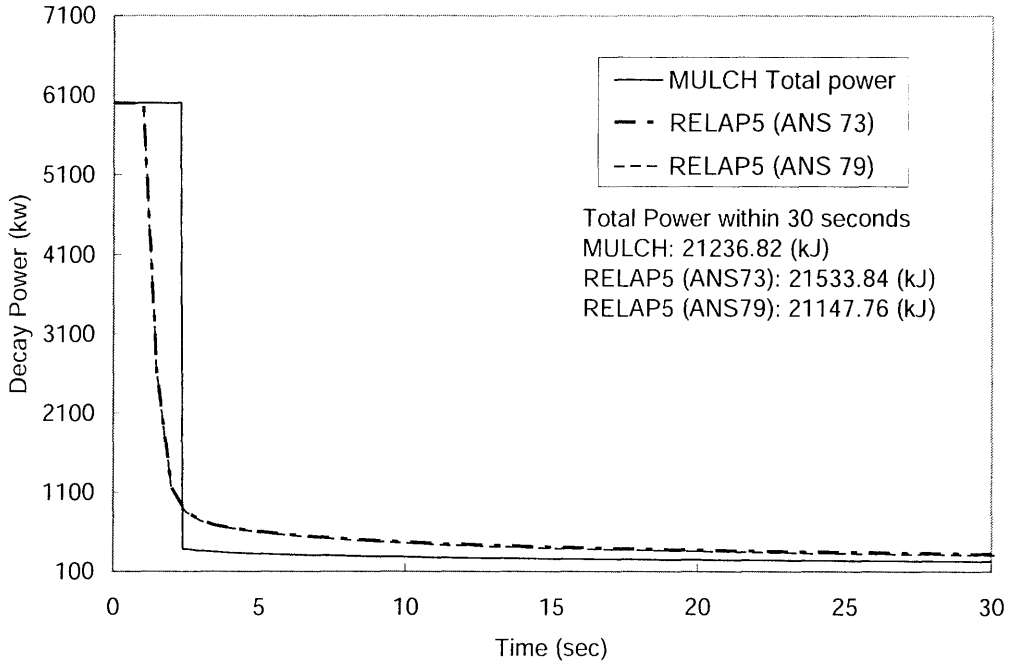

Figure 4-26 Comparison of total power

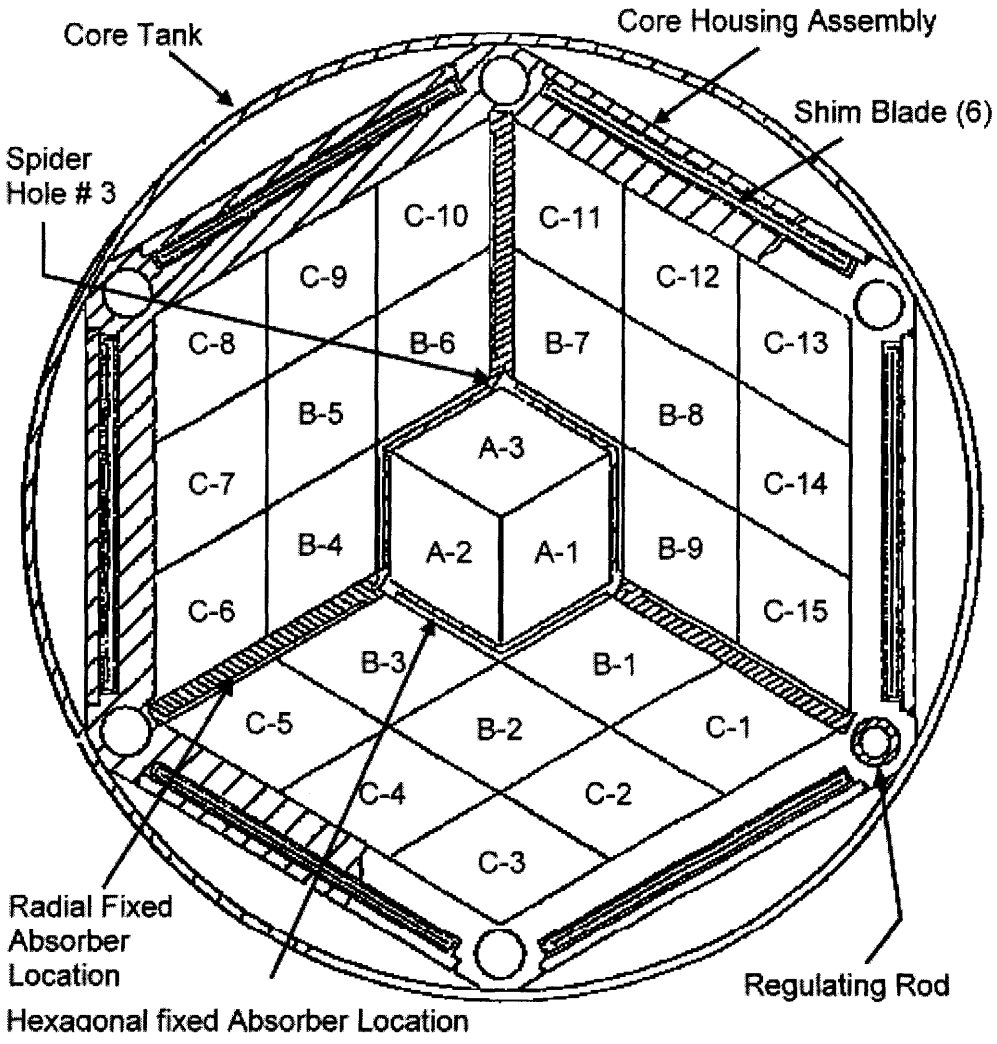

Figure 4-27 Core Section of MITR-II

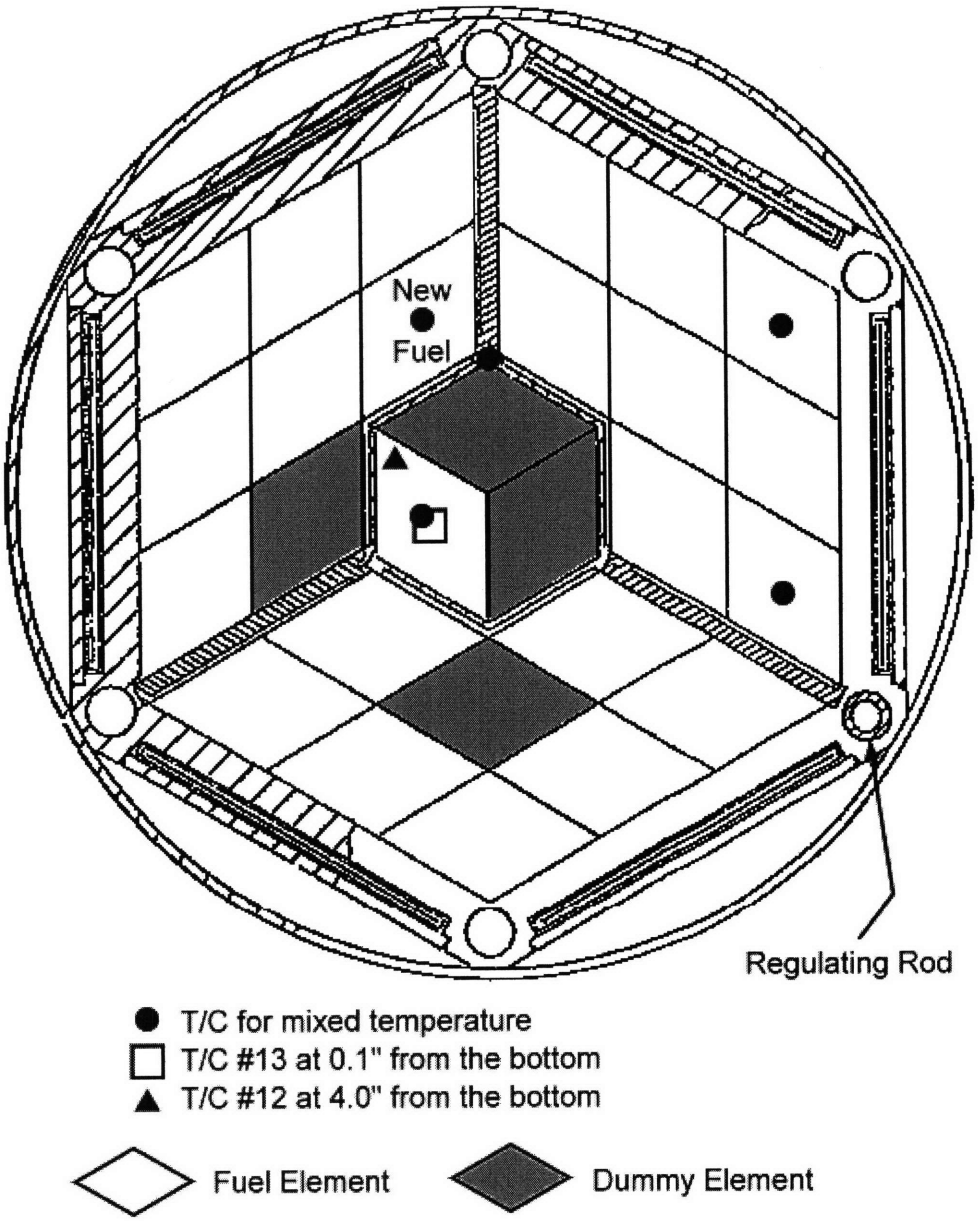

Figure 4-28 Incore Thermocouple Position

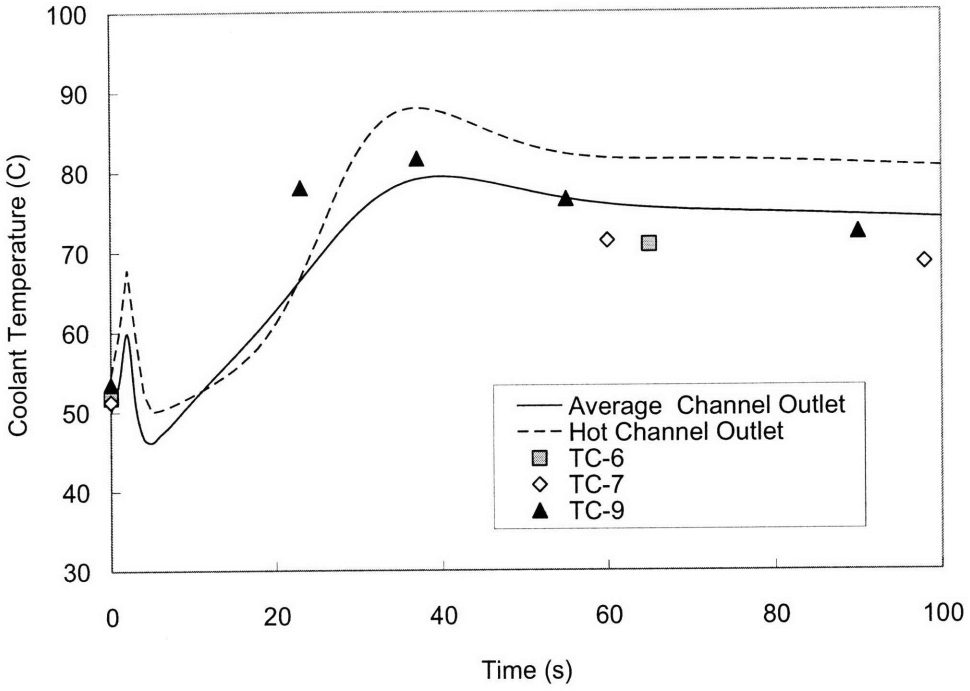

Figure 4-29a Comparison of MULCH and measurement (Case 1, 4.83MW/18 hours)

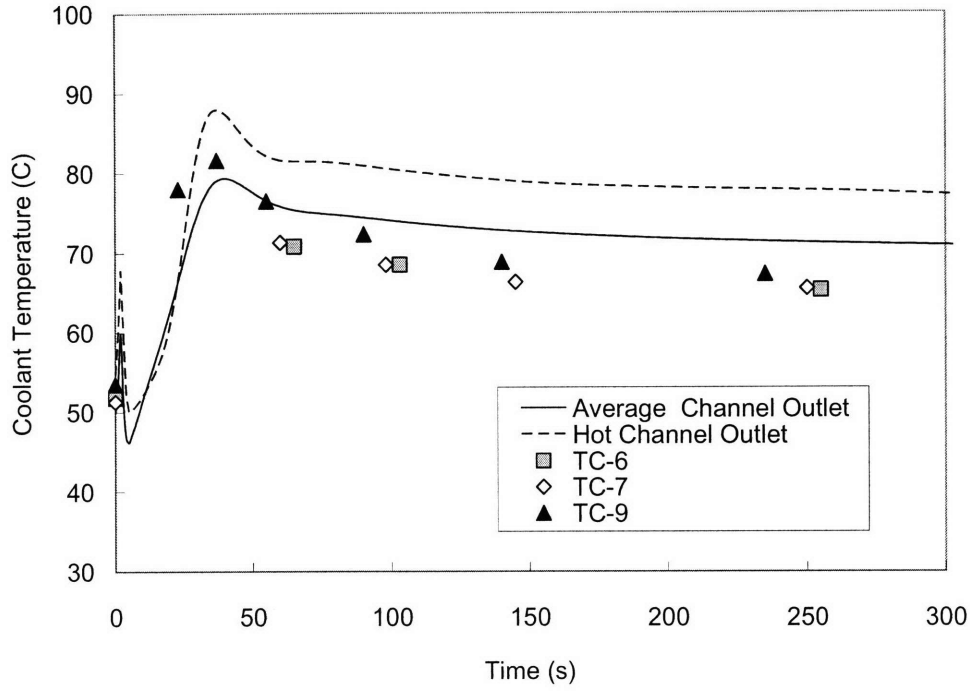

Figure 4-29b Comparison of MULCH and measurement (Case 1, 4.83MW/18 hours)

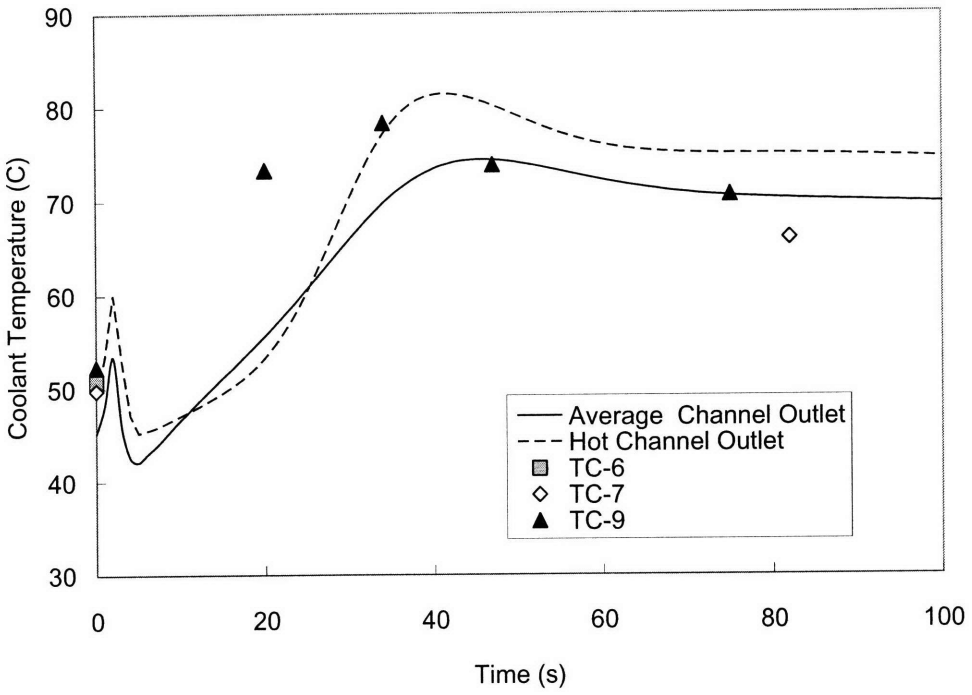

Figure 4-30 Comparison of MULCH and measurement (Case 2, 4.0MW/11.5 hours)

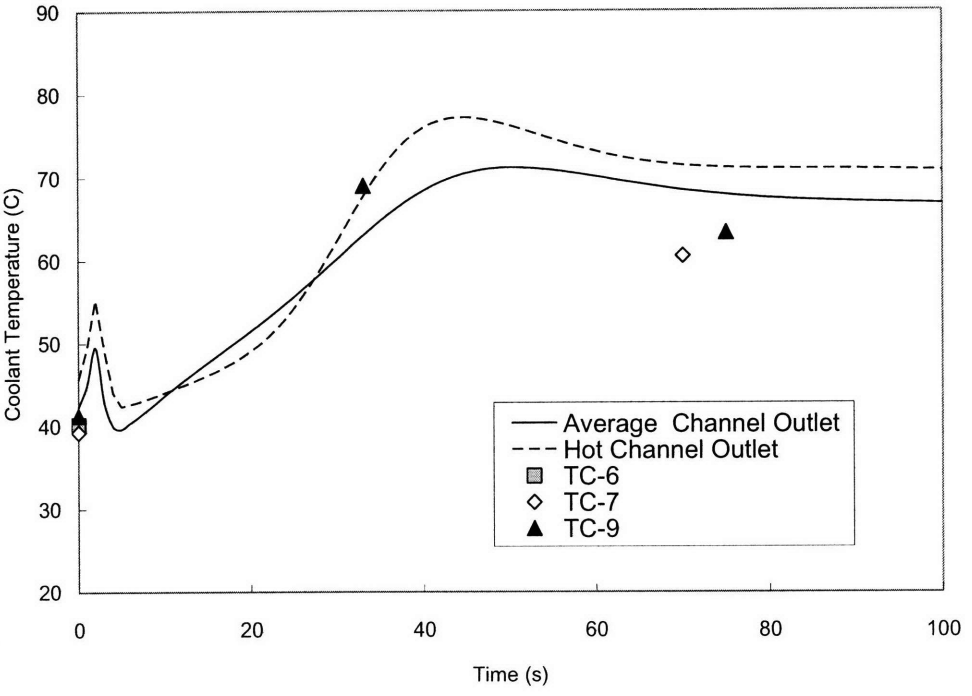

Figure 4-31 Comparison of MULCH and measurement (Case 3, 3.5MW/6.6 hours)

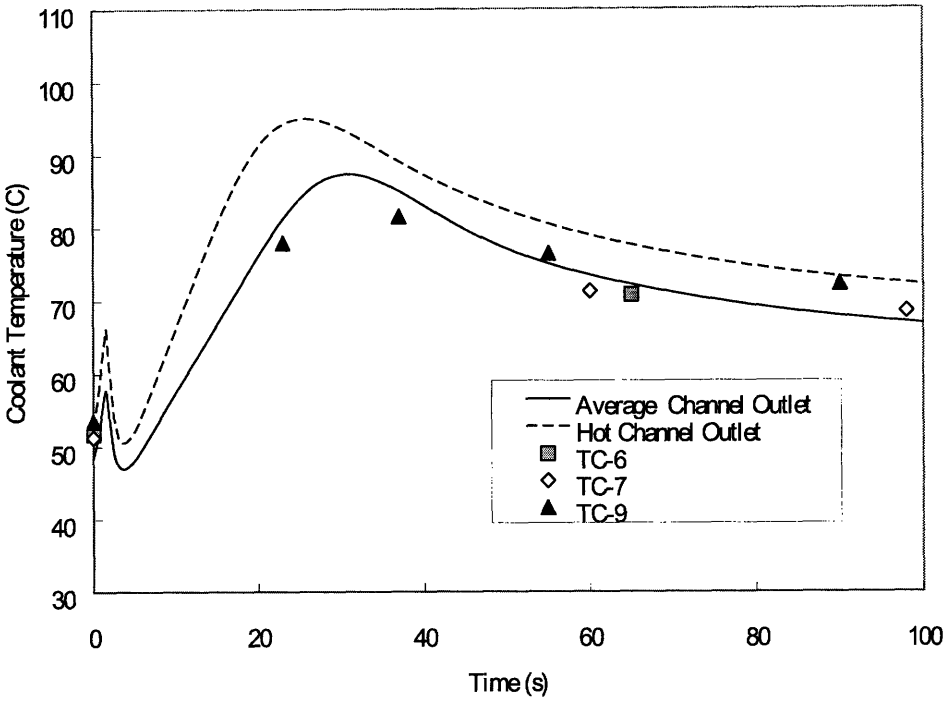

Figure 4-32a Comparison of RELAP5 and measurement (Case 1, 4.83MW/18 hours)

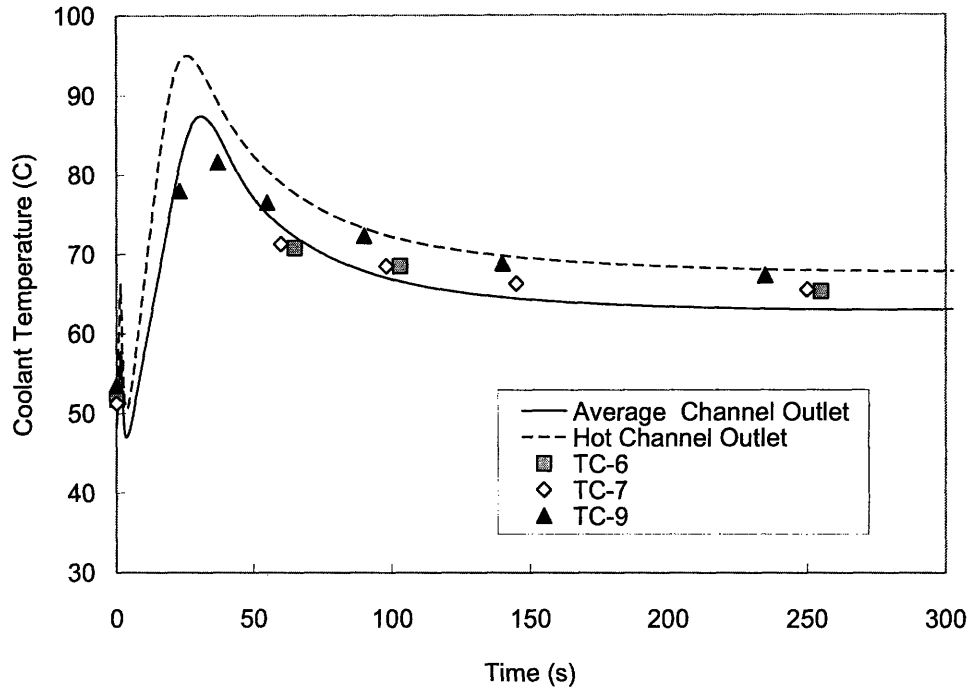

Figure 4-32b Comparison of RELAP5 and measurement (Case 1, 4.83MW/18 hours)

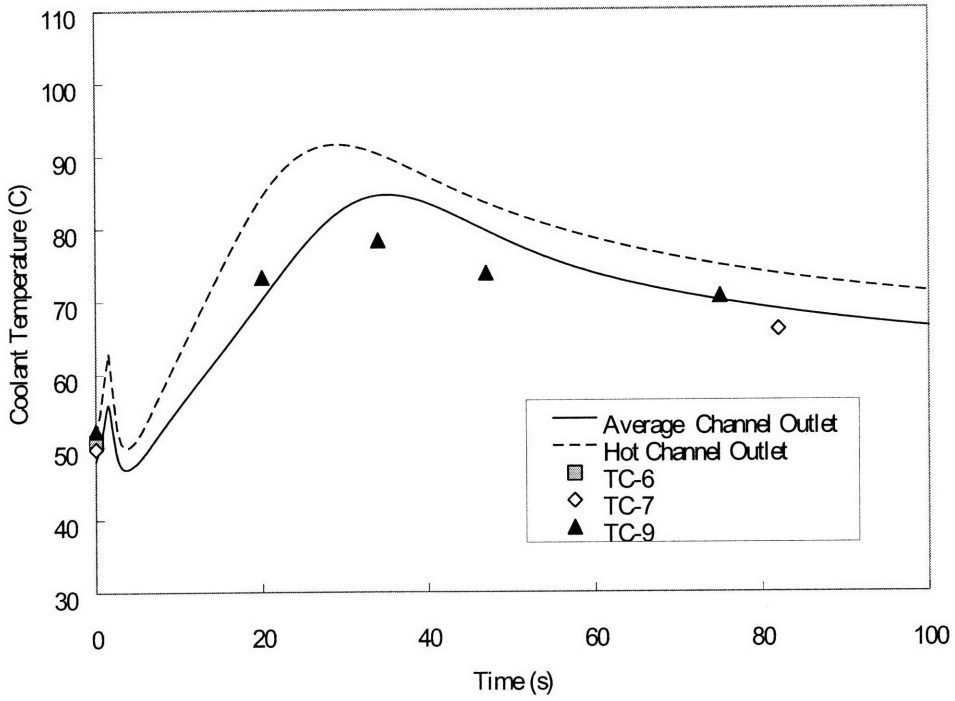

Figure 4-33 Comparison of RELAP5 and measurement (Case 2, 4.0MW/11.5 hours)

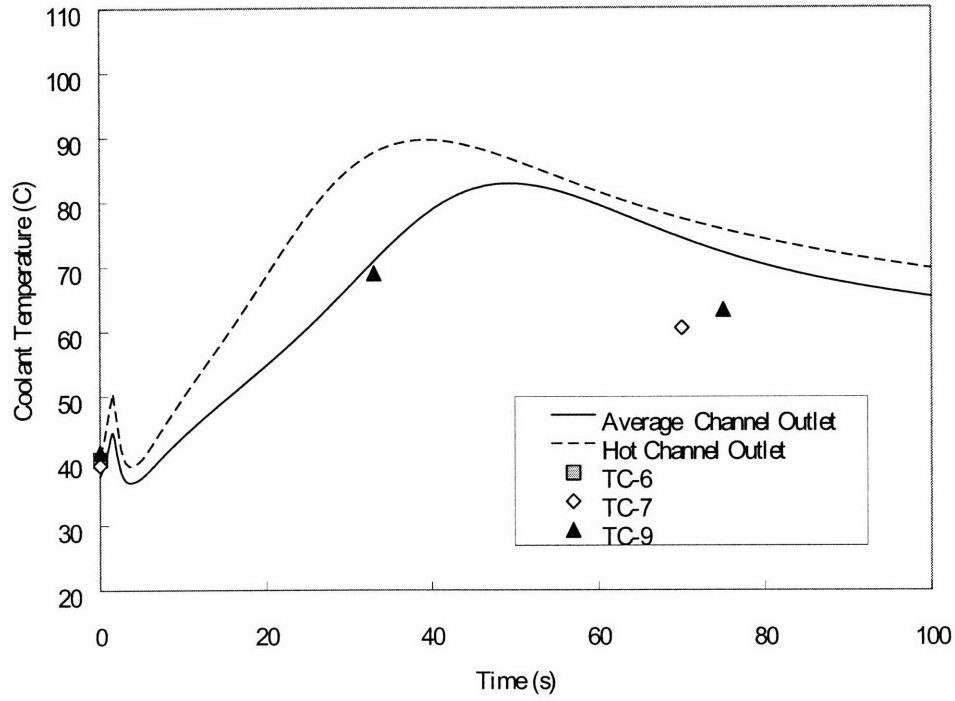

Figure 4-34 Comparison of RELAP5 and measurement (Case 3, 3.5MW/6.6 hours)

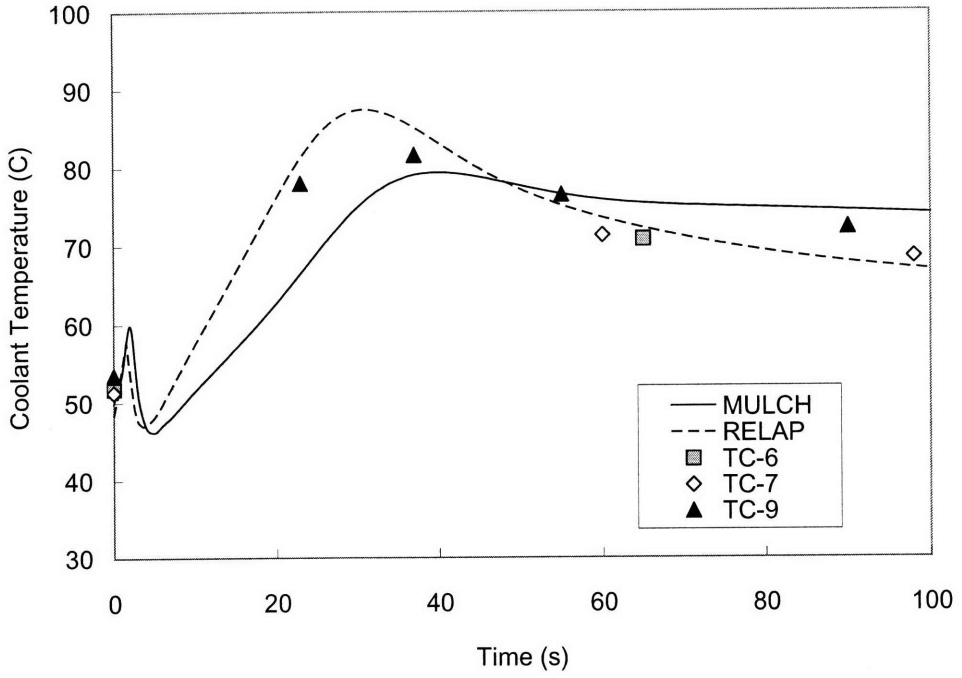

Figure 4-35 Comparison of average channel results with measurement (Case 1)

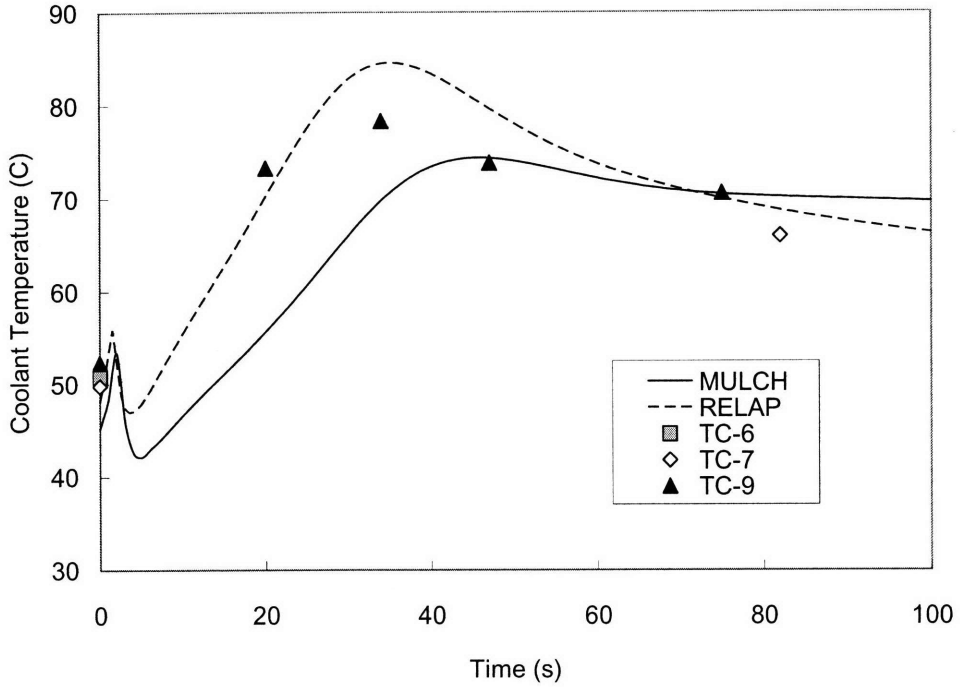

Figure 4-36 Comparison of average channel results with measurement (Case 2)

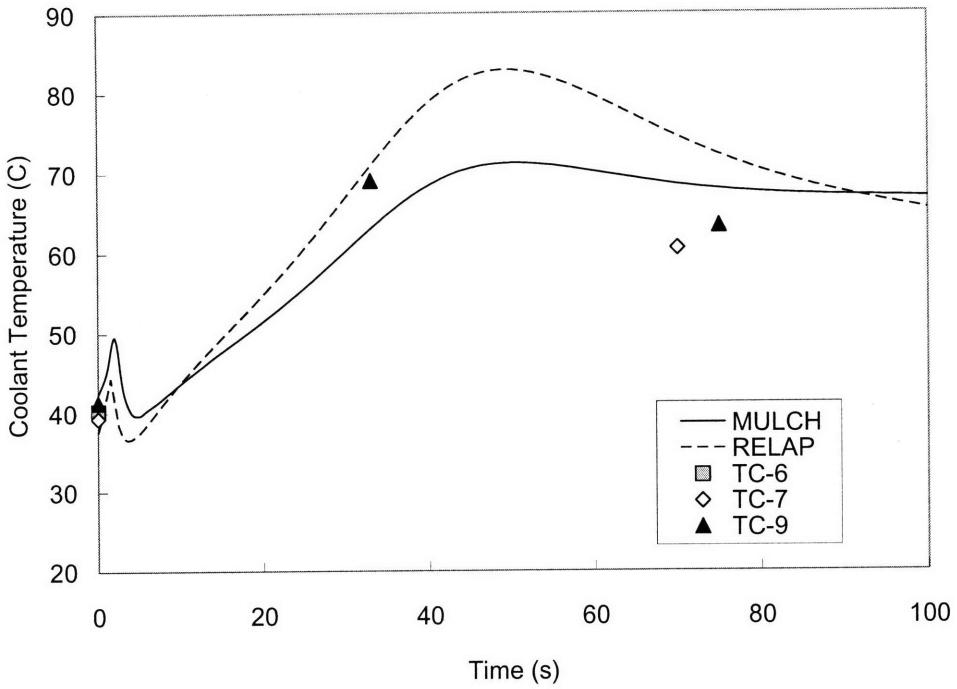

Figure 4-37 Comparison of average channel results with measurement (Case 3)

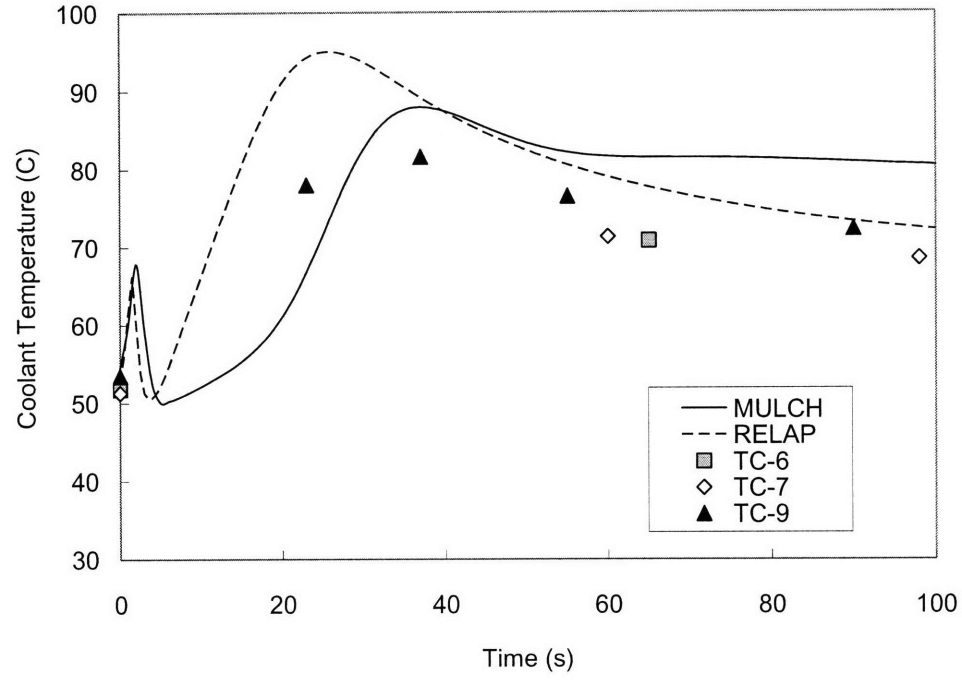

Figure 4-38 Comparison of hot channel results with measurement (Case 1)

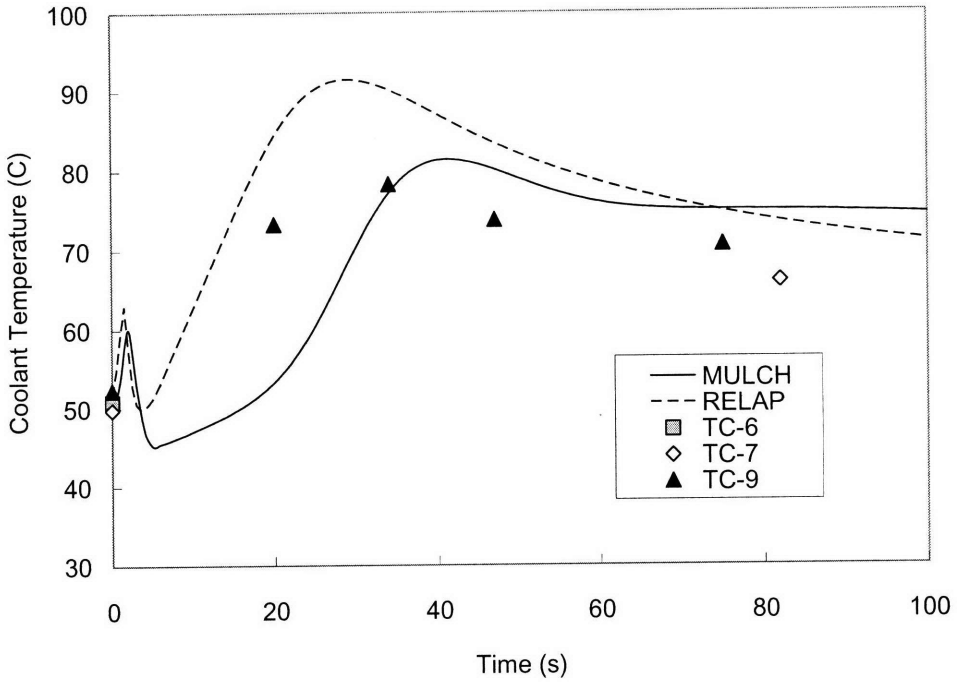

Figure 4-39 Comparison of hot channel results with measurement (Case 2)

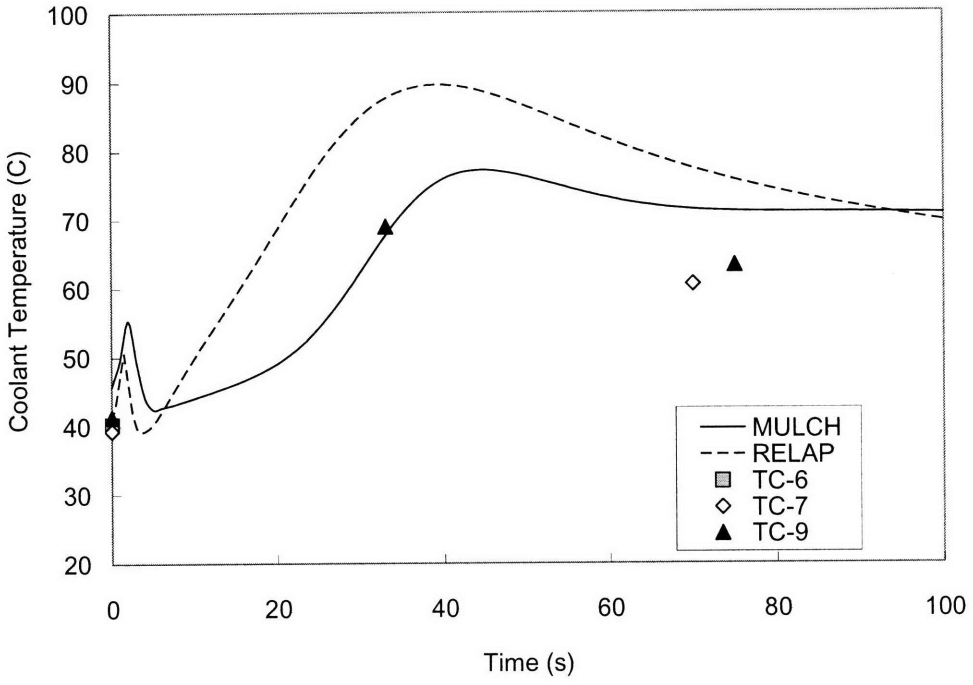

Figure 4-40 Comparison of hot channel results with measurement (Case 3)

Chapter 5
Thermal-hydraulic Analysis for the LEU Core

5.1. Introduction

This chapter consists of two parts. First, thermal-hydraulic performances of HEU and LEU cores are compared. The LEU core design proposed by Newton in his PhD thesis is chosen for this basic comparison. Second, analyses are performed for optimization of the LEU core design. Thermal hydraulic limits and loss of primary flow transient are studied for a number of LEU core configurations. Natural convection analysis for the MITR is also included in this chapter.

The objective of the optimization analyses is to evaluate the LEU fuel/core design options that would meet the thermal-hydraulic criteria for both steady-state operation and loss-of-flow transient. These criteria are the Limiting Safety System Settings (ONB) and core tank pressure loading limit for steady-state, and maximum cladding temperature for loss of primary flow transient.

5.2. Comparison of HEU and LEU thermal-hydraulic performance

The reference LEU core design was proposed by Thomas H. Newton in 2006 as part of his PhD thesis [22]. Table 5-1 lists the core design parameters of the HEU and LEU cores. The dimension of fins is the same for HEU and LEU. There are 110 fins on each side of a fuel plate. Figure 5-1 illustrates the MITR fuel plate cross section. Coolant flow area and the equivalent diameter are calculated based on the "plate to plate distance" and "water gap". The "plate to plate distance" varies with different core configurations. The "water gap" is calculated on a "half fin" basis.

Table 5-2 summarizes the HEU and LEU axial power profiles. Neutron fluxes in the average and hot channels are different and are calculated separately. The HEU core axial power profiles were previously calculated and documented in MITR-III Safety Analysis Report (MITR-III SAR) [23]. The LEU core axial power profiles were calculated by Newton using the MCNP code [21]. Figure 5-2 and 5-3 show the power distributions. A normalized power shape factor is given for each node. The sum of these shape factors is ten. Figure 5-4 and 5-5 show the average channel and hot channel local axial peaking factors. The local axial peaking factor represents the peak value of heat generation within the specific node. In these figures, node 1 represents the bottom and node 10 represents the top the core. It should be noted that both HEU and LEU have higher power peaking at the bottom. This is due to the presence of the D_2O reflector and shim blades. The hot channel is conservatively chosen as one that has the highest radial and axial peaking factors, and the lowest flow disparity. Although this is

rarely the case, however, this approach simplifies the analysis of multiple coolant channels that may potentially result in the highest clad temperature. Because during a fuel cycle the power peaking factors would vary, it is essential that detailed neutronic analysis be performed to provide the licensing basis that encompasses a wide range of refueling and in-core experiment configuration scenarios.

5.2.1 Transient scenario and assumptions

A loss of primary flow (LOF) accident is studied using the MULCH code. The initiating event is assumed to be a pump coast down accident in which both primary pumps are de-energized. Initial conditions are such that the reactor operates at 6 MW with a primary flow rate of 2000 gpm before the accident occurs. The assumed delay time is 2.3 seconds (one second for signal transmission and 1.3 seconds for shim blade insertion. Two different axial power profiles are utilized for the purpose of sensitivity study. In the first case, "LEU#1a" uses the same neutron distribution and local axial peaking factors as the current HEU core. In the second case, "LEU#1b" utilizes Newton proposed LEU axial power profile which is evaluated using the MCNP code. Both LEU#1a and LEU#1b are given a hot channel factor of 1.76 based on the previous calculation [22].

5.2.2 Simulation results

The core flow rate is shown in Fig. 5-6. Table 5-3 summarizes the change of core flow rate through the accident. At the beginning of the transient, HEU and LEU almost have the same core flow rate. After ASV and NCV open (at 4.4 second), the core flow rate of HEU becomes higher than LEU. Once the natural convection flow is established, the core flow rate would be steady and equal to the sum of ASV and NCV flow rates. The steady-state core flow rate after 30 seconds into the transient for HEU, LEU#1a and LEU#1b are 1.52 (kg/s), 1.43 (kg/s) and 1.39 (kg/s) respectively. The natural convection flow rate is lower for the LEU core because the LEU design has thinner flow channels than the HEU core and therefore higher pressure drop through the core region. The higher pressure drop thus results in a lower core flow rate.

Figure 5-7 and 5-8 show the flow rates through ASVs and NCVs. It can be seen that the HEU core has both higher ASV flow rate and NCV flow rate because of the lower pressure drop. The steady state ASV and NCV flow rates are summarized in Table 5-4.

Figure 5-9 and 5-10 show the comparison of exit coolant temperature in the average channel and the hot channel. It should be noted that in the hot channel, LEU has a lower peaking at the beginning of the transient. Overall, the two figures show that LEU has higher coolant temperature in the average channel but lower coolant temperature in the hot channel. The steady state exit coolant temperature in hot channel is at saturation temperature of 107.46 °C, which indicates the occurrence of nucleate boiling for both HEU and LEU cores. However, a critical heat flux will not occur although there is bulk boiling at the outlet of the flow channel

[23].

Figure 5-11 compares the cladding temperature on the hottest axial node (node#5). For the cladding temperature in the average channel, at the beginning HEU has a higher peak than LEU does. Then LEU#1a increases in a faster way and finally surpasses those of HEU and LEU#1b. HEU has a prediction between LEU#1a and LEU#1b which means that within a certain range, LEU has an average channel cladding temperature close to the HEU core. Figure 5-12 shows that LEU has a lower temperature at the hot spot (hot channel plus hottest node), due to the lower heat flux than the HEU case. Table 5-4 summarizes the maximum temperature in the hot and average channels.

Based on this basic comparison, it is concluded that the LEU fuel is promising and has potential to improve reactor thermal-hydraulic performance.

5.3 Analyses for optimization of the LEU core design

There are many variables involved in designing the LEU core. For the neutronic aspect, the axial peaking factor, radial peaking factor, usage of full or half elements and so on are key factors that should be examined to improve the power distribution and fuel management. For the thermal-hydraulic aspect, number of plates per element, water gap thickness, number of fins, and the dimension of fins will have great impacts on thermal-hydraulic performance, such as pressure drop through the core, natural convection flow rate and so on. In order to optimize the LEU core design, it is essential to consider all these variables. However, it will be very time-consuming and will make the design process very complicated to evaluate the impact for each variable. Certain dimensional changes are not practical and/or increase uncertainty of the design. Therefore, in the following analyses, only three variables are chosen for the design optimization work, these are: radial peaking factor, fuel meat thickness and number of plates per element. Impacts of these three variables on the LEU thermal-hydraulic performance are discussed below.

5.3.1 Steady state analyses for the LEU Core design options

The Limited Safety System Settings (LSSS) and constraints for the core tank design pressure limit are the criteria chosen for the steady state thermal-hydraulic analyses.

5.3.1.1 Calculation of the Limited Safety System Settings

The LSSS are established to allow a sufficient margin between normal operating conditions and the safety limits. Onset of nucleate boiling (ONB) is chosen as the criterion for the LSSS derivation. Determination of LSSS takes into account design uncertainties, i.e., engineering hot channel factors. The reactor is assumed to operate with a coolant height of 10 ft. and a primary flow rate of 1800 gpm, which are the current LSSS in the MITR-III SAR. Operation

within the LSSS envelope ensures that boiling will not occur anywhere in the fueled region. Table 5-5 lists the scram set points and LSSS of the existing HEU core (rated power 6 MW). The difference between scram set points and LSSS provides additional safety margin which prevents the MITR from exceeding LSSS during normal operation and credible transients.

Table 5-6 lists the proposed LEU core configurations. Two sets of LEU core options are evaluated. The first set adopts a fuel thickness of 0.762 mm (LEU#a-series). The second set adopts a thinner fuel thickness of 0.508 mm (LEU#b-series). For each set, the number of fuel plates per elements varies from 15 to 20 by changing the water gap dimension. Clad thickness, fin dimension, axial peaking factors and other parameters are fixed. Three values (1.6, 1.76 and 2.0) are proposed for the hot channel factors (radial peaking factor). 2.0 is considered as a conservative one which is the same as the HEU hot channel factor assumed for licensing. 1.6 and 1.76 are proposed because these two values were estimated by MCNP for the fresh LEU cores.

The LSSS power is calculated by the MULCH code. The conditions are set that the coolant outlet temperature, coolant height and the primary flow rate are in accordance with the LSSS listed in Table 5-5. Then the LSSS power is calculated to represent the minimum power where the ONB will take place during the steady state operation. The engineering hot channel factors have great impacts on the LSSS power. Table 5-7 lists the engineering hot channel factors applied in the MITR-III [4]. These engineering hot channel factors are used in all MULCH calculations in this study and are assumed to be the same for the HEU and LEU core.

The LEU LSSS power results are summarized in Table 5-8, Fig. 5-13 and Fig. 5-14. It can be observed that using more plates or thicker fuel plates will enhance the LSSS power. It is expected because given the primary mass flow rate (1800 gpm), using more plates would reduce the heat flux per plate. In addition, using more and thicker fuel plates would both narrow the coolant channel as well as increase the coolant velocity. Therefore, heat transfer will increase as the coolant velocity increases. Besides, Fig. 5-13 and Fig. 5-14 also show that a slight change in the hot channel factor has great impacts on the LSSS power.

In this thesis, the rated power of MITR is assumed to be 6 MW after the conversion. It is recommended that the LEU core design should have the LSSS power equal or larger than the existing HEU LSSS power. For the existing HEU core (MITR-III), the LSSS power of 7.4 MW is calculated [4]. At this design stage, assuming a rated power of 6 MW, a fixed LSSS power of 7.4 MW is chosen as a criterion for the LEU core design options. It should be noted that the LEU core may operate at a power slightly greater than 6 MW to meet the neutron flux demand, if the LSSS power is calculated higher than 7.4 MW.

5.3.1.2 Calculation of the core tank pressure loading

Another constraint to be considered for the LEU core design is the core tank design pressure.

The core tank was constructed and installed during the MITR-II upgrade in the early 1970's. The design pressure is 24 psig according to the MITR-II Reactor Systems Manual. The pressure loading on the core tank is the sum of the gravity pressure head, equivalent to 3.8 m of light water, and the friction pressure drop through the reactor core.

Calculations were performed to estimate the total pressure loading for both LEU core design series (LEU#a-series and LEU#b-series). The primary coolant flow rate is assumed to be 2200 gpm, which is the maximum allowable flow rate and would result in the largest pressure loading. Table 5-9 lists the results of the calculated total pressure loading for the core tank. The total pressure loadings are calculated for an average coolant temperature of 10 °C and 40 °C for each fuel element design. Note that 10 °C is the set point of low secondary temperature. It is used as a conservative estimate of the primary coolant temperature since the pressure loading increases at low temperature due to higher viscosity and density.

Because the condition of the core tank cannot be readily determined and measurements of actual pressure loading have not been made, it is recommended that the LEU core design be limited to equal or below the current pressure loading of the HEU core. Hence, as shown in Fig. 5-15, the possible design options are LEU#a1, #a2, #b1, #b2, #b3, and #b4. More specifically, the fuel element should not have more than 18 plates, given the chosen fuel thicknesses.

5.3.1.3 Steady state operation qualified LEU core design options

Based on the previous analyses, it is found that a smaller coolant channel is desirable for the LSSS power but would increase the core tank pressure loading. The LEU core design should compromise between these two issues. One way is to use more plates with thinner fuel meat. The existing HEU fuel meat has a thickness of 0.762 mm. The possibility of using a thinner fuel meat has been estimated and concluded as preferable for the conversion task [21]. Therefore, the following analyses will focus on the LEU#b-series (fuel meat thickness = 0.508 mm). Figure 5-16 shows the qualified LEU core options based on the LSSS power and results of pressure loading limitation. These qualified LEU core options are LEU#b1, #b2, #b3 and #b4 with a hot channel factor of 1.6 and LEU#b3 and #b4 with a hot channel factor of 1.76. No design option with a hot channel factor equal to 2.0 is qualified at this stage. The six qualified design options that are identified by red circles in Fig. 5-16 will be analyzed in the next section for the thermal-hydraulic performance through the loss-of-flow transient.

5.3.2 Loss-of-flow analyses for the LEU Core design options

The six LEU core design options identified in fig. 5-16 are analyzed using RELAP5 in this section. The purpose of this loss-of-flow analysis is to understand their respective thermal-hydraulic performance during the LOF transient, especially for the maximum cladding temperature and flow instability phenomenon. The transient scenario and assumptions are the same as those described in section 4.4 (refer to Table 4.2). However, the

initial conditions are different from the previous LOF simulations. The LSSS are chosen as initial settings for the simulated cases. Namely, the reactor is 7.4 MW and the bulk coolant outlet temperature is deliberately set to 60°C by changing the coolant inlet temperature. Coolant height is 4 inches below overflow and the primary flow rate is 112.5 kg/s (1800 gpm). The existing HEU core configuration with 22 fuel elements is also analyzed for comparison, which is the case designated as MITR-III in Fig. 5-16.

Figure 5-17 and 5-18 show the laminar (natural convection flow) and turbulent (forced convection flow) pressure drop through the core, respectively. It can be observed that within 18 plates per element, the LEU core would have less pressure drop than HEU core does. It happens for both laminar and turbulent flow and is consistent with the previous analytical results (refer to Fig. 5-15). Table 5-10 lists the RELAP results of pressure loss through core region and natural convection flow rate.

Figure 5-19 and 5-20 are the coolant outlet temperature and clad outlet temperature in the average channel, respectively. The results show that using more plates per element would have lower steady state temperature; however, it also gives higher peak temperature during the transient. The reasons are as follows: Assuming the primary flow rate is fixed (1800 gpm for all cases), using more plates per element results in the narrower coolant channel and increases steady state core flow rate, therefore improves heat transfer. On the other hand, during natural circulation the core flow rate is basically dependent on the initial driving force and pressure loss. Since the reactor power before shut down is also fixed (7.4 MW), the driving force can be assumed the same for all cases. The narrower coolant channel leads to higher friction loss hence decreases the core flow rate and heat transfer. Besides, neither ONB nor flow instability is found in the average channel.

Figure 5-21 is the coolant outlet temperature in the hot channel. It can be observed in this figure that HEU has a significant temperature oscillation at the beginning of the transient. This temperature oscillation lasts around 35 seconds and then the temperature variation decays gradually with time. Except for a slight oscillation in LEU#b4, other LEU cases have no obvious temperature oscillation. Their temperatures mostly follow the same trend as the average channel.

Figure 5-22 is the clad temperature in the hot channel. Node 5 is plotted because it is the hottest node within this channel. As shown in Fig. 5-22, HEU has a very high temperature peak (~ 156 °C) when the pump coast-down happens. About 2 seconds later the reactor scrams and then the temperature drops. Flow instability follows and causes a temperature oscillation. Still, LEU cases have no obvious temperature oscillation mainly because of the lower hot channel factor.

Figure 5-23 and 5-24 reveal the impacts of hot channel factor (HCF). In Fig. 5-23, a higher HCF does not give an obvious oscillation if 17 plates are used in the fuel element (LEU#b3). In case of LEU#b4 (Fig. 5-34), it adopts 18 plates per element, changing the HCF from 1.6 to

1.76 results in an obvious temperature oscillation. However, considering its frequency and magnitude this temperature oscillation can be seen as acceptable.

5.4 Conclusions

Two tasks are completed in this chapter. First, thermal-hydraulic performance of highly enriched uranium and low enriched uranium cores are compared. Second, analyses for LEU core optimization are performed. A number of LEU core configurations are analyzed to understand their thermal-hydraulic performance through LSSS power and loss of primary flow transient. Natural convection analysis for the MITR is also included in this chapter.

The comparison between the existing HEU core and the LEU core proposed by Newton [22] shows that the LEU fuel is promising and has the potential to improve reactor thermal-hydraulic performance.

Results of the steady state analyses for the LEU core show that a smaller coolant channel is desirable for the LSSS power but would increase the core tank pressure loading. The LEU core design should be chosen as a compromise between these two issues. Results of the LOF analyses show that HEU has a significant oscillation of coolant and clad temperature in the hot channel during the transient. No temperature oscillations were observed in the LEU cases. Therefore, it is concluded that the LEU#b-series design with 15~18 plates per element and HCF less than 1.76 are qualified based on the LOF transient. The HCF of 1.76 is lower than what used before in case of MITR-III (when it was assumed to be 2.0). However, it is still a higher factor than what was obtained in practice.

Table 5-1 Design parameters of the HEU and LEU cores

	HEU	LEU
Fuel material	UAlx	Monolithic U-7Mo
Number of total fuel plates	345	378
Fuel thickness (mm)	0.76	0.55
Aluminum cladding thickness (mm)	0.38	0.25
Number of fins per plate	220	220
Fin height (mm)	0.254	0.254
Fin Width (mm)	0.254	0.254
Coolant channel width (cm)	6.48	6.48
Plate to plate distance (mm)	4.013	3.353
Water gap (mm)	2.24	2.054
Flow area of coolant channel (m^2)	1.249 E-4	1.1383 E-4
De of coolant channel (m)	2.1864 E-3	1.996 E-3
Nuclear hot channel factor	2.0	1.76
Neutron flux distribution	See Table 5-2 and Fig.5-2 & 5-3	
Local axial peaking factor	See Table 5-2	

Table 5-2 Comparison of HEU and LEU axial power profiles

	Power distribution in AVERAGE channel (Shape)									
	Node #1	**Node #2**	**Node #3**	**Node #4**	**Node #5**	**Node #6**	**Node #7**	**Node #8**	**Node #9**	**Node #10**
HEU	1.166	1.143	1.257	1.299	1.23	1.061	0.917	0.767	0.61	0.55
LEU	0.998	1.049	1.125	1.222	1.199	1.14	1.028	0.912	0.707	0.62
	Local axial peaking factor for each node in AVERAGE channel (Peak)									
	Node #1	**Node #2**	**Node #3**	**Node #4**	**Node #5**	**Node #6**	**Node #7**	**Node #8**	**Node #9**	**Node #10**
HEU	1.622	1.059	1.026	1.009	1.048	0.976	1.074	1.083	1.106	1.589
LEU	1.08	1.078	1.09	1.075	1.021	1.054	1.101	1.156	1.261	1.193
	Power distribution in HOT channel (Shape)									
	Node #1	**Node #2**	**Node #3**	**Node #4**	**Node #5**	**Node #6**	**Node #7**	**Node #8**	**Node #9**	**Node #10**
HEU	1.462	1.503	1.568	1.631	1.407	0.87	0.571	0.407	0.339	0.241
LEU	1.537	1.626	1.735	1.66	1.146	0.7	0.537	0.446	0.341	0.271
	Local axial peaking factor for each node in HOT channel (Peak)									
	Node #1	**Node #2**	**Node #3**	**Node #4**	**Node #5**	**Node #6**	**Node #7**	**Node #8**	**Node #9**	**Node #10**
HEU	1.45	1.037	1.098	1.089	1.169	1.307	1.206	1.091	1.201	1.266
LEU	1.049	1.049	1.074	1.048	1.43	1.612	1.276	1.197	1.325	1.269

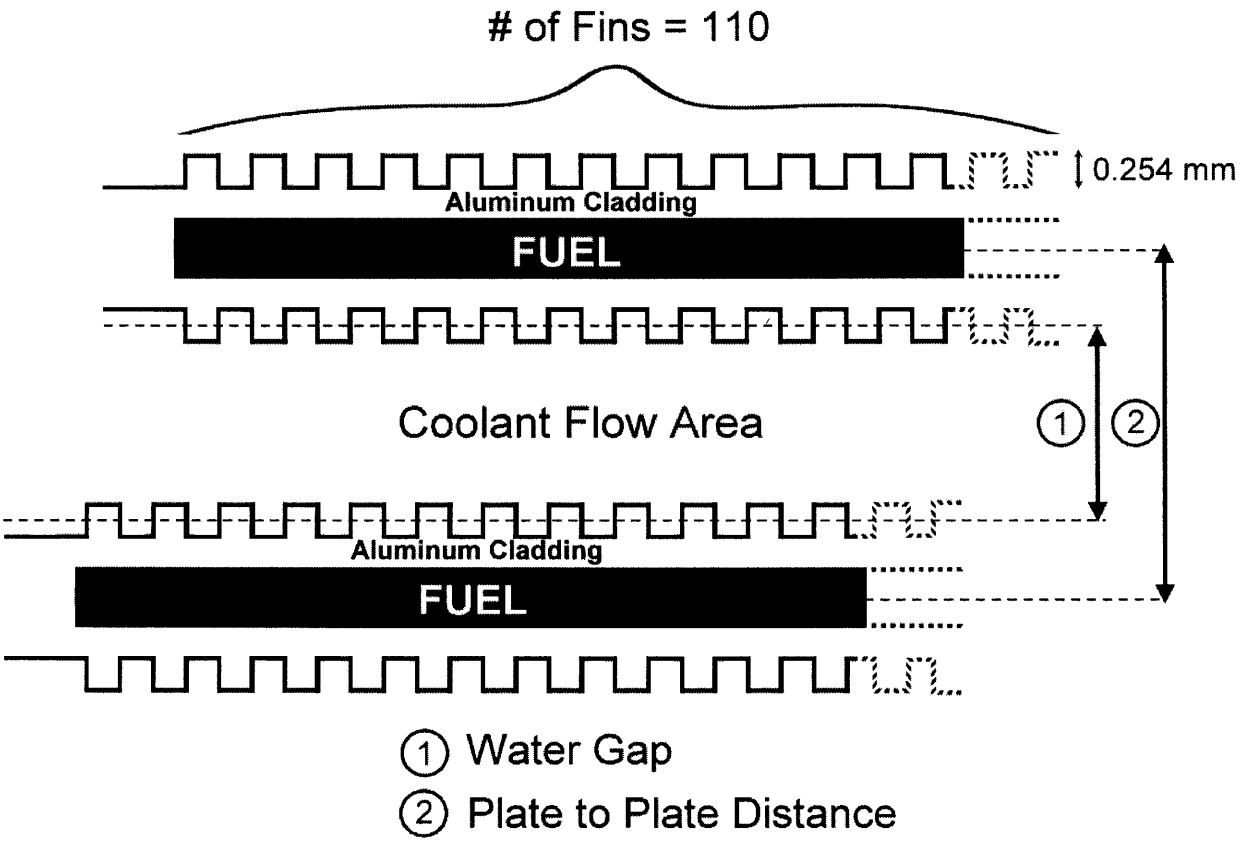

Figure. 5-1 MITR finned fuel plates

Table 5-3 Comparison of core flow rate

Time (sec)	Core flow rate (kg/s)		
	HEU	LEU#1a	LEU#1b
0.0	115.1	115.06	115.06
1.0	63.2	63.20	63.20
1.5	46.5	46.47	46.47
2.0	34.2	34.25	34.25
2.5	25.2	25.24	25.24
3.0	18.6	18.58	18.58
3.5	13.6	13.63	13.63
4.0	9.96	9.96	9.96
4.5	5.80	6.14	7.24
5.0	3.46	3.19	3.33
6.0	1.74	1.49	1.50
7.0	1.08	0.93	0.93
8.0	0.77	0.67	0.67
9.0	0.68	0.61	0.60
10.0	0.69	0.63	0.62
15.0	1.02	0.95	0.94
20.0	1.35	1.26	1.23
25.0	1.51	1.42	1.39
30.0	1.52	1.43	1.39

Table 5-4 Comparison of loss-of-flow results (HEU vs LEU)

	HEU	LEU#1a	LEU#1b
Steady state pressure drop (Pa)	50,081	54,583	54,634
Core flow rate (kg/s)*	1.524	1.431	1.392
ASV flow rate (kg/s)*	1.371	1.363	1.360
NCV flow rate (kg/s)*	0.285	0.192	0.152
Max coolant temperature in average channel (°C)	84.57	87.84	88.48
Max coolant temperature in hot channel (°C)	107.46	107.46	107.46
Max cladding temperature in average channel (°C)	79.27	81.06	78.56
Max cladding temperature in hot channel (°C)	124.61	120.11	119.34

*After natural convection established.

Table 5-5 Scram set points and LSSS for the existing HEU core (6 MW)

Parameter	Scram set points	LSSS
Power	6.6 MW	7.4 MW (max)
Primary Coolant Flow	1900 gpm	1800 gpm (min)
Steady-State Average Core Outlet Temperature	55 °C	60 °C (max)
Coolant Height	No overflow	4" below overflow (min), or 10 feet above top of fuel plates

Table 5-6 Proposed LEU core configurations for the LSSS Calculation

	Plates per element	Total # of plates	De (m)	Fuel thickness (mm)	Hot Channel Factor	Coolant Channel area (m^2)	Peaking factors
HEU	15	330	2.1864 E-03	0.762	2.0	1.249E-04	HEU*
LEU# a1	15	330	2.44E-03	0.762	1.6, 1.76, 2.0	1.40E-04	LEU**
LEU# a2	16	352	2.20E-03	0.762	1.6, 1.76, 2.0	1.26E-04	LEU
LEU# a3	17	374	1.99E-03	0.762	1.6, 1.76, 2.0	1.13E-04	LEU
LEU# a4	18	396	1.80E-03	0.762	1.6, 1.76, 2.0	1.02E-04	LEU
LEU# a5	19	418	1.63E-03	0.762	1.6, 1.76, 2.0	9.25E-05	LEU
LEU# a6	20	440	1.47E-03	0.762	1.6, 1.76, 2.0	8.37E-05	LEU
LEU# b1	15	330	2.68E-03	0.508	1.6, 1.76, 2.0	1.54E-04	LEU
LEU# b2	16	352	2.44E-03	0.508	1.6, 1.76, 2.0	1.40E-04	LEU
LEU# b3	17	374	2.23E-03	0.508	1.6, 1.76, 2.0	1.28E-04	LEU
LEU# b4	18	396	2.05E-03	0.508	1.6, 1.76, 2.0	1.17E-04	LEU
LEU# b5	19	418	1.87E-03	0.508	1.6, 1.76, 2.0	1.07E-04	LEU
LEU# b6	20	440	1.72E-03	0.508	1.6, 1.76, 2.0	9.79E-05	LEU

***Refer to the HEU peaking factors in Table 5-2**
**** Refer to the LEU peaking factors in Table 5-2**

Table 5-7 Engineering Hot Channel Factors Applied in the MITR-III [4]

Enthalpy Rise			
Reactor power measurement			1.05
Power density measurement/calculation			1.10
Plenum chamber flow			1.08
Flow measurement			1.05
Fuel density tolerances			1.026
Flow channel tolerances			1.089
Eccentricity			1.001
	F_H,	Statistical	1.173
Film Temperature Rise			
Reactor power measurement			1.05
Power density measurement/calculation			1.10
Plenum chamber flow			1.06
Flow measurement			1.04
Fuel density tolerances			1.05
Flow channel tolerances			1.124
Eccentricity			1.003
Heat transfer coefficient			1.200
	$F_{\Delta T}$,	Statistical	1.275
Heat Flux			
Reactor power measurement			1.05
Power density measurement/calculation			1.10
Fuel density tolerances			1.05
Eccentricity			1.003
	F_Q	Statistical	1.123

Table 5-8 LSSS power results

	Hot channel factor	LSSS Power (MW)
HEU	2.0	7.4
LEU# a1	1.6	8.2
	1.76	7.3
	2.0	6.2
LEU# a2	1.6	8.9
	1.76	7.8
	2.0	6.7
LEU# a3	1.6	9.8
	1.76	8.6
	2.0	7.3
LEU# a4	1.6	10.6
	1.76	9.3
	2.0	7.8
LEU# a5	1.6	11.5
	1.76	10.0
	2.0	8.6
LEU# a6	1.6	12.1
	1.76	10.8
	2.0	9.2
LEU# b1	1.6	7.5
	1.76	6.7
	2.0	5.7
LEU# b2	1.6	8.1
	1.76	7.2
	2.0	6.2
LEU# b3	1.6	9.0
	1.76	8.1
	2.0	6.7
LEU# b4	1.6	9.6
	1.76	8.6
	2.0	7.3
LEU# b5	1.6	10.2
	1.76	9.2
	2.0	7.9
LEU# b6	1.6	11.2
	1.76	9.7
	2.0	8.4

Table 5-9 Total pressure loading for the core tank

	Plates per element	Total # of plates	De (m)	Fuel thickness (mm)	Coolant Channel area (m^2)	Total pressure loading at 10°C (psig)	Total pressure loading at 40°C (psig)
HEU	15	330	2.1864E-03	0.762	1.249E-04	16.20	14.02
LEU# a1	15	330	2.44E-03	0.762	1.40E-04	13.24	11.68
LEU# a2	16	352	2.20E-03	0.762	1.26E-04	14.80	12.88
LEU# a3	17	374	1.99E-03	0.762	1.13E-04	16.81	14.43
LEU# a4	18	396	1.80E-03	0.762	1.02E-04	19.18	17.03
LEU# a5	19	418	1.63E-03	0.762	9.25E-05	22.02	19.40
LEU# a6	20	440	1.47E-03	0.762	8.37E-05	25.73	22.49
LEU# b1	15	330	2.68E-03	0.508	1.54E-04	11.40	10.21
LEU# b2	16	352	2.44E-03	0.508	1.40E-04	12.39	10.97
LEU# b3	17	374	2.23E-03	0.508	1.28E-04	13.49	11.81
LEU# b4	18	396	2.05E-03	0.508	1.17E-04	14.78	13.32
LEU# b5	19	418	1.87E-03	0.508	1.07E-04	16.43	14.70
LEU# b6	20	440	1.72E-03	0.508	9.79E-05	18.32	16.28

* Total pressure loading is calculated by adding a gravity pressure head of 3.8 m of primary coolant, which is equivalent to 5.40 psi at 10°C or 5.36 at 40°C, and the friction pressure drop based on a primary flow rate of 2200 gpm. The core tank was installed during the MITR-II upgrade. The design pressure is 24 psig, according to the Reactor System Manual.

Table 5-10 RELAP5 Results: Pressure drop through core and core flow rates

	Plates per element	Total # of plates	Clad thickness (mm)	Fuel thickness (mm)	De (m)	Pressure drop through core (Pa)		Natural convection core flow rate (kg/s)
						Laminar Flow (Natural convection)	Turbulent Flow (Forced convection)	
LEU# b1	15	330	0.25	0.508	2.68E-03	5689	26893	2.37
LEU# b2	16	352	0.25	0.508	2.44E-03	5698	30673	2.26
LEU# b3	17	374	0.25	0.508	2.23E-03	5709	35107	2.15
LEU# b4	18	396	0.25	0.508	2.05E-03	5719	39934	2.04
HEU	15	330	0.38	0.762	2.186E-03	5722	41403	2.12

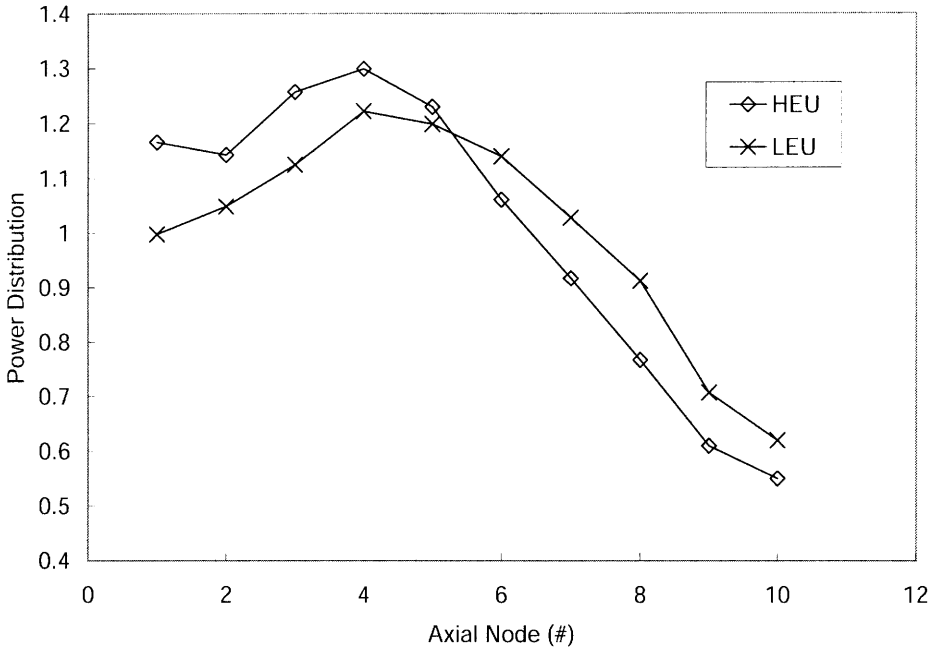

Figure 5-2 Power distribution in AVERAGE channel (Shape)

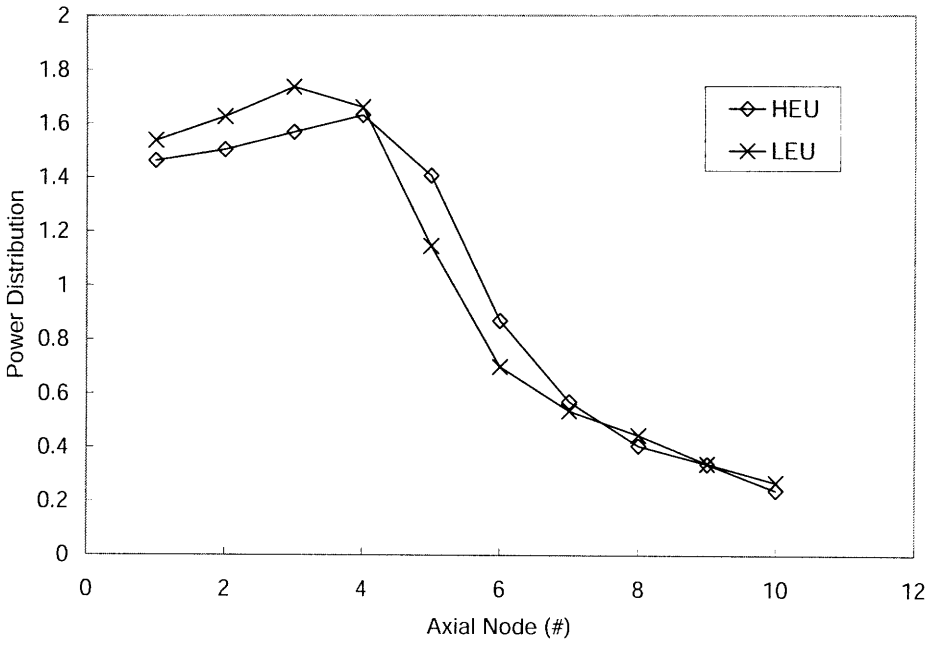

Figure 5-3 Power distribution in HOT channel (Shape)

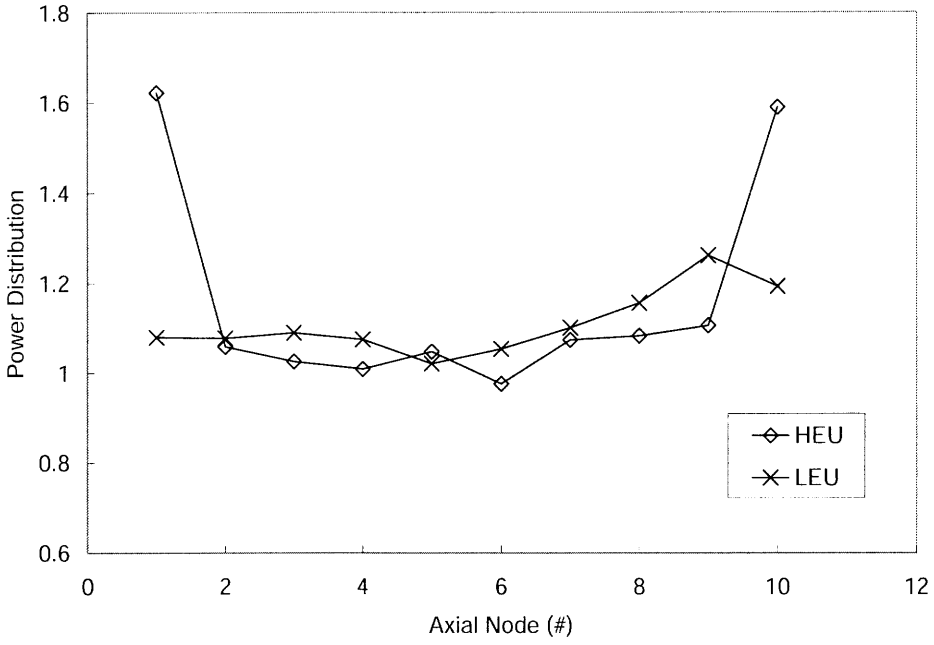

Figure 5-4 Local axial peaking factor for each node in AVERAGE channel

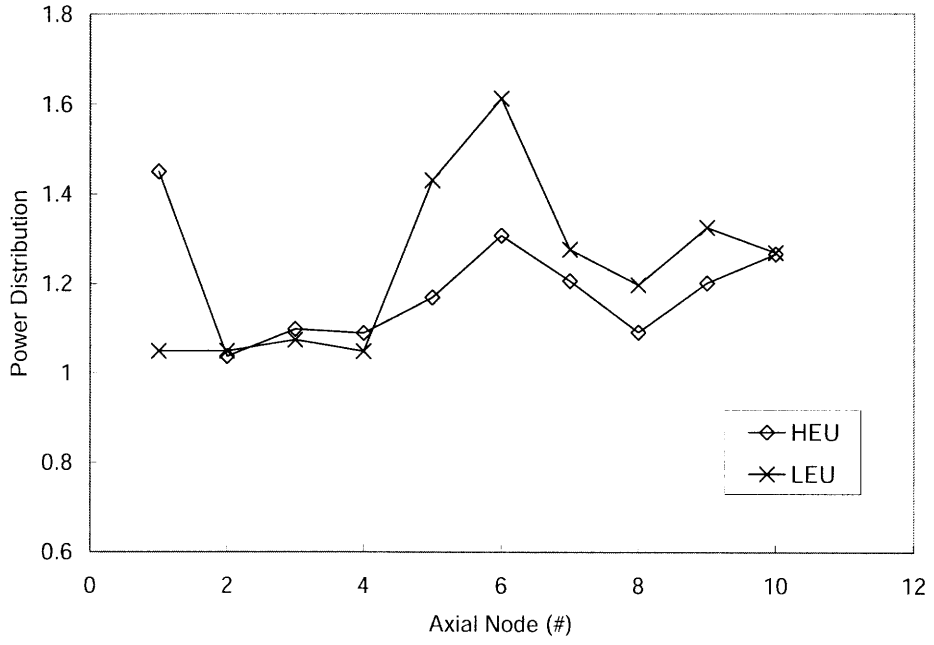

Figure 5-5 Local axial peaking factor for each node in HOT channel

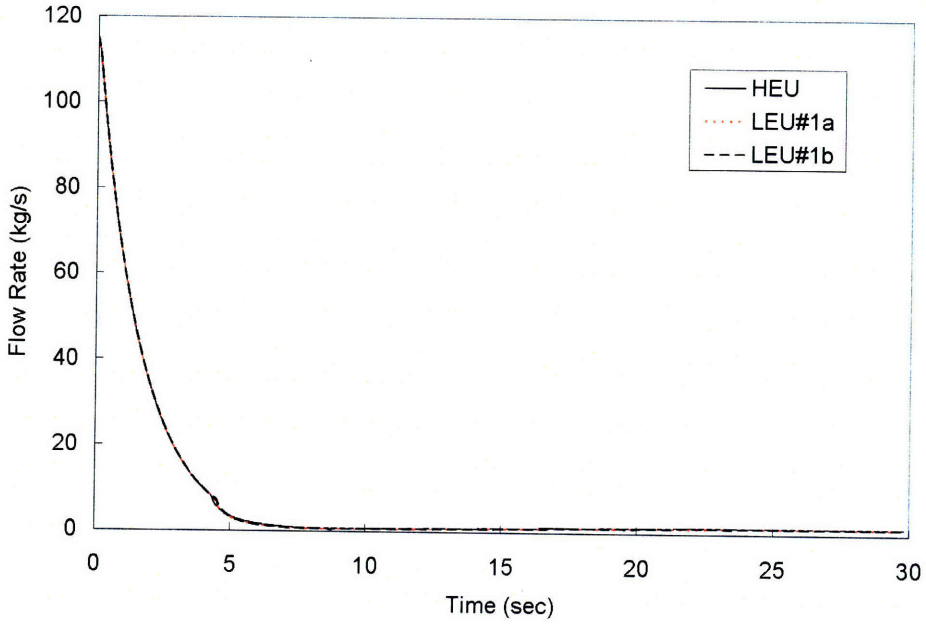

Figure 5-6 Comparison of Core Flow rate

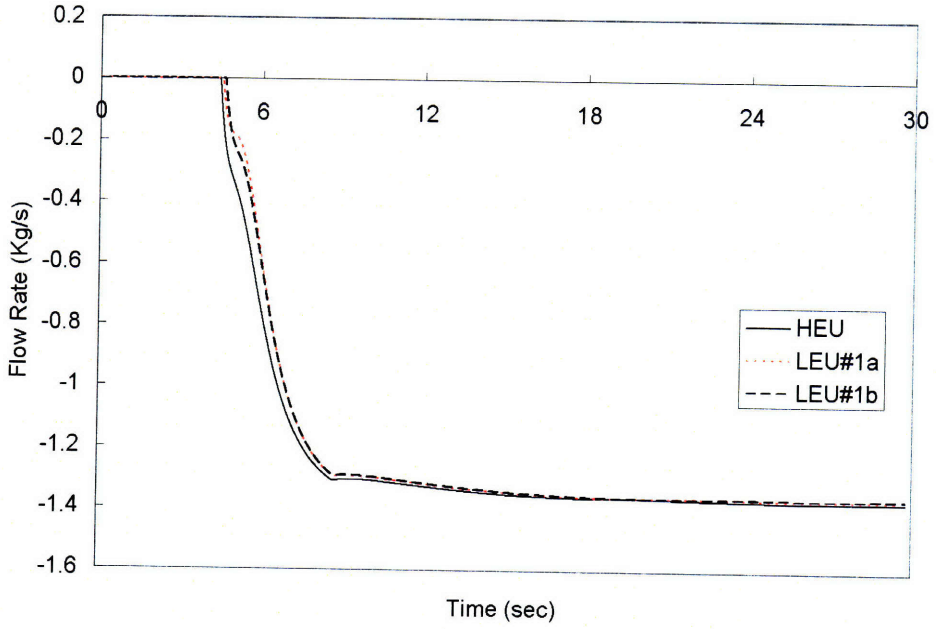

Figure 5-7 Comparison of ASV Flow rate

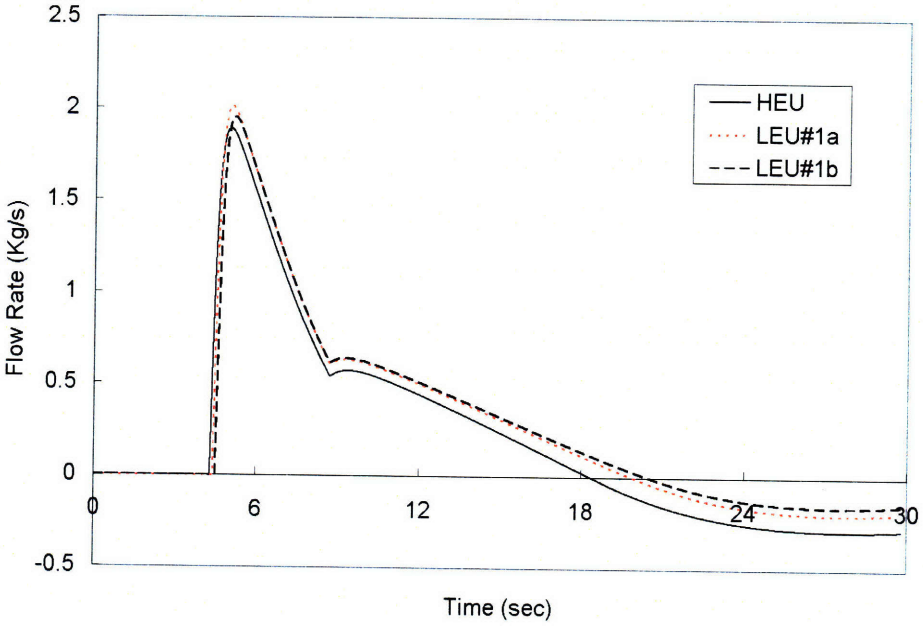

Figure 5-8 Comparison of NCV Flow rate

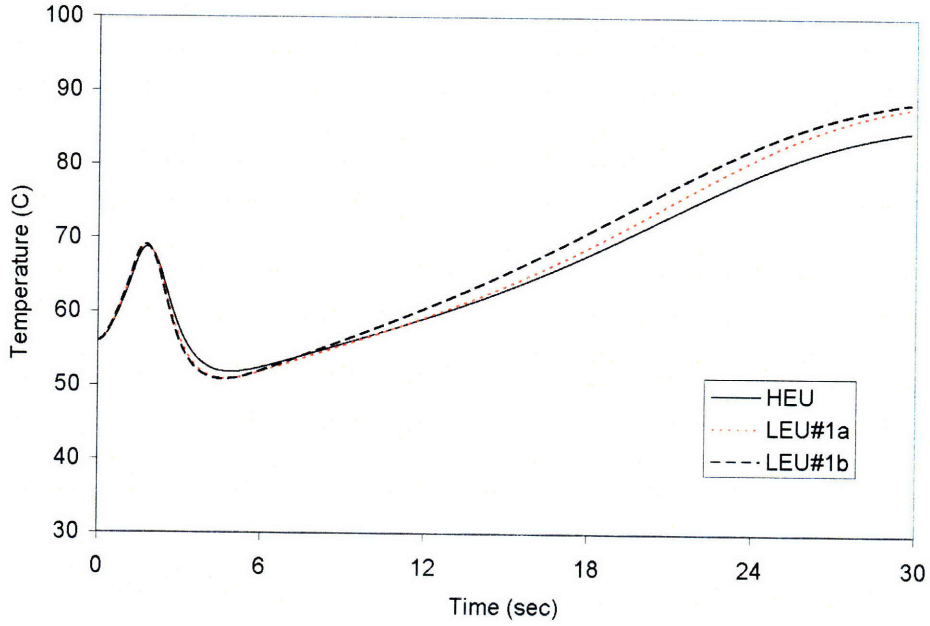

Figure 5-9 Comparison of Exit Coolant Temperature (Average Channel)

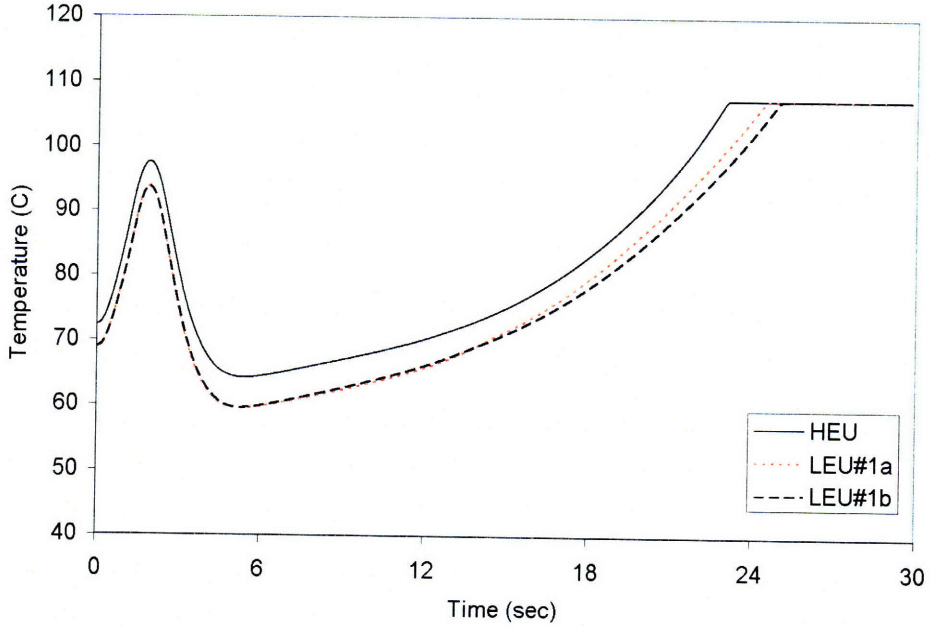

Figure 5-10 Comparison of Exit Coolant Temperature (Hot Channel)

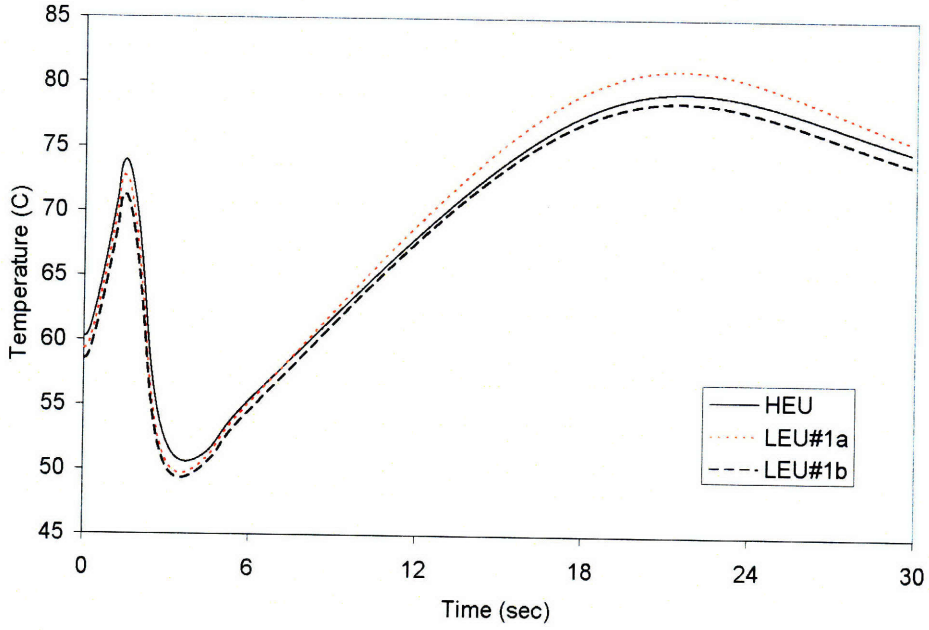

Figure 5-11 Comparison of Cladding Temperature (Average Channel, Node#5)

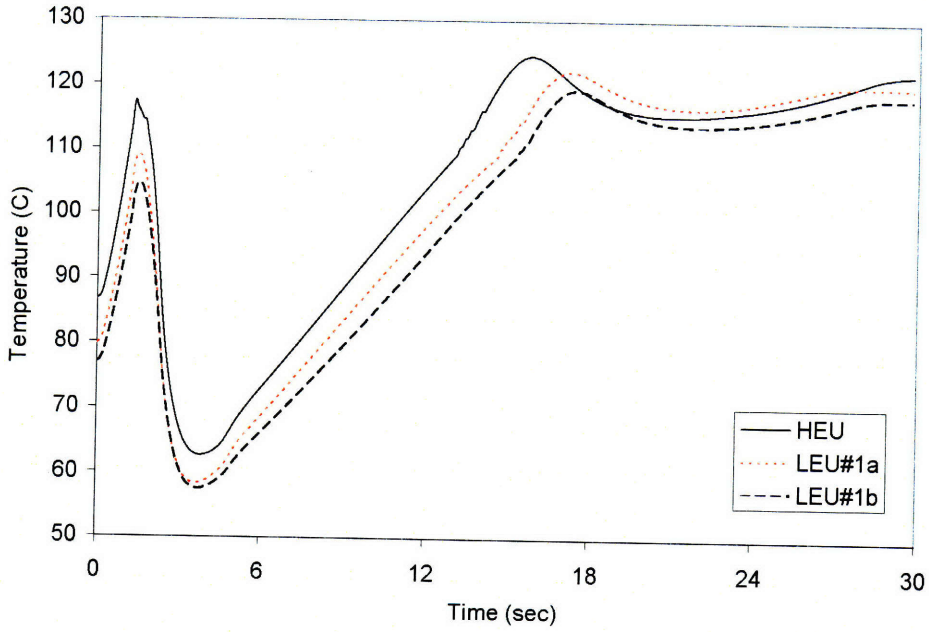

Figure 5-12 Comparison of Cladding Temperature (Hot Channel. Node#5)

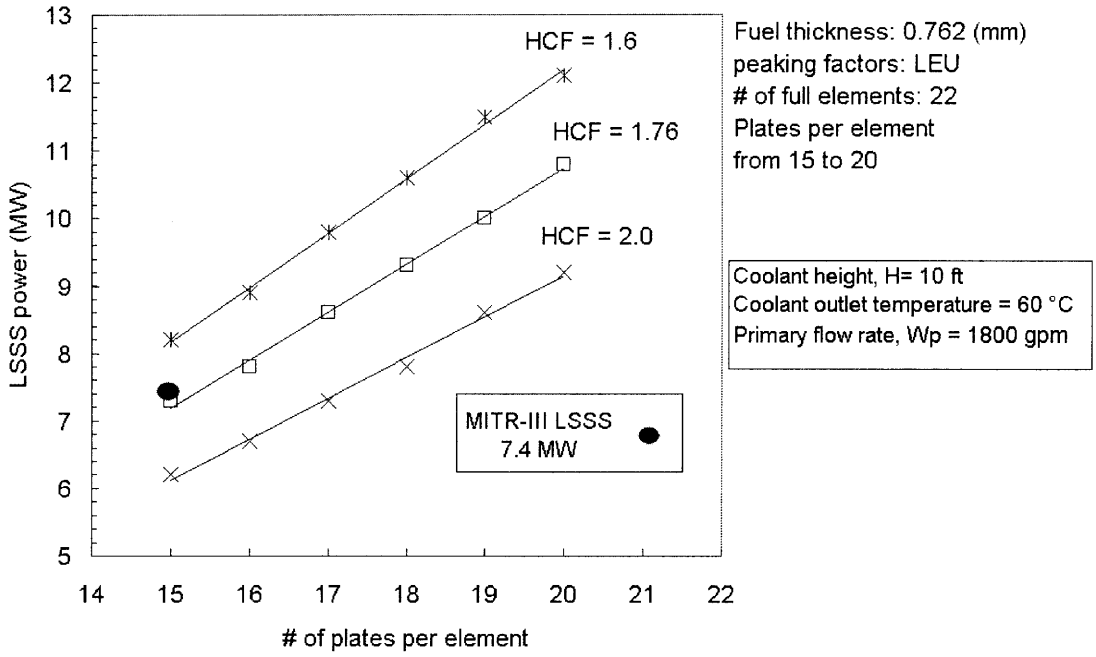

Figure 5-13 LEU LSSS Power (fuel thickness = 0.762 mm)

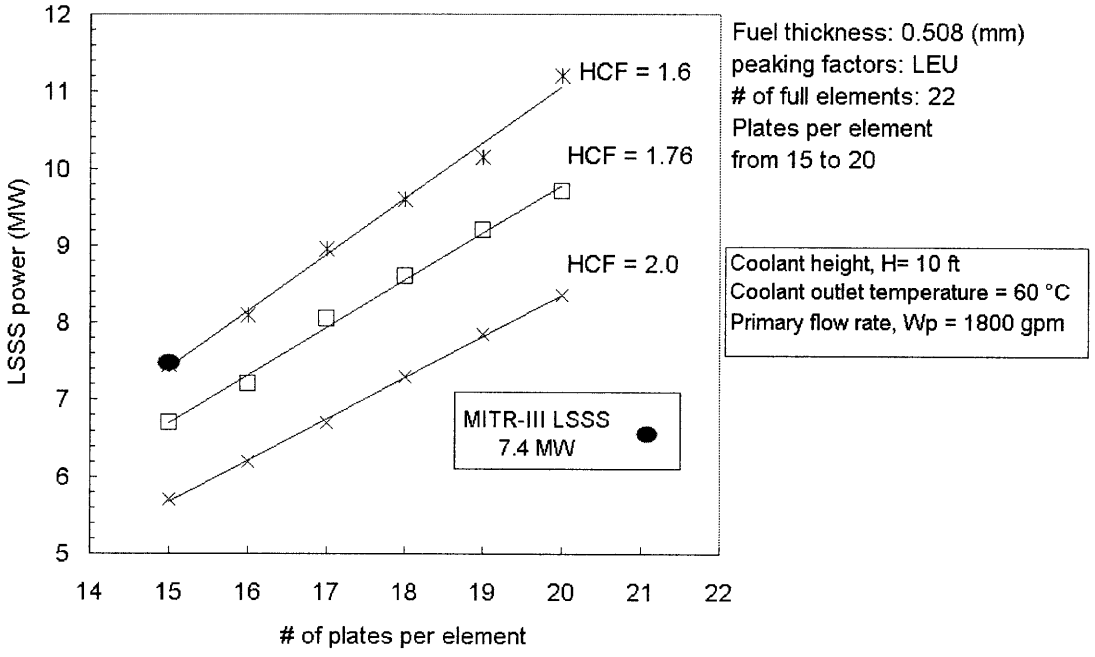

Figure 5-14 LEU LSSS Power (fuel thickness = 0.508 mm)

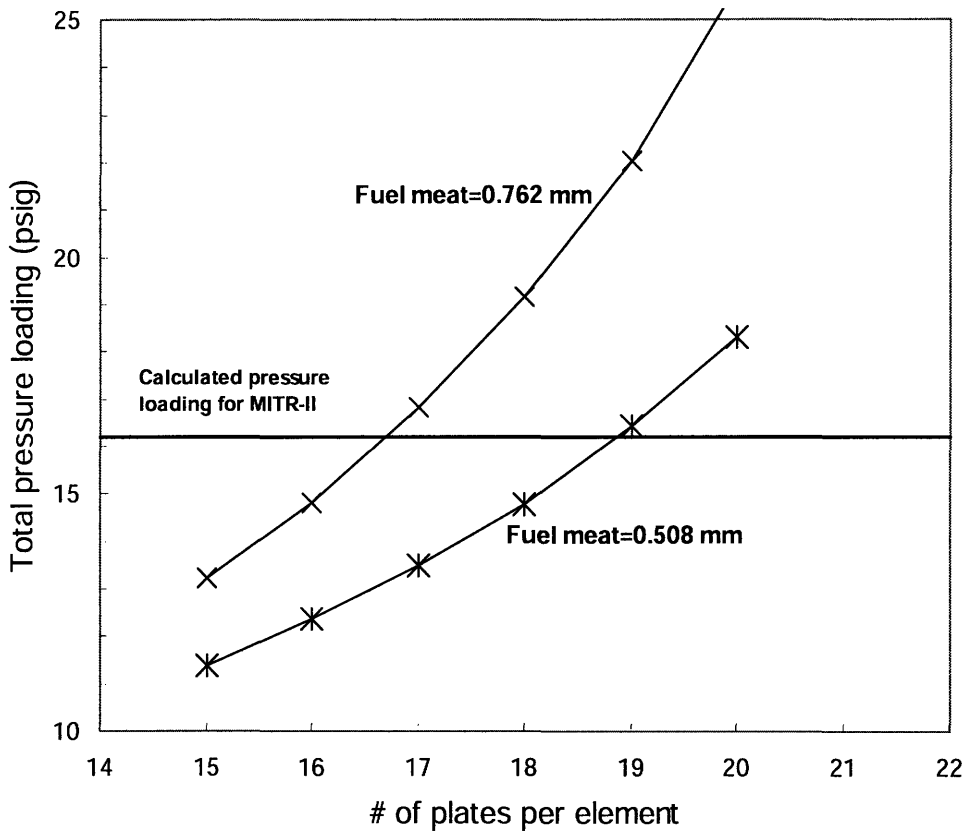

Figure 5-15 Estimated pressure loading on the MITR core tank

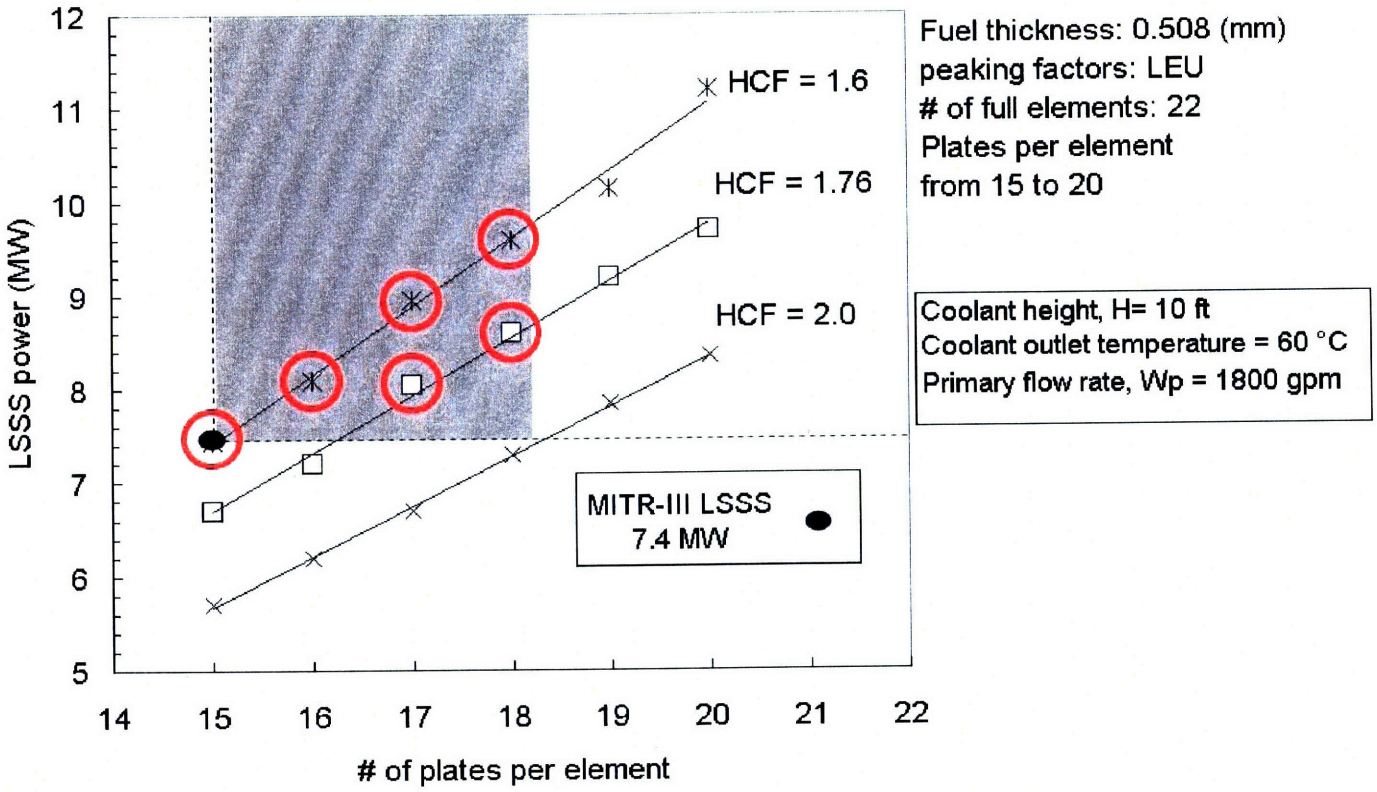

Figure 5-16 Sensitivity study of hot channel factors for LEU core design options
(Red circles indicates the cases selected for LOF analysis)

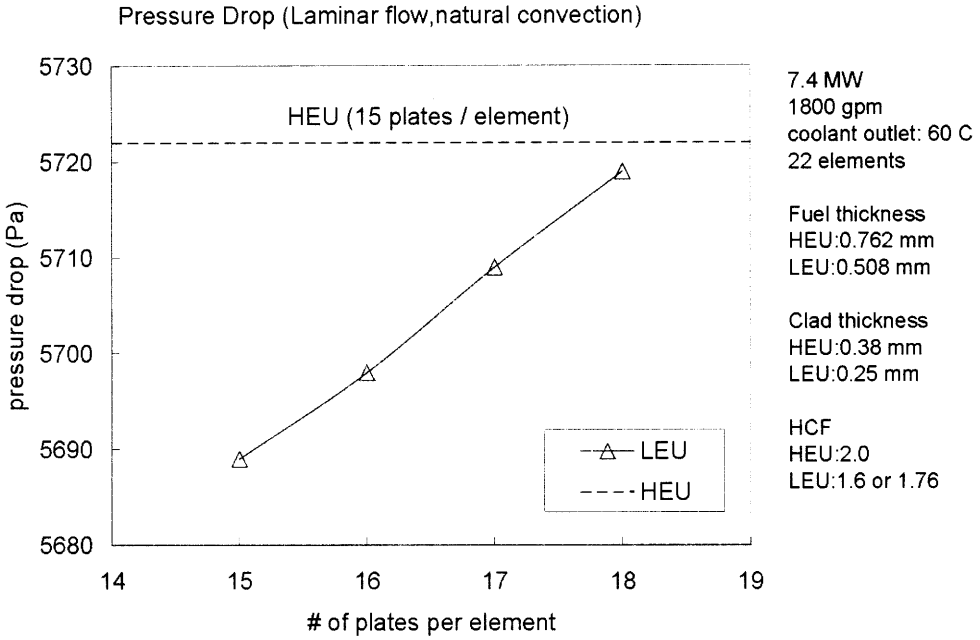

Figure 5-17 RELAP5 calculated Laminar flow pressure drop

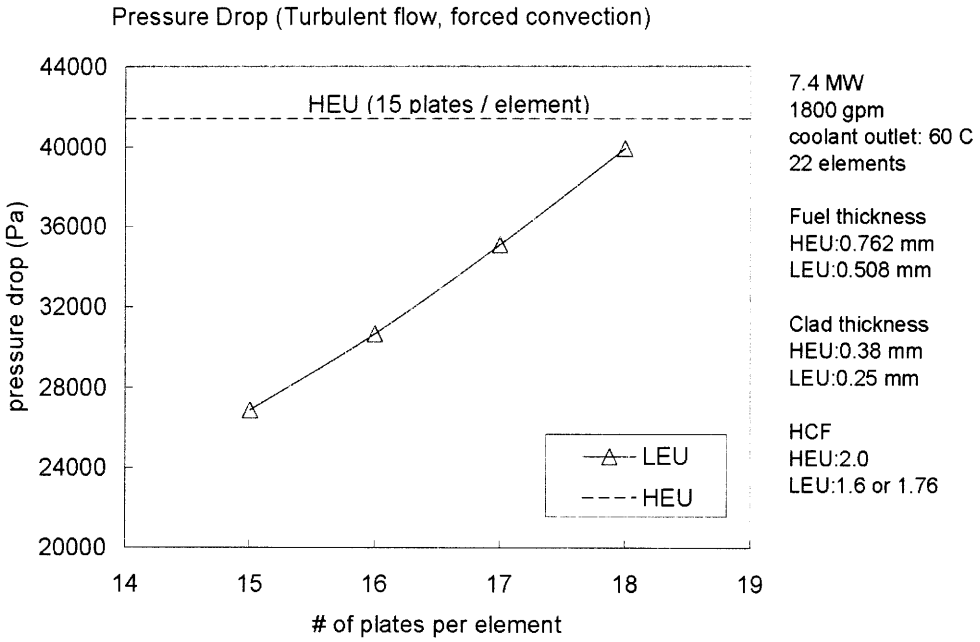

Figure 5-18 RELAP5 calculated Turbulent flow pressure drop

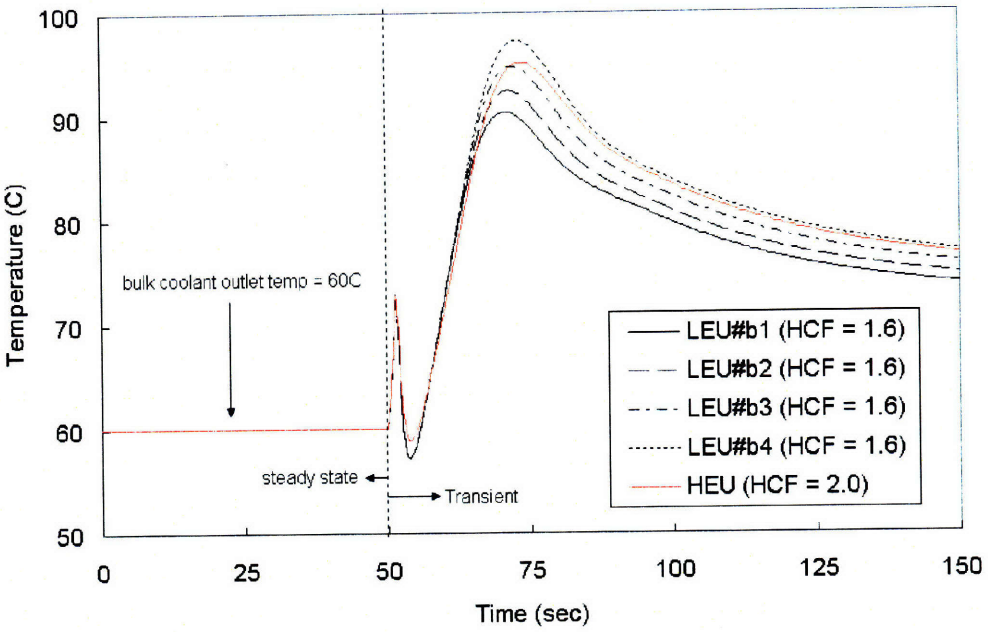

Figure 5-19 Comparison of coolant outlet temperature in the average channel

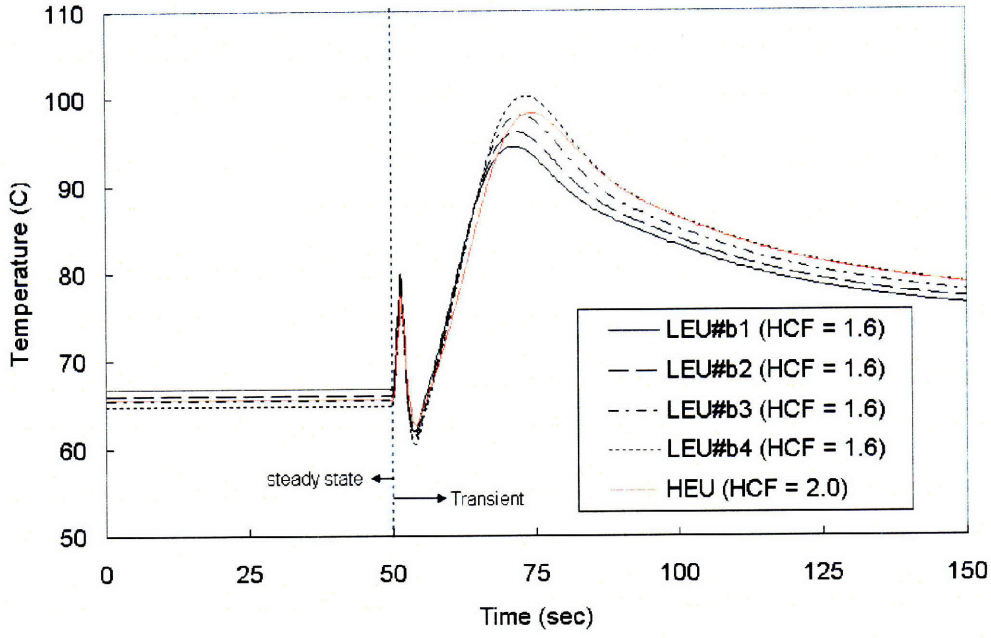

Figure 5-20 Comparison of clad outlet temperature in the average channel

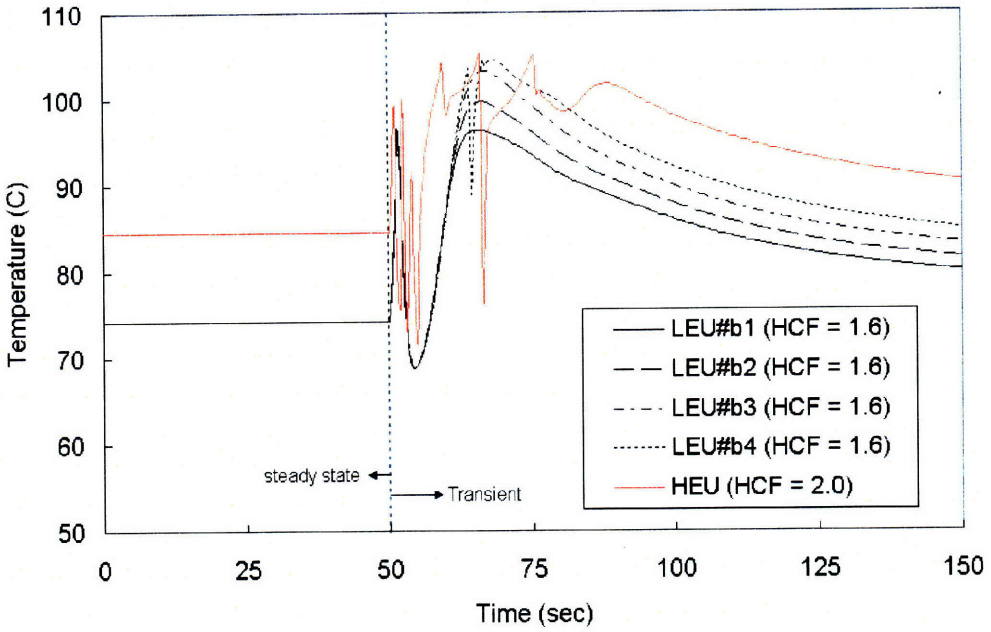

Figure 5-21 Comparison of coolant outlet temperature in the hot channel

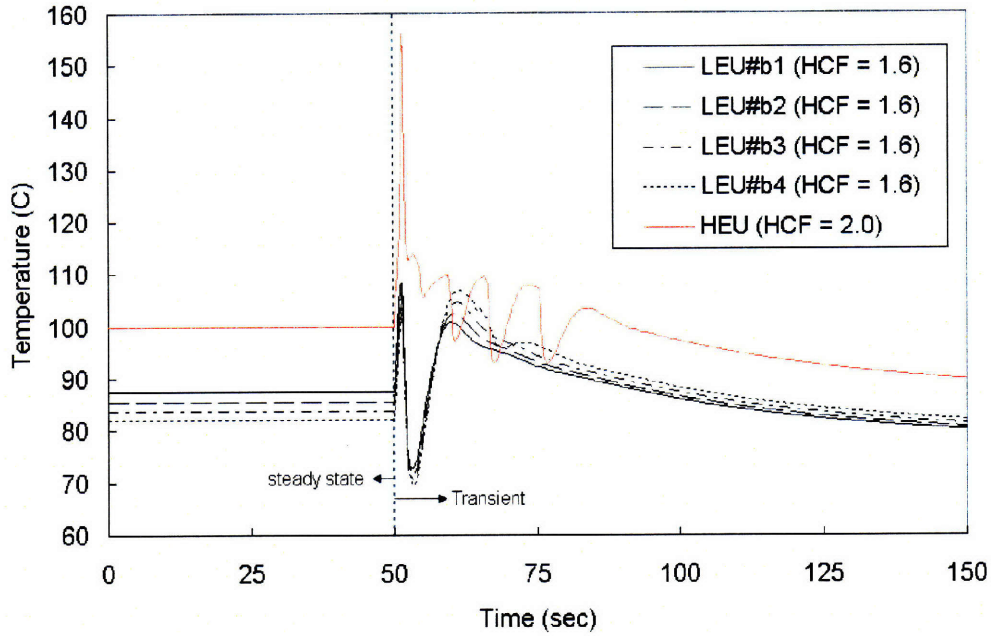

Figure 5-22 Comparison of clad temperature in the hot channel

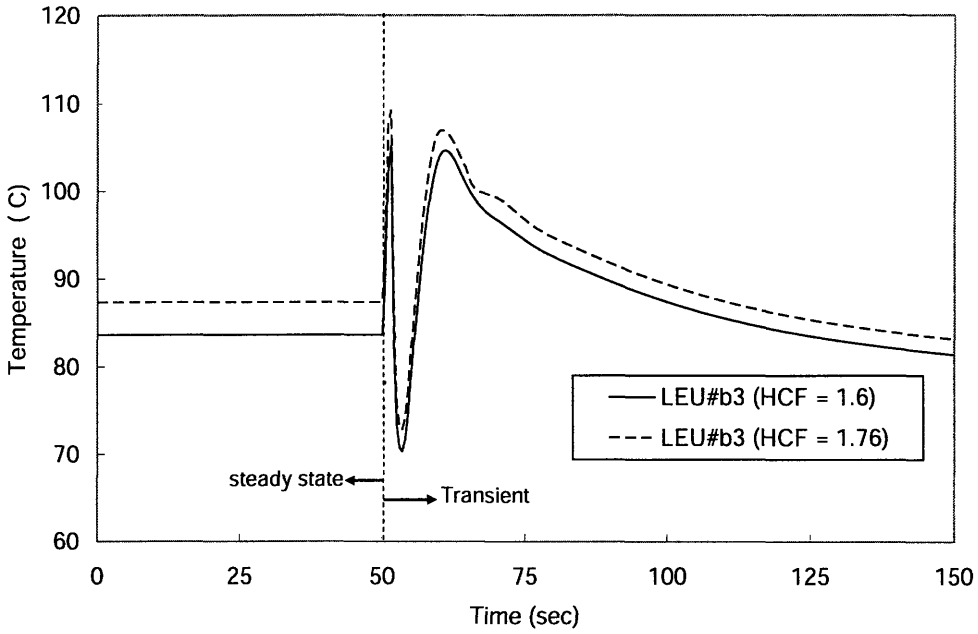

Figure 5-23 Comparison of clad temperature with different hot channel factors (LEU#b3)

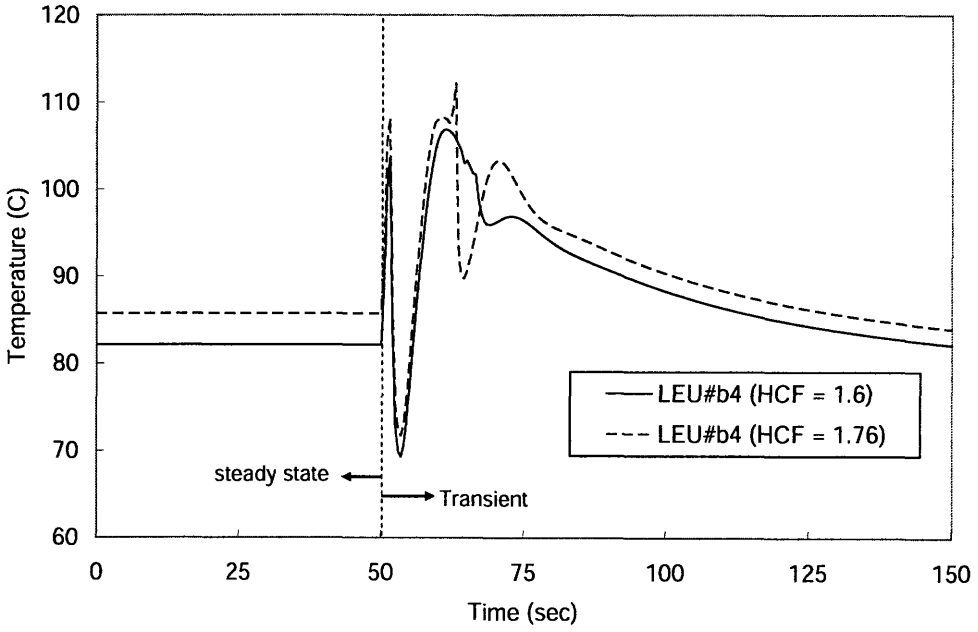

Figure 5-24 Comparison of clad temperature with different hot channel factors (LEU#b4)

Chapter 6
Summary of Conclusions and Recommendations

6.1 Summary of Steady State Benchmark Study

The objective of this benchmark study is to evaluate the capability and accuracy of the MITR in-house thermal-hydraulics code, MULCH. Since MULCH will be used to perform the thermal-hydraulic calculation for the proposed LEU core design, it is very important to assure the adequacy of using the MULCH code.

The MULCH code does not model the temperature distribution within the fuel plate since during steady-state and credible transient scenarios the temperature difference between fuel centerline and clad outer surface is small. MULCH does take into account the conduction resistance between the fuel meat outer surface and coolant due to crud. The crud here means oxidation layers formed during regular reactor operation. Default outputs of MULCH for outer clad temperatures are the crud outer surface temperatures. By setting crud thickness to zero, MULCH can provide the clad outer surface temperatures. In this benchmark study, it is assumed that no crud has been formed on the clad surface. Appendix B summarizes the calculated temperature difference between fuel centerline and coolant for the hot channel as a function of reactor power.

Two cases using PLTEMP and one case using RELAP5 are simulated to benchmark MULCH for steady state analyses. Assuming fin effectiveness is zero, the results predicted by MULCH and PLTEMP are very close. To consider the presence of fins, since both PLTEMP and RELAP5 cannot model the fin effectiveness, the heat transfer area on cladding surface is increased to account for the effect of fins. Results are in good agreement among PLTEMPT, RELAP5 and MULCH. Since the steady state results of MULCH are in agreement with PLTEMPT and RELAP5, it is concluded that MULCH is qualified to perform steady state analysis for the MIT reactor.

6.2 Summary of Loss of Flow Benchmark Study

The MIT Research Reactor is intended to operate with a primary coolant flow rate of 2000 gpm under steady state conditions. A low primary flow (below 1900 gpm) will automatically initiate a scram. There are two initiating events that can cause a loss of primary coolant flow accident. The first is a loss of off-site electrical power which will stop the primary pumps and scram the reactor by dropping all six shim blades simultaneously. This is a credible scenario. The second is a pump coast down accident

that occurs because of primary pump power supply failures or malfunctions of the pump motors. This is not considered to be a credible accident because the probability for both pumps to fail at the same time is very small. However the latter scenario is selected for this study since it provides a more conservative estimate of peak clad temperature due to the instrument delay time.

The loss-of-flow (LOF) benchmark study consists of two parts. First, LOF accidents initiated by pump coast-down are simulated by RELAP5 and MULCH based on a steady-state reactor power of 6 MW with an initial flow rate at 2000 gpm for the existing highly enriched uranium core. Second, the measurements from MITR-II startup test are used to compare with the prediction of MULCH and RELAP5. Results of loss of primary flow transients show that RELAP5 predicts higher ASV, NCV and core flow when natural circulation is established. For the comparison of temperature, RELAP5 predicts higher coolant and cladding temperature in the average channel but lower coolant and cladding temperature in the hot channel. The decay energy is also compared. Results show that MULCH predicts a total decay energy of 8347.6 kJ during the transient, which is slightly less than RELAP5's prediction of 8564.0 kJ.

Comparison between calculated values and measurements shows that RELAP5 seems to over-predict the peak temperature but the predicted trend and values match the measured values well. MULCH is somewhat less conservative than RELAP5 in peak temperature prediction. It is therefore determined that MULCH can be used for design analysis for LEU cores, however RELAP5 will also be used to obtain more accurate results, e.g., temperature oscillations due to OFI, for reactor safety analysis.

6.3 Summary of Analyses for the LEU Core options

Steady state analyses for the LEU core design options consist of LSSS power calculation and pressure loading for the core tank. In this thesis, the rated power of the LEU core is assumed to remain at 6 MW. The criterion for the LEU core design is that the LSSS power be equal or larger than the existing HEU LSSS power of 7.4 MW. It is preferable to achieve a larger LSSS power because the LEU core may operate at a power slightly greater than 6 MW to meet the neutron flux demand. The LSSS results revealed that by increasing the number of plates per element and by reducing the plate thickness a higher core power can be realized. However, it is found that a smaller coolant channel is good for the LSSS power but would increase core friction pressure drop and therefore core tank pressure loading which is another constraint to be considered for the LEU core design.

Because the condition of the core tank cannot be readily determined and measurements of actual pressure loading have not been made, it is recommended that the LEU core design should be limited to equal or below the current pressure loading of the HEU core. More specifically, the fuel element should not have more than 18 plates if the fuel thickness remains at or above 0.508 mm. The existing HEU fuel meat has a thickness of 0.762 mm. Usage of a thinner fuel plate is also recommended to better meet the pressure loading criterion.

The LEU#b-series design with 15~18 plates per element are analyzed for loss-of-flow transient. The LSSS are chosen as initial settings for the simulated cases. The existing HEU core with 22 fuel elements is also analyzed for comparison. Variation of the coolant outlet temperature in the average channel shows that using more plates per element would result in lower steady state temperature; however, it also gives a higher peak temperature during the transient. HEU has a significant oscillation of coolant temperature in the hot channel at the beginning of the transient. But no temperature oscillation was found in the LEU cases, at a lower peaking factor.

Results of clad temperature show that HEU has a very high peak (~ 156 °C) and flow instability at the onset of the transient. LEU cases have no obvious temperature oscillation mainly because of the lower hot channel factor. For the LEU core design with 17 and 18 plates, a higher HCF may result in an obvious temperature oscillation. However, considering the frequency and magnitude this temperature oscillation may be acceptable.

Based on the results of steady state and loss-of-flow simulation, it is recommended that a desirable design for the LEU core should encompass low peaking factors to increase the LSSS power and to decrease the maximum clad temperature during the transient. Moreover, it is important to optimize the configuration in order to have the highest possible LSSS power, to prevent significant temperature oscillation during LOF transient, and to limit core tank pressure loading. At this stage, the LEU#b-series design with 15~18 plates per element and hot channel factor less than 1.76 are qualified to comply with the thermal-hydraulic criteria.

A LEU core design with a thinner fuel meat was proposed to increase the LSSS power. If a higher LSSS power can be attained, the LEU core may operate at higher power. The thermal-hydraulic analyses of a thinner fuel plate are summarized in Appendix F. It is concluded that using a thinner fuel provides limited benefit for the LSSS power. Raising the core flow rate will be a better way to increase the LSSS power and safety margin.

6.4 Recommendations for the Future Work

Through this thesis, some issues are recommended to be considered in the future. These issues are worthy of further investigation because addressing these issues can improve MIT reactor operation and/or consolidate the LEU core design options. These issues are:

(1) Detailed neutronic calculations are needed to obtain the radial and axial peaking:

Radial and axial peaking factors are the key parameters on reactor's thermal-hydraulic performance, for example, the LSSS power. The LEU core design needs detailed neutronic calculations with fuel burnup in order to establish a reasonable design margin and to ensure that it can attain the experimental demand of neutron flux in compliance with the safety limits.

(2) A updated pump coast-down curve:

The pump coast-down curve used in the thesis is based on the existing heat exchangers. New heat exchangers are planed to be installed for the 6 MW MITR-III core in summer 2008. The new heat exchanger is of plate-and-frame type and is expected to have much higher viscous pressure drop than the current ones. Therefore, the pump coast-down curve may be affected adversely and the LOF transient should be re-analyzed.

(3) Investigation of flow disparity:

The flow disparity factor used in the thesis is obtained from the MITR-II startup report for the existing HEU core. Since the new LEU core may use different fuel configuration, such as different clad and fuel thickness, a usage of half element and so on, it will be necessary to evaluate the flow disparity factor for the new LEU core design.

(4) Investigation of friction factors and form loss coefficients:

The friction factors and form loss coefficients used in the thesis are obtained from correlations or experimental data [5, 31, 35]. Since the effect of fins on viscous pressure loss for MITR fuel has not been confirmed previously, it is suggested that measurements be made for new geometries proposed for LEU fuel designs to confirm previous analyses.

(5) Updated neutron kinetics model and thermal-hydraulic correlations for the MULCH code

As discussed in the section 4.7, the point kinetics model in MULCH should also be improved. The MULCH code will be more reliable for loss of primary flow transient if the decay power prediction after reactor scram is improved. In addition, introducing the updated thermal-hydraulic correlations for the MULCH code should also be considered. For example, in the RELAP5 code, Petukhov correlation [36] and Elenbaas correlation [37] are used for the parallel-plate-type fuel.

(6) Evaluation of the Engineering Hot Channel Factors for New Fuel Design

Engineering hot channel factors account for the manufacturing tolerances, analysis, and measurement uncertainties relevant to reactor design and operations. For the LSSS analysis described in this thesis, the factors developed for the HEU core are adopted. For new fuel design, the manufacturing tolerances for the new fuel matrix and geometry may vary and thus these factors should be re-evaluated.

References

[1] U.S. Department of Energy, "Reduced Enrichment for Research and Test Reactors, http://www.nnsa.doe.gov/na-20/rertr.shtml

[2] DOE Press release No. R-05-099, April 11, 2005

[3] T. H. Newton Jr., "Development of a Low Enrichment Uranium Core for the MIT Reactor", Chapter 1, PhD Thesis, MIT NSE Dept., Feb. 2006

[4] MITR Staff, "Safety Analysis Report for the MIT Research Reactor (MITR-III)", Chapter 1, MIT Nuclear Reactor Laboratory, July 1999.

[5] M. J. McGuire, "An Analysis of the Proposed MITR-III Core to Establish Thermal-Hydraulic Limits at 10 MW", PhD Thesis, MIT Nucl. Eng. Dept., June 1995

[6] L.-W. Hu and J. A. Bernard, "Development and Benchmarking of a Thermal-Hydraulics Code for the MIT Nuclear Research Reactor," Proceedings of the ANS Joint International Conference on Mathematical Methods and Super-Computing for Nuclear Applications, Saratoga, NY, Oct. 5-7, 1997.

[7] L.-W. Hu and J. A. Bernard, "Thermal-Hydraulic Analysis for the Upgraded MIT Nuclear Research Reactor," *IEEE Transactions on Nuclear Science*, Vol. 45, No. 3, Part I, June 1998.

[8] S. A. Abdelkader, "Thermal Analysis of the Reflector System of the Massachusetts Institute of Technology Research Reactor (MITR-III)", Master Thesis, MIT Nucl. Eng. Dept., May 1996

[9] G.C. Allen, "The reactor engineering of the MITR-II construction and startup", PhD Thesis, MIT Nucl. Eng. Dept., June. 1976

[10] F. Bamadad-Haghighi, "Natural convection analysis of the MITR-II during loss of flow accident", Master Thesis, MIT Nucl. Eng. Dept., August 1977

[11] Arne P. Olson and M. Kalimullah, "A Users Guide to The PLTEMP/ANL Code", Argonne National Laboratory, May 2006

[12] W. Shaw and J. Tigg. Applied Mathematica. Addison Wesley, Menlo Park, Ca., 1994.

[13] The RELAP5 Code Development Team, "RELAP5/MOD3 Code Manual", USA: Idaho National Engineering Laboratory, 1995.

[14] C. B. Davis, C. D. Fletcher, and S. B. Rodriguez, Benchmarking the RELAP5 L-Reactor Model with Savannah River Reactor Test Data, EGG-EAST- 8336, April 1989.

[15] R. G. Ambrosek and R. P. Wadkins, "RELAP5 Benchmarking with ATR Star-Up Tests," Transactions of the American Nuclear Society, June 1990.

[16] J. S. Bollinger and C. B. Davis "Benchmarking the RELAP5/MOD2.5 Model r-R of an SRS (Savannah River Site) Reactor to the 1989 L-Reactor Tests," 1990 Joint RELAP5 and TRAC-BWR International User Seminar, Chicago, IL, September 17-21, 1990.

[17] J.L. Snelgrove, P. Lemoine, P. Adelfang, and N. Arkhangelsky, "Qualification and Licensing of U-Mo Fuel," Proceedings of the Research Reactor Fuel Management Conference, Aix-en-Provence, France, March, 2003.

[18] J.L. Snelgrove, and A. Languille, "Qualification of Uranium-Molybdenum Alloy

Fuel – Conclusions of and International Workshop," Proceedings of the Research Reactor Fuel Management Conference, Colmar, France, March, 2000.

[19] T. H. Newton Jr., "Development of a Low Enrichment Uranium Core for the MIT Reactor", Chapter 3, PhD Thesis, MIT NSE Dept., , Feb. 2006

[20] T. H. Newton Jr., "Development of a Low Enrichment Uranium Core for the MIT Reactor", Chapter 4, PhD Thesis, MIT NSE Dept., Feb. 2006

[21] T. H. Newton Jr., "Development of a Low Enrichment Uranium Core for the MIT Reactor", Chapter 5, PhD Thesis, MIT NSE Dept., Feb. 2006

[22] T. H. Newton Jr., "Development of a Low Enrichment Uranium Core for the MIT Reactor", Chapter 8, PhD Thesis, MIT NSE Dept., Feb. 2006

[23] MITR Staff, "Safety Analysis Report for the MIT Research Reactor (MITR-III)", Chapter 4, MIT Nuclear Reactor Laboratory, July 1999.

[24] F. W. Dittus and L. M. K. Boelter, "Heat Transfer in Automobile Radiators of the Tubular Type," Publications in Engineering, 2, University of California, Berkeley, 1930, pp. 443-461.

[25] F. Kreith and M. S. Bohn, Principles of Heat Transfer, 4th Edition, New York: Harper and Row, 1986.

[26] J. C. Chen, "A Correlation for Boiling Heat Transfer to Saturated Fluids in Convective Flow," Process Design and Development, 5, 1966, pp. 322-327.

[27] W. M. Kays, "Numerical Solution for Laminar Flow Heat Transfer in Circular Tubes," Transactions of the ASME, 77, 1955, pp. 1265-1274.

[28] S. W. Churchill and H. H. S. Chu, "Correlating Equations for Laminar and Turbulent Free Convection from a Vertical Plate," International Journal of Heat and Mass Transfer, 18, 1975, pp. 1323-1329.

[29] MITR Staff, "Safety Analysis Report for the MIT Research Reactor (MITR-III)", Chapter 13, MIT Nuclear Reactor Laboratory, July 1999.

[30] H. G. Trosman, "computer Simulation for Transient analysis of MITR Loop Components", Master thesis, MIT Department of Nuclear Engineering, 1994.

[31] C. Kao, "Simulation of MITR-II Primary System in Steady State," MIT Department of Nuclear Engineering Internal Report, 1992.

[32] F. Bamadad-Haghighi, "Natural convection analysis of the MITR-II during loss of flow accident", Chapter 2, Master Thesis, MIT Nucl. Eng. Dept., August 1977

[33] "American National Standards Institute/American Nuclear Society Standard for Decay Heat Power in Light Water Reactors," ANSI/ANS-5.1-1979, August 1979.

[34] W. B. Wilson, T. R. England, R. J. LaBauve, and D. C. George, "DKPOWR: A Code for Calculating Decay Power, Energy, Activity, and p* + Y Spectra in LWR Fuel Using Fission Pulse Functions," prepared for publication by the Electric Power Research Institute, May 1984.

[35] Lin-Wen Hu, "Thermal Hydraulic Mixing Transients in the MIT Research Reactor Core Tank", PhD Thesis, MIT Nucl. Eng. Dept., Febuaray.1996

[36] B. S. Petukhov, "Heat Transfer and Friction in Turbulent Pipe Flow with Variable Physical Properties," Advances in Heat Transfer, New York: Academic Press, 1970, pp. 503-565.

[37] F. P. Incropera and D. P. DeWitt, Introduction to Heat Transfer, New York: Wiley, 1990, p. 501.

Appendix A
MULCH-II Input Instructions

Units: temperature (°C), power (W), flow rate (kg/s), height, length, width, thickness and elevation (m), area (m^2), volume (m^3)

Line #	
1	**Title**
2	<Blank>
3	**Initial Conditions**: power, cooling tower outlet temp, primary flow, secondary flow, cooling tower efficiency (~0.8), reference coolant temperature (~50 °C), height from water/air interface to top of flow guide (2.31m)
4	Type of transient to be simulated, hours of steady-state operation before transient (hr)
5	Time step (sec), total simulation time (sec)
6	**Scram Set Points**: reactor power set point, primary flow set point, secondary flow set point, core inlet temperature set point ,core outlet temperature set point, secondary inlet temperature set point, secondary outlet temperature set point
7	Instrument delay time to initiate scram (sec), blade drop time for 80% blade in (sec)
8	<Blank>
9	**Pump Coast-down Curve**: coefficients Ac(1), Ac(2) , Ac(3) , Ac(4) , Ac(5) , Ac(6)
10	**Hot Leg Primary**: flow area, volume, De, elevation, K factor, # of channels
11	**HX Primary Side**: flow area, volume, De, elevation, K factor, # of channels
12	**Cold Leg Primary**: flow area, volume, De, elevation, K factor, # of channels
13	**Downcomer 1**: flow area, volume, De, elevation, K factor, # of channels
14	**Downcomer 2**: flow area, volume, De, elevation, K factor, # of channels
15	**Downcomer 3**: flow area, volume, De, elevation, K factor, # of channels
16	**Downcomer 4**: flow area, volume, De, elevation, K factor, # of channels
17	**Core**: flow area, volume, De, elevation, K factor, # of channels
18	**Flow Guide**: flow area, volume, De, elevation, K factor, # of channels
19	**Mixing Area**: flow area, volume, De, elevation, K factor, # of channels
20	**Cold Leg Secondary**: flow area, volume, De, elevation, K factor, # of channels
21	**HX Secondary Side**: flow area, volume, De, elevation, K factor, # of channels
22	**Hot Leg Secondary**: flow area, volume, De, elevation, K factor, # of channels

23	**ASV:** float contact area, reference area for loss coefficient, float volume, length, K factor (up flow), K factor (down flow), # of valves
24	**NCV:** float contact area, reference area for loss coefficient, float volume, length, K factor (up flow), K factor (down flow), # of valves
25	<Blank>
26	**Fuel:** # of elements, fuel meat thickness, fuel clad thickness, crud thickness, fuel width, fuel meat length, fin effectiveness
27	**Bypass Flow:** ratio of forced flow through fueled core region
28	**HX fouling factor:** fouling factor (primary + secondary side)
29	<Blank>
30	**Power Distribution in Systems:** fuel, coolant, D_2O, graphite
31	Hot channel factor
32	**Neutron flux distribution for average channel, Shape (1:10)** (summation of these numbers should equal 10)
33	**Neutron flux distribution for hot channel, Shape (1:10)** (summation of these numbers should equal 10)
34	**Local axial peaking factor for each node in average channel, Peak (1:10)**
35	**Local axial peaking factor for each node in hot channel, Peak (1:10)**
36	**Flow disparity for the hot channel (assume the hit channel gets the minimum flow in the core)**
37	**Engineering Hot Channel Factors:** enthalpy rise (F_H), film temperature rise ($F_{\triangle T}$), heat flux (F_Q)
38	Minimum CHF ratio, Minimum DNB ratio
39	<Blank>

Appendix B.
Temperature difference between fuel centerline, clad and crud

The analysis presented here is based on the analytical solution of a fuel plate model as shown below. The objective is to provide an estimate of the temperature differences between the fuel centerline and the clad outer surface, and those between the fuel centerline and the crud outer surface, as a supplement to the steady-state analysis performed using MULCH-II which does not have a conduction model within the fuel plate. The thermal conductivities used in this calculation are 41.2 W/m K, 186 W/m K, and 2.08 W/m K for fuel meat, cladding, and crud, respectively. The thickness of fuel meat, cladding, and crud are 0.762 mm, 0.508 mm and 0.0254 mm, respectively. These are the same values as those in the MULCH-II calculations for HEU fuel described in this report. The volumetric heat generation rate in the fuel meat is calculated based on 23 fuel elements in the core, and a hot channel factor of 2.0. The axial power distribution is not taken into account in this analysis.

The temperature difference is calculated using the following equations:

$$T_{\max} - T_{co} = q''\left|\frac{a1}{2k_{fuel}} + \frac{a2}{k_{clad}}\right|$$

$$T_{\max} - T_{crud} = q''\left|\frac{a1}{2k_{fuel}} + \frac{a2}{k_{clad}} + \frac{a3}{k_{crud}}\right|$$

where a1 is the half-thickness of the fuel meat, a2 is the thickness of the cladding, and a3 is the thickness of crud. The heat flux q'' is calculated base on the interface area between the fuel meat and the clad. Below is a schematic of the fuel plate model.

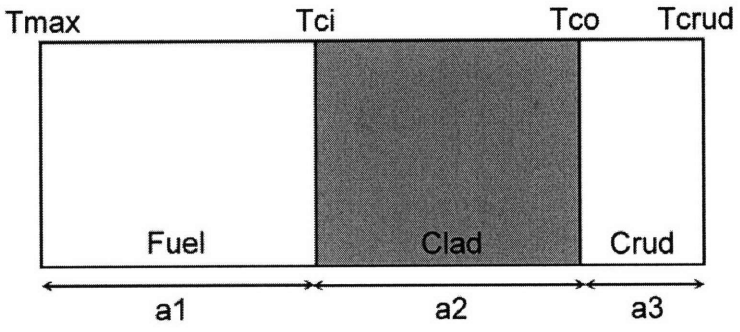

a1 = Fuel thickness
a2 = Clad thickness
a3 = Crud thickness

The figure below illustrates the temperature differences as a function of reactor power. It is evident that due to the lower thermal conductivity of the crud, the temperature difference between the fuel centerline and crud outer surface is much higher than that between fuel centerline and the clad outer surface.

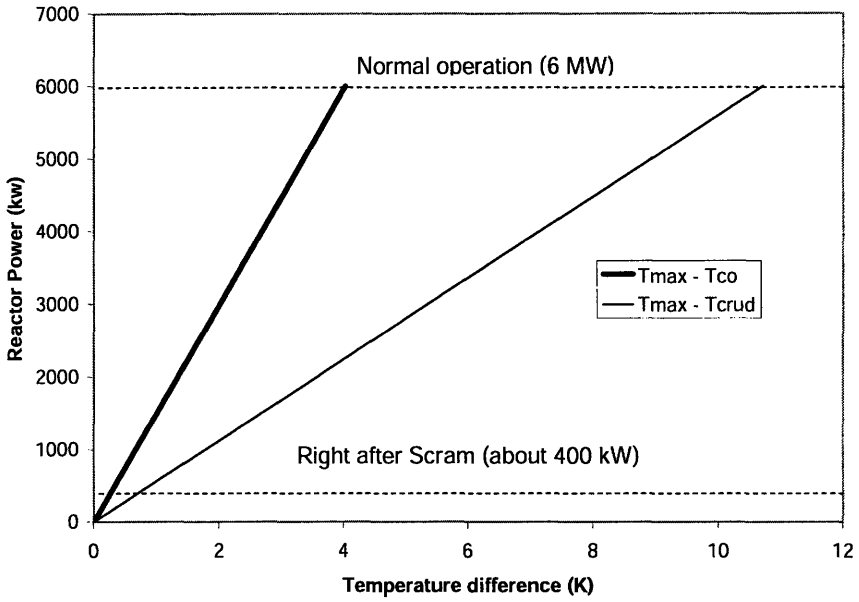

As shown in the table below, during 6 MW steady-state operation the temperature difference within the fuel plate is ~ 11 °C. After reactor scram, the temperature difference is < 1 °C.

Reactor power	Tmax – Tco (K)	Tmax – Tcrud (K)
6 MW (Normal operation)	4.03	10.71
400 kW (After Scram)	0.27	0.71

Appendix C.
MULCH-II input files for MIT reactor

```
MITR-III 6 MW with existing equipment PLTEMP benchmark 9/16/06
-------------------------------------------
6e6,17.9,125.0,103.0,0.8,50.0,2.31      ! 112.2 kg/s is 1800gpm @ 50C; 125 kg/s is 2000
gpm
0,1.e10                                          ! 4" below overflow
0.1,0.1
6.6e6,100.0,50,40.,55.,50.,50.
1.0,1.0
-------------------------------------------
-1.87,0.41,2.95,-0.68,0.5136,1.492          ! pump coast down curve
0.032,0.427,0.203,-7.08,4.58,1
3.8870e-5,1.6792e-4,7.04e-3,0.0,7.30,1770
0.032,0.468,0.203,6.97,2.17,1
0.339,0.413,0.180,-1.22,0.0,1
0.111,0.076,0.063,-0.69,0.3,1
0.0044,0.016,0.22,-0.01,0.18,1
0.029,0.018,0.04,-0.61,0.0,1
1.2490e-4,8.2434e-5,2.1864e-3,0.66,2.05,345 !min 23 elements
0.13,0.099,0.387,0.76,0.0,1
0.923,1.92,1.084,1.22,0.0,1
0.032,0.427,0.203,-7.08,4.58,1
9.003e-5,3.8895e-4,3.010e-3,0.0,7.3,1770
0.032,0.468,0.203,6.97,2.17,1
1.78e-3,3.837e-3,1.059e-4,2715.0,7.9,6.9,2
2.71e-3,8.107e-3,2.04e-4,2715.0,46.3,52.0,4
-------------------------------------------------
23,7.62e-4,5.08e-4,2.54e-5,0.05588,0.5683,1.0     !min 23 elements
0.9205
3.5E-4
-------------------------------------------------
1.0,0.0,0.0,0.0
2.0                                    ! 1.41 even bank, assume 1 blade drop 1.645
1.166,1.143,1.257,1.299,1.23,1.061,0.917,0.767,0.61,0.55
1.462,1.503,1.568,1.631,1.407,0.87,0.571,0.407,0.339,0.241
1.622,1.059,1.026,1.009,1.048,0.976,1.074,1.083,1.106,1.959
1.45,1.037,1.098,1.089,1.169,1.307,1.206,1.091,1.201,5.56
0.864
1.173,1.275,1.123,1.0                          ! new e-factors 1/26/99
1.5,1.5
0,0
```

Appendix D.
PLTEMP/ANL input files for MIT reactor

```
MITR-3 HEU Benchmark 6.0 MW Single Plate Model
! mitr_6mw_avg_v3.inp     Sept. 20 2006
! assume clad thickness is that without fins
! Dittus-Boelter h
    1    0    5    1    0    1    1    1
! flow driven mode; type 0310 needed for mass flow rates
    1    3 0.0              1.000          1.000          1.000
   11   11 1.00
    1    1    1
 1.299
! coolant channel geometry
!   area          Dh              L              Resistance
! L=22.375" from Fig. 4-3 MITR3 Fuel Element
! end box: assume same shape as end of meat section
! flow area=2 3/8 x 1 7/8"=.002873 m^2
 2.87300E-03 5.32300E-02 0.0
 0.0             0.0             0.5683         0.0
 2.87300E-03 5.32300E-02 0.0
! Blasius equation for Re<30000, per Newton thesis p. 102
  0.316             0.25
! fuel plate geometry and properties
! clad is 6061 with k=180 W/mK; UALx k=42.5 from T. H. Newton thesis 2006 p. 101
! clad thickness=.015
    2    3    0.000E-00 0.5683         0.38100E-03 180.0          0.76200E-03      42.5
! coolant channel cross section data
! half-channel area; full channel Dh
!    area          Dh          Perimeter     Heated P
  0.6245E-04   2.1864E-03 0.12350       0.0
  0.6245E-04   2.1864E-03 0.12350       0.0
! plate width
 0.10620
! radial peaking
 1.00
! flow rates kg/s, card 0310
! average channel data: divided by 2
! for 23 element core, 0.920 fraction core flow, 125 kg/s
! flow disparity factor=.864
 0.16667       0.16667
! assume 100% of heat generated is deposited in the fuel plate
! DP0           DDP             DPMAX          power, MW      Tin            Pin
! power = 1.0*6.0MW/(23*15)
 0.140         0.0005          0.190          0.017391       43.6           0.170
```

```
! QFCLAD        QFCOOL: assume no heat deposited directly to clad or to coolant
  0.              0.0
! Whittle & Forgan eta=25.
  100 0.10000E-03     25.0              0.0                0.0
 -11
    0.00            0.050          1.166
    0.10            0.150          1.143
    0.20            0.250          1.257
    0.30            0.350          1.299
    0.40            0.450          1.230
    0.50            0.550          1.061
    0.60            0.650          0.917
    0.70            0.750          0.767
    0.80            0.850          0.610
    0.90            0.950          0.550
! node last value set to value at 0.90
    1.00            1.000          0.550
     2
```

Appendix E.
RELAP5-3D input files for MIT reactor

```
= MIT case1, pump coast-down
*     first 50 seconds is a null transient, pump trips at 50 s
100 new transnt
102 si si * use SI units
105 5.0 6.0 1000. * max computer time = 1000 seconds
*
*       time step
*
* 201 50. 1.0-6 .02 31 10 10 200 * force to run 50 seconds of transient
* 201 50. 1.0-6 .005 31 100 1000 500 * force to run 50 seconds of transient
* 201 100. 1.0-6 .005 31 100 1000 500 * force to run 100 seconds of transient
* change minimum time step from 10-6 to 10-7 becos
* Thermodynamic property error with minimum time step, transient being terminated
* 201 100. 1.0-7 .005 31 100 1000 500 * force to run 100 seconds of transient
201 150. 1.0-9 .005 31 100 1000 500 * YCK 030907 force to run 150 seconds of transient

*
*                   minor edit variables
*
301 count 0
302 cputime 0
303 dt 0
304 dtcrnt 0
*
*                 trips, open ASV and NCV
*
401 time 1 ge null 1 54.4 1 * trip ASV at t = 54.4 and latch
402 time 1 ge null 1 54.4 1 * trip NCV at t = 54.4 and latch
*
*                   hydrodynamic components
*
1000000 snkref tmdpvol * sink reference volume, sets system pressure
1000101 1.0 1.0 1.0 0. 0. 0. .00001 0. 0000000
1000200 103
```

```
* 1000201 0. 1.02+5 333.15 * initial p, T
1000201 0. 1.02+5 328.0 * initial p, T, by MULCH S.S. compinent #1 YCK 032207
*
1010000 outlet sngljun
1010101 103010002 100010001 .032 1.0 1.0 100 1.0 1.0 1.0
1010201 1 125. 0. 0.
*
1020000 cldleg tmdpvol * cold leg inlet temperature
1020101 1.0 1.0 1.0 0. 0. 0. .00001 0. 0000000
1020200 103
* 1020201 0. 1.03+5 320.4 * initial p, T by MULCH S.S. compinent #2 YCK 032207
1020201 0. 1.03+5 316.6 * initial p, T
*
1030000 upppln snglvol
1030101 .923 .1 .0923 0. 90. .1 .00001 1.1 11000
1030200 103 1.025+5 333.15 * initial p, T
*
1040000 uppjn1 sngljun
1040101    105010002 103010001 .5 .01 .01 100 1.0 1.0 1.0
1040201 1 125. 0. 0.
*
1050000 uppl2 snglvol * middle volume for upper plenum
* 1050101 .923 1.11 1.02453 0. 90. 1.11 .00001 1.1 11000
1050101 .923 1.12 1.03376 0. 90. 1.12 .00001 1.1 11000 *YCK 022807
1050200 103 1.04+5 333.15 * initial p, T
*
1060000 uppjn2 sngljun
1060101 108010002 105010001 .13 .01 .01 100 1.0 1.0 1.0
1060201 1 125. 0. 0. * initial flow rate
*
1070000 uppjn3 sngljun
1070101 105010001 109010001 .5 .01 .01 100 1.0 1.0 1.0
1070201 1 0. 0. 0.
*
1080000 uppl3 snglvol
1080101 .130 .76 .0988 0. 90. .76 .00001 .387 11000    *YCK 022807
```

```
* 1080101 .130 .84 .1092 0. 90. .84 .00001 .387 11000
1080200 103 1.05+5 333.15 * initial p, T
*
1090000 uppl4 snglvol
* 1090101 .90 .76 .684 0. -90. -.76 .00001 1.282 11000
* 1090101 .973 .76 .73948 0. -90. -.76 .00001 1.282 11000    *YCK 022807
1090101 .973 .80 .7784 0. -90. -.80 .00001 1.282 11000    *YCK2 022807
1090200 103 1.05+5 333.15 * initial p, T
*
1100000 inltpl snglvol
* 1100101 .130 .05 .0065 0. 90. .05 .00001 .387 11000
1100101 .130 .0658 .008554 0. 90. .0658 .00001 .387 11000    *YCK 022807
1100200 103 1.10+5 320.4 * initial p, T
*
2010000 pump tmdpjun * pump
2010101 102010002 203010001 .032
2010200 1
2010201 0. 125. 0. 0. * t,w    pump coastdown starts at 50 s
2010202 50. 125. 0. 0.
2010203 50.1 108.43 0. 0.
2010204 50.2 101.69 0. 0.
2010205 50.3 95.40 0. 0.
2010206 50.4 89.53 0. 0.
2010207 50.6 78.92 0. 0.
2010208 50.8 69.65 0. 0.
2010209 51.0 61.52 0. 0.
2010210 51.5 45.23 0. 0.
2010211 52.0 33.34 0. 0.
2010212 52.5 24.57 0. 0.
2010213 53.0 18.08 0. 0.
2010214 53.5 13.27 0. 0.
2010215 54.0 9.69 0. 0.
2010216 54.5 6.23 0. 0.
2010217 55.0 4.04 0. 0.
2010218 56.0 2.09 0. 0.
2010219 57.0 1.43 0. 0.
```

```
2010220 58.0 1.104 0. 0.
2010221 60.0 0.0 0. 0.
2010222 100000.0 0.0 0. 0.
*
2020000 ASV valve
2020101 105010002 203010001 .007674 6.90 7.90 100 1.0 1.0 1.0 * 2 valves
2020201 1 0. 0. 0. * initial flow rate
2020300 trpvlv * trip valve
2020301 401 * trip 401
*
2030000 regn1 pipe * region 1
2030001 10 * number of nodes
2030101 .339,10 * area
* 2030301 .117,10 * node lengths
2030301 .122,10 * node lengths * YCK 022807
2030601 -90.,10 *    vertical angles
2030801 .00001,.180,10 * roughness, Dh
2031001 11000,10 * volume control flags
2031101 1020,9 * junction control flags
2031201 103,1.04+5,320.4,0.,0.,0.,10 * initial pressure, temperature
2031300 1 * use mass flows below
2031301 125.0,0.,0.,9 * initial junction flow rates
*
2040000 rgn1to2 sngljun * region 1 to region 2 junction
* 2040101 203100002 205010001 .111 .4 .8 100
2040101 203100002 205010001 .111 .3 .3 100 *YCK 022807
2040201 1 125. 0. 0. * initial flow rate
*
2050000 regn2 pipe * region 2
2050001 10 * number of nodes
2050101 .111,10 * area
* 2050301 .146,10 * node lengths
2050301 .06899,10 * node lengths    YCK 022807
* 2050601 -28.2,10 * vertical angles
2050601 -90.,10 * vertical angles    YCK 022807
2050801 .00001,.063,10 * roughness, Dh
```

```
2051001 11000,10 * volume control flags
2051101 1020,9 * junction control flags
2051201 103,1.05+5,320.4,0.,0.,0.,10 * initial pressure, temperature
2051300 1 * use mass flows below
2051301 125.0,0.,0.,9 * initial junction flow rates
*
2060000 rgn2to3 sngljun * region 2 to region 3 junction
2060101 205100002 207010001 .0044 .18 .18 100    * YCK 022807
* 2060101 205100002 207010001 .029 .4 .9 100
2060201 1 125. 0. 0. * initial flow rate
*
2070000 regn3 pipe * region 3
2070001 10 * number of nodes
2070101 .0044,10 * area    * YCK 022807
* 2070101 .029,10 * area
* 2070301 .025,10 * node lengths
2070301 .364,10 * node lengths    * YCK 022807
* 2070601 -2.3,10 * vertical angles
2070601 -0.16,10 * vertical angles * YCK 022807
2070801 .00001,.220,10 * roughness, Dh
2071001 11000,10 * volume control flags
2071101 1020,9 * junction control flags
2071201 103,1.06+5,320.4,0.,0.,0.,10 * initial pressure, temperature
2071300 1 * use mass flows below
2071301 125.0,0.,0.,9 * initial junction flow rates
*
2080000 NCV valve * NCV
* 2080101 109010002 210010001 .03244 52.0 46.3 100 1.0 1.0 1.0 * 4 valves    * YCK 022807
2080101 109010002 210010001 .029 52.0 46.3 100 1.0 1.0 1.0 * 4 valves
2080201 1 0. 0. 0. * initial flow rate
2080300 trpvlv * trip valve
2080301 402 * trip 402
*
2090000 rgn3to4 sngljun * region 3 to region 4 junction
2090101 207100002 210010001 .0044 .1 .1 100    * YCK 022807
2090201 1 125. 0. 0. * initial flow rate
```

```
*
2100000 regn4 pipe * region 4
2100001 10 * number of nodes
* 2100101 .029,10 * area
2100101 .029,10 * area
* 2100301 .07142,10 * node lengths
2100301 .061,10 * node lengths    * YCK 022807
2100601 -90.,10 *    vertical angles
2100801 .00001,.040,10 * roughness, Dh
2101001 11000,10 * volume control flags
2101101 1020,9 * junction control flags
2101201 103,1.07+5,320.4,0.,0.,0.,10 * initial pressure, temperature
2101300 1 * use mass flows below
2101301 125.0,0.,0.,9 * initial junction flow rates
*
2110000 rgn4toi sngljun * region 4 to inlet plenum
* 2110101 210100002 110010001 .029 .1 .1 100
2110101 210100002 110010001 .029 2.05 2.05 100 * YCK 022807
2110201 1 125. 0. 0. * initial flow rate
*
*               302 represents 329 average core channels
*               402 represents 1 hot channel
*
3010000 avginl sngljun * inlet to the average core channel
* 3010101 110010002 302010001 .041 .1 .1 100
3010101 110010002 302010001 .04 .1 .1 100    * YCK 022807
3010201 1 114.8 0. 0. * initial flow rate * YCK 032407
*
3020000 avgchn pipe * average core channel
3020001 10 * number of nodes
* 3020101 .041,10 * area
3020101 .04,10 * area    * YCK 022807
3020301 .06478,1 .05683,9 .06478,10 * node lengths
3020601 90.,10 * vertical angles
3020801 .00001,.0021864,10 * roughness, Dh
3021001 11000,10 * volume control flags
```

```
3021101 1020,9 * junction control flags
3021201 103,1.08+5,320.4,0.,0.,0.,10 * initial pressure, temperature
3021300 1 * use mass flows below
3021301 114.8,0.,0.,9 * initial junction flow rates * YCK 032407
*
3030000 avgout sngljun * outlet from the average core channel
* 3030101 302100002 108010001 .041 .6 .3 100
3030101 302100002 108010001 .04 .1 .1 100    * YCK 022807
3030201 1 114.8 0. 0. * initial flow rate * YCK 032407
*
*          average fuel plate
*
13021000 10 9 1 0 0. 0 0 2 * 658 average half-plates
13021100 0 2 * mesh flags
13021101 .00009525,8 * mesh intervals
13021201 1,4 2,8 * compositions
13021301 0.,4 1.,8 * radial source distribution
13021401 320.4,9 * initial temperatures
* 13021501 302010000,10000,1,0,3.761,10 * left boundary condition
13021501 302010000,10000,1,0,3.929,10 * left boundary condition * YCK 032407
* 13021601 0,0,0,0,3.761,10 * right boundary condition, insulated
13021601 0,0,0,0,3.929,10 * right boundary condition, insulated * YCK 032407
* 13021701 1000 38.36 0. 0. 1 * axial source distribution, 329 av. plates
* 13021702 1000 37.60 0. 0. 2
* 13021703 1000 41.36 0. 0. 3
* 13021704 1000 42.73 0. 0. 4
* 13021705 1000 40.47 0. 0. 5
* 13021706 1000 34.91 0. 0. 6
* 13021707 1000 30.17 0. 0. 7
* 13021708 1000 25.23 0. 0. 8
* 13021709 1000 20.07 0. 0. 9
* 13021710 1000 18.10 0. 0. 10
13021701 1000 40.11 0. 0. 1 * axial source distribution, 329 av. plates * YCK 030907
13021702 1000 39.32 0. 0. 2 * YCK 030907
13021703 1000 43.24 0. 0. 3 * YCK 030907
13021704 1000 44.69 0. 0. 4 * YCK 030907
```

```
13021705 1000 42.31 0. 0. 5 * YCK 030907
13021706 1000 36.50 0. 0. 6 * YCK 030907
13021707 1000 31.54 0. 0. 7 * YCK 030907
13021708 1000 26.38 0. 0. 8 * YCK 030907
13021709 1000 20.98 0. 0. 9 * YCK 030907
13021710 1000 18.92 0. 0. 10 * YCK 030907
13021800 0
13021801 .0021864,10.,10.,0.,0.,0.,0.,1.0,10 * additional left boundary * YCK 032407
13021900 0
13021901 .0021864,10.,10.,0.,0.,0.,0.,1.0,10 * additional right boundary * YCK 032407
*
*       ENGINEERING FACTOR FOR HOT CHANNEL FLOW RATE = 1.275,
*       reduce flow area by the same factor
4010000 avginl sngljun * inlet to the average core channel
* 4010101 110010002 402010001 1.249-4 .1 .1 100
* 4010101 110010002 402010001 1.015-4 .1 .1 100
4010101 110010002 402010001 1.0-4 .1 .1 100    * YCK 022807
* 4010201 1 .339 0. 0. * initial flow rate
4010201 1 .288 0. 0. * initial flow rate * YCK 032407
*
4020000 hotchn pipe * hot core channel
4020001 10 * number of nodes
* 4020101 1.015-4,10 * area
4020101 1.0-4,10 * area    * YCK 022807
4020301 .06478,1 .05683,9 .06478,10 * node lengths
4020601 90.,10 * vertical angles
4020801 .00001,.0021864,10 * roughness, Dh
4021001 11000,10 * volume control flags
4021101 1020,9 * junction control flags
4021201 103,1.08+5,320.4,0.,0.,0.,10 * initial pressure, temperature
4021300 1 * use mass flows below
4021301 .288,0.,0.,9 * initial junction flow rates * YCK 032407
*
4030000 avgout sngljun * outlet from the average core channel
* 4030101 402100002 108010001 1.015-4 .6 .3 100
4030101 402100002 108010001 1.0-4 .1 .1 100    * YCK 022807
```

```
4030201 1 .288 0. 0. * initial flow rate * YCK 032407
*
*
*          peak fuel plate
*
14021000 10 9 1 0 0. 0 0 2 * 2 peak half-plates
14021100 0 2 * mesh flags
14021101 .00009525,8 * mesh intervals
14021201 1,4 2,8 * compositions
14021301 0.,4 1.,8 * radial source distribution
14021401 320.4,9 * initial temperatures
* 14021501 402010000,10000,1,0,.01143,10 * left boundary condition
* 14021601 0,0,0,0,.01143,10 * right boundary condition, insulated
14021501 402010000,10000,1,0,.0114,10 * left boundary condition * YCK 032407
14021601 0,0,0,0,.0114,10 * right boundary condition, insulated * YCK 032407

* 14021701 1000 .1462 0. 0. 1 * axial source distribution, 2 peak half plates
* 14021702 1000 .1503 0. 0. 2
* 14021703 1000 .1568 0. 0. 3
* 14021704 1000 .1631 0. 0. 4
* 14021705 1000 .1407 0. 0. 5
* 14021706 1000 .0870 0. 0. 6
* 14021707 1000 .0571 0. 0. 7
* 14021708 1000 .0407 0. 0. 8
* 14021709 1000 .0339 0. 0. 9
* 14021710 1000 .0241 0. 0. 10
14021701 1000 .2924 0. 0. 1 * axial source distribution, 2 peak half plates * YCK 030907
14021702 1000 .3006 0. 0. 2 * YCK 030907
14021703 1000 .3136 0. 0. 3 * YCK 030907
14021704 1000 .3262 0. 0. 4 * YCK 030907
14021705 1000 .2814 0. 0. 5 * YCK 030907
14021706 1000 .1740 0. 0. 6 * YCK 030907
14021707 1000 .1142 0. 0. 7 * YCK 030907
14021708 1000 .0814 0. 0. 8 * YCK 030907
14021709 1000 .0678 0. 0. 9 * YCK 030907
14021710 1000 .0482 0. 0. 10 * YCK 030907
```

```
14021800 0
14021801 .0021864,10.,10.,0.,0.,0.,0.,1.0,10 * additional left boundary * YCK 032407
14021900 0
14021901 .0021864,10.,10.,0.,0.,0.,0.,1.0,10 * additional right boundary * YCK 032407
*
5010000 bypinl sngljun * inlet to the bypass flow
* 5010101 110010002 502010001 3.66-3 .1 .1 100
5010101 110010002 502010001 3.44-3 .1 .1 100    * YCK 022807
5010201 1 9.9 0. 0. * initial flow rate * YCK 032407
*
5020000 bypass pipe * bypass flow
5020001 10 * number of nodes
* 5020101 3.66-3,10 * area
5020101 3.44-3,10 * area    * YCK 022807
5020301 .06478,1 .05683,9 .06478,10 * node lengthss
5020601 90.,10 * vertical angles
5020801 .00001,.0021864,10 * roughness, Dh
5021001 11000,10 * volume control flags
5021101 1020,9 * junction control flags
5021201 103,1.08+5,320.4,0.,0.,0.,10 * initial pressure, temperature
5021300 1 * use mass flows below
5021301 9.9,0.,0.,9 * initial junction flow rates * YCK 032407
*
5030000 bypout sngljun * outlet from the bypass flow
* 5030101 502100002 108010001 3.66-3 .6 .3 100
5030101 502100002 108010001 3.44-3 .1 .1 100    * YCK 022807
5030201 1 9.9 0. 0. * initial flow rate * YCK 032407
*
*
*
*              tables
*
20100100 tbl/fctn 1 1 * thermal properties table 1 for Al
* 20100101 180. * Al thermal conductivity
* 20100101 100. * Al thermal conductivity/1.8
* 20100151 2.42e6 * Al rho*Cp
```

```
* 20100151 1.34e6 * Al rho*Cp/1.8
20100101 180. * Al thermal conductivity *YCK 032407
20100151 2.42e6 * Al rho*Cp *YCK 032407
*
20100200 tbl/fctn 1 1 * thermal properties table 2 for leu fuel
* 20100201 40. * thermal conductivity
* 20100201 22.2 * thermal conductivity
* 20100251 2.24e6 * rho*Cp
* 20100251 1.24e6 * rho*Cp/1.8
* 20100201 42.5 * thermal conductivity *YCK 031407
20100201 42. * thermal conductivity *YCK 032407
20100251 2.24e6 * rho*Cp *YCK 032407
*
20200100 reac-t * General table 1, scram reactivity
20200101 0. 0.* t, reactivity ($)
20200102 51.3 0.    * YCK 030907
20200103 52.3 -7.5    * YCK 060207
20200104 53.3 -10.0    * YCK 060207
20200105 10000. -10.0
*
*    point kinetics
*
30000000 point separabl
* 30000001 gamma 909.09 0. 150. 1.0 1.0 2.0 52. wk * power/half plate/axial node
* 30000001 gamma 18181.8 0. 150. 1.0 1.0 2.0 52. wk * power/plate
30000001 gamma 17391.3 0. 150. 1.0 1.0 2.0 52. wk * power/plate * YCK 030907
30000002 ans79-1
30000401 17391.3 52. wk * YCK 030907
30000011 1
30000501 500. 0. * moderator density reactivity
30000502 2000. 0.
30000601 300. 0. * doppler reactivity
30000602 1000. 0.
30000701 302010000 0 1. 0. * Volume weighting factors
30000801 3021001 0 1.0 0.
.    end of input file
```

Appendix F
Thermal-hydraulic analyses of a 15-mil-thick fuel meat for the LEU core design

A LEU core design with a thinner fuel meat was proposed to increase the LSSS power. If a higher LSSS power can be attained, the LEU core may operate at higher power. In chapter 5, a fuel meat with a thickness of 0.508 mm (20 mils) and 18 plates per element is considered as an optimal design at this stage. In the Appendix F, an alternative design of a thinner fuel meat with a thickness of 0.381 mm (15 mils) is evaluated and the results are summarized.

As discussed in 5.3.1.2, the existing HEU core pressure loading for the core tank is chosen as an upper limit for the LEU core designs. To evaluate the feasibility of applying the 15-mil-thick fuel (LEU #c-series), first we examine the pressure drop. For simplicity, here we use the core pressure drop as a criterion. Figure F-1 shows the steady-state (forced convection) pressure drop through the core. These results are calculated by MULCH. It can be seen that the 15-mil-thick fuel, even with 20 plates per element, can meet the pressure drop criterion.

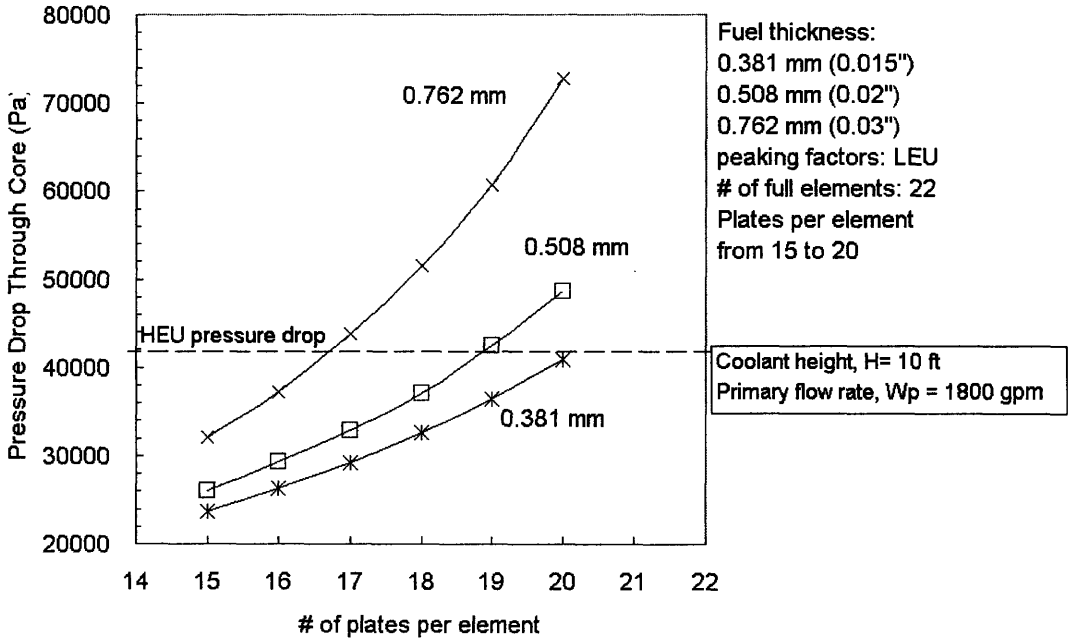

Figure F-1. Steady-state forced convection pressure drop (prediction of MULCH)

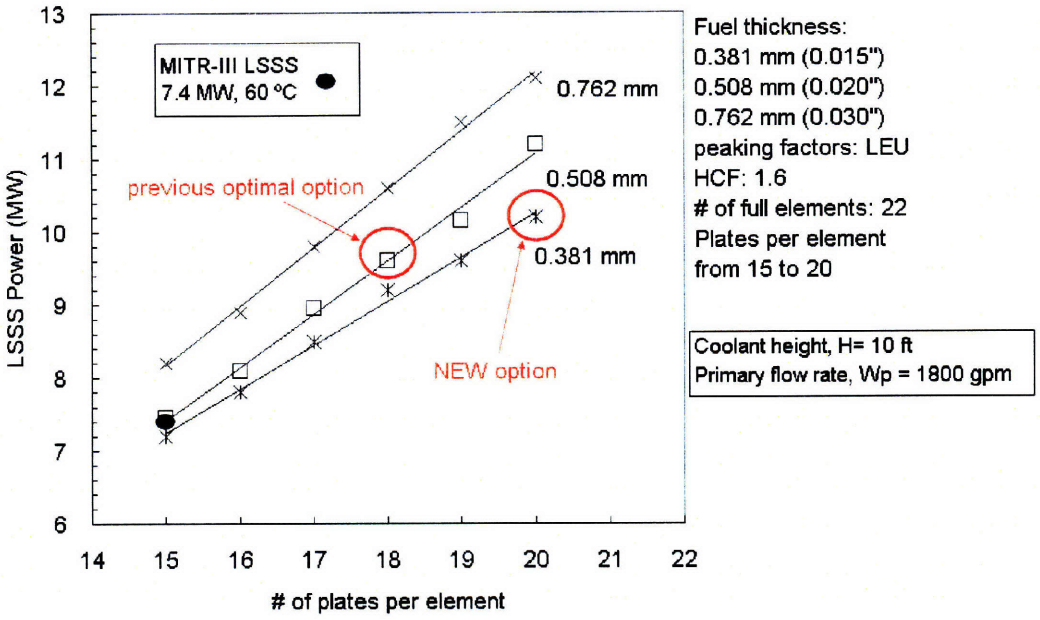

Figure F-2. LSSS power (prediction of MULCH)

Next we compare the LSSS power for different LEU core designs. In Fig. F-2, the 15-mil-thick fuel with 20 plates per element (LEU #C1) gives the highest LSSS power. Compared to the previous optimal option (a 20-mil-thick fuel with 18 plates per element, LEU #b4), the LSSS power can be increased from 9.6 MW to 10.2 MW if the LEU#C1 is selected.

The loss-of-flow transient simulation for LEU#C1 is performed by RELAP5. Figure F-3 is the maximum cladding temperature in the hot channel. It shows that both LEU#b4 and LEU#C1 would not have a drastic thermal spike at the beginning of the transient. Also, there is no significant flow instability happened for these two LEU core design options.

The LEU#C1 design looks fine and promising. However, RELAP5 gives a different result of steady state pressure drop. Table F-1 summarizes the pressure prop results. As shown in Table F-1, RELAP5 predicts that the LEU#C1 will have a slightly larger pressure drop than the HEU core does. This result is opposite to the prediction of MULCH. To deal with it conservatively, if we use a 15-mil-thick fuel with 19 plates per element, it can be expected that the pressure drop criterion can be met. However, this design gives a LSSS power of 9.6 MW, which is equal to our previous best option (LEU#b4).

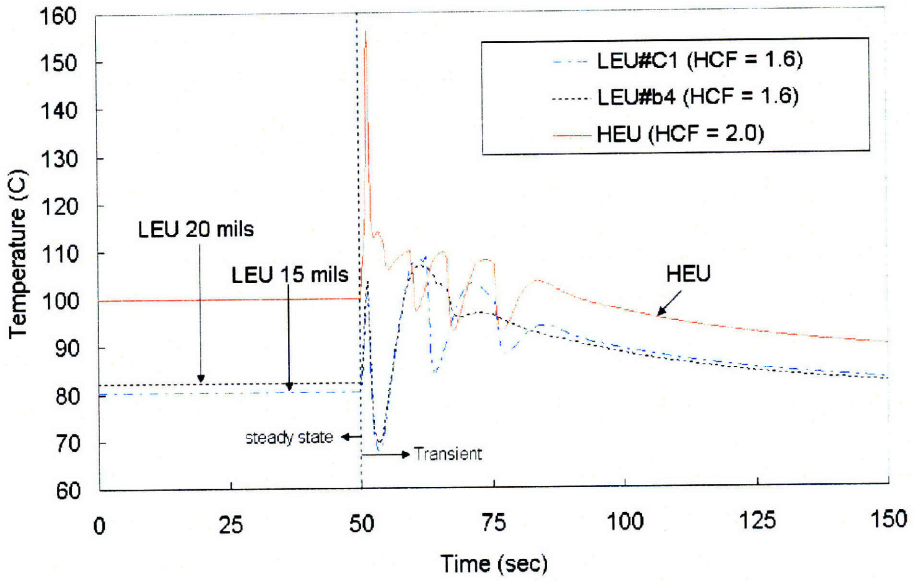

Figure F-3. Maximum clad temperature (prediction of RELAP5)

Table F-1. Design option data and pressure drop results

	Plates per element	Total # of plates	Fuel thickness (mm)	De (m)	Pressure drop through the core (Pa)	
					MULCH	RELAP5
HEU	15	330	0.762 (30 mils)	2.186 E-03	44389	44508
LEU# b4	18	396	0.508 (20 mils)	2.050 E-03	39320	39934
LEU# C1	20	440	0.381 (15 mils)	1.844 E-03	43505	44721

Even if the LEU#C1 is applicable, the increase of LSSS power is not significant (from 9.6 MW to 10.2 MW, an increase of 6%). Besides, the fabrication of the thinner fuel meats may be more difficult and could involve greater engineering uncertainty

Therefore, it can be concluded that using a thinner fuel may not provide much additional benefit for the LSSS power.